TECHNICAL REPORT STANDARD TITLE PAGE

1. Report No.	2. Government Accession No.	3. Recipient's Catalog No.
FHWA/TX-79/09+207-5		

4. Title and Subtitle	5. Report Date
METHODOLOGY FOR PREDICTING THE REFLECTION CRACKING LIFE OF ASPHALT CONCRETE OVERLAYS	March, 1979
	6. Performing Organization Code
7. Author(s)	8. Performing Organization Report No.
Frederick P. Germann, and Robert L. Lytton	Research Report 207-5
9. Performing Organization Name and Address	10. Work Unit No.
Texas Transportation Institute Texas A&M University College Station, Texas 77843	11. Contract or Grant No. Study 2-8-75-207
	13. Type of Report and Period Covered
12. Sponsoring Agency Name and Address	Interim- September, 1974 March, 1979
Texas State Department of Highways and Public Transportation Transportation Planning Division P. O. Box 5051; Austin, Texas 78763	14. Sponsoring Agency Code

15. Supplementary Notes

Work done in cooperation with FHWA, DOT.
Study Title: Flexible Pavement Evaluation and Rehabilitation

16. Abstract

An experimental testing procedure has been established in the report, for quantitative analysis of overlays designed to reduce reflection cracking. From this testing procedure the overlay scheme that shows the most resistance to cracking can be chosen. The procedure uses crack propagation tests on overlay samples which are conducted on a machine called the "overlay tester." This machine was specifically built to stimulate the displacements resulting from temperature changes in the cracked or jointed pavement or base materials that are beneath an overlay.

Various types of overlay samples were investigated on the overlay tester. These include samples with fabric, such as "Petromat," and samples composed of different grades of asphalt, AC-5, AC-10, and AC-20; various gradations, open graded, dense graded, and hot sand mixes; and different overlay thickness of one, two, and three inches.

In order to design an overlay, determining its proper thickness and reinforcing as well as the quantities of the constituents used in the mix, its reflection cracking life must be predicted so that the proposed overlay's resistance to cracking can be easily seen. One way to determine the fatigue life is to perform fatigue tests on overlay samples using the overlay tester. These tests can be time consuming and costly. Another method to find the fatigue life is to use a method of stress analysis that considers the concentration of stresses near the crack tip, known as "fracture mechanics." To use fracture mechanics, two material constants have to be determined. These material (continued on back)

17. Key Words	18. Distribution Statement
Reflection cracking, thermal cycling, asphalt concrete overlays.	No Restrictions. This document is available to the public through the National Technical Information Service, Springfield, Virginia 22161

19 Security Classif. (of this report)	20. Security Classif. (of this page)	21. No. of Pages	22. Price
Unclassified	Unclassified	147	

Form DOT F 1700.7 (8-69)

constants can be determined by fatigue tests, but elimination of these fatigue tests is desirable. As the name implies, these constants are properties of the material in which cracking occurs. Dr. R. A. Schapery of Texas A&M University has recently developed a theory using material properties to determine the two material constants for viscoelastic materials. The material properties used in his theory are creep compliance, D(t), tensile strength, σ_m, and fracture energy, Γ. This investigation explains what these properties are and shows how these properties are determined and applied to predict the reflection cracking life of an overlay.

METHODOLOGY FOR PREDICTING THE REFLECTION CRACKING LIFE OF ASPHALT CONCRETE OVERLAYS

by

Frederick P. Germann
Robert L. Lytton

Research Report Number 207-5

Flexible Pavement Evaluation and Rehabilitation

Research Project 2-8-75-207

Conducted for

The Texas State Department of Highways
and Public Transportation

in cooperation with the
U. S. Department of Transportation
Federal Highway Administration

by the

TEXAS TRANSPORTATION INSTITUTE
Texas A&M University
College Station, Texas

March 1979

PREFACE

This report gives a complete description of reflection cracking due to thermal cycling. It tells what the important material properties are and shows several new ways of measuring them, including the use of the duomorph and the measurement of crack lengths with ultrasonic waves.

The report presents the results of a series of reflection cracking tests that were run on the TTI Overlay Tester. Various thicknesses of overlays that were made with different viscosities of asphalt as well as some that were reinforced with various fabrics were tested and their results are reported herein. A viscoelastic theory which has been proposed to predict crack growth is presented and partially validated. Methods of reducing overlay tester data to determine the important material properties are given in this report.

This report is the fifth in a series of reports from the study entitled, "Flexible Pavement Evaluation and Rehabilitation." The study, sponsored by the State Department of Highways and Public Transportation in cooperation with the Federal Highway Administration, is a comprehensive program to develop new means of evaluating flexible pavements, predicting their performance and distress, and determining optimum management strategies for their rehabilitation and maintenance.

DISCLAIMER

The contents of this report reflect the views of the authors who are responsible for the facts and the accuracy of the data presented herein. The contents do not necessarily reflect the official views or policies of the Federal Highway Administration. This report does not constitute a standard, specification or regulation.

ABSTRACT

An experimental testing procedure has been established in this report, for quantitative analysis of overlays designed to reduce reflection cracking. From this testing procedure the overlay scheme that shows the most resistance to cracking can be chosen. The procedure uses crack propagation tests on overlay samples which are conducted on a machine called the "overlay tester." This machine was specifically built to simulate the displacements resulting from temperature changes in the cracked or jointed pavement or base materials that are beneath an overlay.

Various types of overlay samples were investigated on the overlay tester. These include samples with fabric, such as "Petromat," and samples composed of different grades of asphalt, AC-5, AC-10, and AC-20; various gradations, open graded, dense graded, and hot sand mixes; and different overlay thicknesses of one, two, and three inches.

In order to design an overlay, determining its proper thickness and reinforcing as well as the quantities of the constituents used in the mix, its reflection cracking life must be predicted so that the proposed overlay's resistance to cracking can be easily seen. One way to determine the fatigue

life is to perform fatigue tests on overlay samples using the overlay tester. These tests can be time consuming and costly. Another method to find the fatigue life is to use a method of stress analysis that considers the concentration of stresses near the crack tip, known as "fracture mechanics." To use fracture mechanics, two material constants have to be determined. These material constants can be determined by fatigue tests, but elimination of these fatigue tests is desirable. As the name implies, these constants are properties of the material in which cracking occurs. Dr. R. A. Schapery of Texas A&M University has recently developed a theory using material properites to determine the two material constants for viscoelastic materials. The material properties used in his theory are creep compliance, D(t), tensile strength, σ_m, and fracture energy, Γ. This investigation explains what these properties are and shows how these properties are determined and applied to predict the reflection cracking life of an overlay.

IMPLEMENTATION STATEMENT

The results of a series of tests of overlay samples which were performed on the TTI Overlay Tester are given in this report. The samples included some with "Petromat" and other fabrics; different overlay thicknesses of one, two, and three inches; different grades of asphalt, AC-5, AC-10, and AC-20; and various gradations of aggregate, open-graded, dense-graded, and hot sand mixes.

Material properties that are relevant to cracking resistance are given and a method of using them to calculate the reflection cracking life of an overlay is presented. Example calculations are shown.

The methodology that is presented in this report is intended to be a testing and analysis service that TTI can perform for the Texas SDHPT. The service is intended to assist the Materials Division (D-9) in assessing the efficiency of and in developing specifications for new materials that are proposed for use in overlays in various locations around the state.

This methodology will be fully implemented when the Texas SDHPT begins to use TTI's testing and analysis service on a regular basis.

TABLE OF CONTENTS

LIST OF TABLES

LIST OF FIGURES

CHAPTER I

INTRODUCTION

The primary objective of this research is to establish an experimental test procedure for quantitative analysis of overlay methods designed to reduce, eliminate, or delay reflection cracking. From such a testing procedure the overlay scheme that will most likely be successful in the field can be determined, and some pre-construction guidance on rehabilitation projects can be given to the Texas State Department of Highways and Public Transportation (SDHPT).

Experimental tests performed on the overlay schemes are a special kind of fatigue test, and these tests are conducted on a machine called the "overlay tester". The overlay tester was specifically built to model the displacements in the pavement or base materials that result from stresses induced by temperature changes (thermal stresses).

This type of cracking that occurs in asphalt overlays is more commonly known as "reflective cracking". It is caused by the cracked underlying pavement or base course contracting during drops in temperature during which restraining stresses are developed along the underside of the overlay (1). If these restraining stresses are greater than the tensile strength of the asphalt, cracks will form above the existing ones. From these thermal cracks other branch cracks develop and these continue to grow into what is known as "alligator cracking" (2). Water can intrude into these cracks which in turn leads to loss of bond between

the overlay and the original pavement and could also cause localized loss of subgrade support.

The direction in which the thermally induced cracks propagate are from the original pavement then up through the overlay, or the cracks may initiate in the base course and then propagate upward through the pavement. The latter behavior of crack initiation in the base course was observed by Carpenter, Lytton, and Epps (3). They reported that transverse cracking in pavements in west Texas resulted from the thermally active base course materials subjected to freeze thaw cycles which were found to be more susceptible to cracking than the asphalt concrete surface. Lime- and cement-stabilized base courses also cause reflection cracking due to their shrinkage and their thermal cycling. Based on the above observations of pavement cracking, the overlay tester was constructed so that this cracking behavior could be simulated.

Many asphalt overlay schemes have been developed to try to stop reflection cracking or at least minimize it. Some of these schemes tried are listed below:

1. Improved mixes for resurfacing. These include softer asphalts and the use of rubber and polymer-asphalt additives.
2. Intervening layers such as granular materials and open-graded asphalt mixes.
3. Stress-relieving interfaces, rubber tire-aggregate mixes, and some proprietary methods such as "overflex".
4. Reinforced layers of asphalt concrete that are reinforced with wire mesh or a fabric such as "Petromat".

In this investigation two main groups of tests were performed on possible overlay schemes. The first group of tests investigates the

performance of various fabrics, using fatigue tests, that are used to make the pavements more resistant to cracking. In the second group of tests a study is made on the behavior of cracking in asphalt overlays with "hard" and "soft" asphalts and "high" and "low" asphalt contents on open graded, dense graded, and hot sand mixes. Also the effect of cracking, in a standard ASTM dense graded asphalt mix, on three different thicknesses of one, two, and three inches is investigated. All of the above tests are performed at a constant temperature of 77°F (25°C).

For a study concerned with the evaluation of fatigue and fracture resistance of asphalt concrete, two approaches can be used, the phenomenological approach and the mechanistic approach.

The phenomenological approach was developed by Monismith (4-11), Pell (12-14), and others by empirically relating the fatigue life (N_f), the number of load applications to failure of the pavement, to the maximum tensile stress (σ) or tensile strain (ε) occurring on the underside of the pavement caused by traffic loads;

$$N_f = C_1 \left(\frac{1}{\sigma}\right)^{m_1} \quad \text{for controlled stress tests}$$

and

$$N_f = C_2 \left(\frac{1}{\varepsilon}\right)^{m_2} \quad \text{for controlled strain tests.}$$

The constants C_1, C_2, m_1, and m_2 are determined experimentally from simply supported or cantilevered asphalt concrete beams. Since the constants C and m vary with the type of test and boundary conditions, Ramsamooj (15) argued that they cannot be considered as true material

constants. Also, the phenomenological approach cannot take into account the crack initiation and propagation; in other words it cannot explain crack growth (16).

By using fracture mechanics to predict fatigue life and to explain crack growth, a mechanistic model was developed at Ohio State University (15, 17, 18). From fracture mechanics, fatigue life can be described by the process of crack initiation, crack growth, and ultimate fracture:

$$N_f = f(a, A, n, K, K_{Ic})$$

where

K = stress-intensity factor; this controls the rate of crack propagation since K takes into account the effect of external loads and geometry that intensifies the stresses near the crack tip (19, 20).

K_{Ic} = critical stress-intensity factor; when $K = K_{Ic}$ a crack propagates at an uncontrolled rate, like fracture that occurs in glass.

a = crack length

A and n = material constants.

From fatigue tests performed on metals, Paris and Erdogan (19) have shown that A, n, and K are related by the power law equation,

$$\frac{da}{dN} = A K^n \qquad (1\text{-}1)$$

where $\frac{da}{dN}$ is the change in crack length per cycle. Taking the log of both sides of the power law equation gives,

$$\log \frac{da}{dN} = \log A + n \log K$$

This is an equation of a straight line and from a plot of $\log \frac{da}{dN}$ versus log K, the material constants A and n are determined graphically. Log A is the "y-intercept" and n is the slope of the line.

Schapery (21) recently presented a theory of crack growth in viscoelastic materials in which he found a relationship between the material constants A and n and the properties of the material in which the crack is propagating,

$$A = f(\sigma_m, I_1, \nu, D(t), \Gamma, w(t), \Delta t)$$

and

$$n = f(m),$$

where

σ_m = maximum stress a material can withstand before separation of the material occurs

I_1 = an integration of stresses near the crack tip over a small region ahead of the crack tip known as the "failure zone." I_1 has the property that when it is multiplied by a constant, $\frac{2}{\pi}$, the product is equal to the stress-intensity factor K.

ν = Poisson's ratio of the material

$D(t)$ = creep compliance as a function of time, t, found from simple shear or uniaxial tension tests.

Γ = "fracture energy", which is defined as the work done (applied force times the resulting displacement) on a

material to increase its surface area, a unit area (this results from crack growth), and can have the units of $\frac{\text{lb-in}}{\text{in}^2}$.

$w(t)$ = the wave shape of the stress-intensity factor, K, i.e. $K_0 \sin \frac{2\pi t}{\Delta t}$, which represents a sinusoidal fluctuation with amplitude K_0.

Δt = the period of the cyclic loading, that is the time required to complete one cycle of loading.

m = the slope of the log D(t) vs. log t curve at the time, t, required for the crack to propagate the length of the failure zone.

The advantage of using Schapery's theory is that the constants A and n can be found by knowing the material properties as listed above instead of performing very time consuming fatigue tests to determine them experimentally. The results of fatigue tests at different temperatures and sample geometries can be predicted directly as can the fatigue of actual highway pavements. The importance of various material properties (e.g. asphalt, aggregate) can be determined explicitly rather than relying on extensive series of fatigue tests. If Schapery's theory can be shown to apply to reflection cracking fatigue, a number of mathematical inferences will be immediately available for purposes of designing optimum surface courses and overlays to delay, reduce, or prevent reflection cracking.

This leads to the second objective of this investigation, which is to verify Schapery's theory applied to asphalt concrete so that the fatigue life of a potential overlay scheme can be predicted numerically

based on material properties instead of having to rely only upon a series of fatigue tests which are costly in time and money and whose results cannot be applied directly to field conditions.

In the next section the concepts of fracture mechanics and their role in predicting the fatigue life of materials will be presented. Schapery's theory will then be presented and a review of previous research done to design asphalt mixes resistant to fatigue failure and cracking along with field tests will be given. The concluding section gives the experimental procedure, testing apparatus, and methods used for material characterization for evaluating overlays along with the data obtained from the tests.

CHAPTER II

FRACTURE MECHANICS

Basically, fracture mechanics explains why a structural member will fail (fracture) at a load (stress) much smaller than the load (stress) it was designed for. The explanation for this behavior is the existence of flaws (cracks) in the structure which created stress concentrations which in turn cause crack propagation resulting in failure.

There have been many structures which have failed under applied loads much smaller than the allowable designed loads which were based on large safety factors (22). The consequences of these failures sometimes resulted in the loss of human lives. Between 1942 and 1952 seven Liberty ships had broken completely in half which was caused by stress concentrations at square hatch corners. In the mid 1950's two Comet aircraft failed catastrophically while at high altitudes, and from investigations the cause was blamed on small fatigue cracks originating from rivet holes near openings in the fuselage. Bridges have also failed catastrophically such as the Point Pleasant Bridge at Point Pleasant, West Virginia resulting in the loss of 16 lives in 1967. In an attempt to prevent such failures from occurring, researchers have devised a structural analysis which considers crack growth as a function of the applied loads and this type of structural analysis is referred to as "fracture mechanics."

Fortunately when pavements fail due to cracking, the results are not as serious as would be in other types of structures. The advantage of applying fracture mechanics to asphalt concrete pavements is that the rate of crack growth, caused by environment or traffic loads, can be

determined and in turn the life of the pavement can be predicted as will be shown later in this section.

The first analysis of fracture behavior for materials containing cracks was made by Griffith in 1920 (23). Griffith postulated that for brittle materials, fracture (unstable crack growth) occurs when the rate of decrease in elastic strain energy due to an incremental increase in crack length is equal to or greater than the rate of increase in surface energy due to an incremental increase in crack length. Elastic strain energy is the area under that portion of the stress-strain curve for which Hooke's law is applicable.

Griffith considered an infinite plate of unit thickness that contains a through thickness crack of length 2a and is subjected to a uniform tensile stress, σ, applied at infinity as shown in Figure 1. The total potential energy of this system is

$$U = U_o - U_a + U_\gamma$$

where

U_o = elastic strain energy of uncracked plate

U_a = decrease in the elastic strain energy caused by introducing the crack in the plate

U_γ = increase in the surface energy caused by the formation of the crack surfaces, and stored on the surfaces of the crack.

Using a stress analysis that was developed by Inglis (24), Griffith showed that

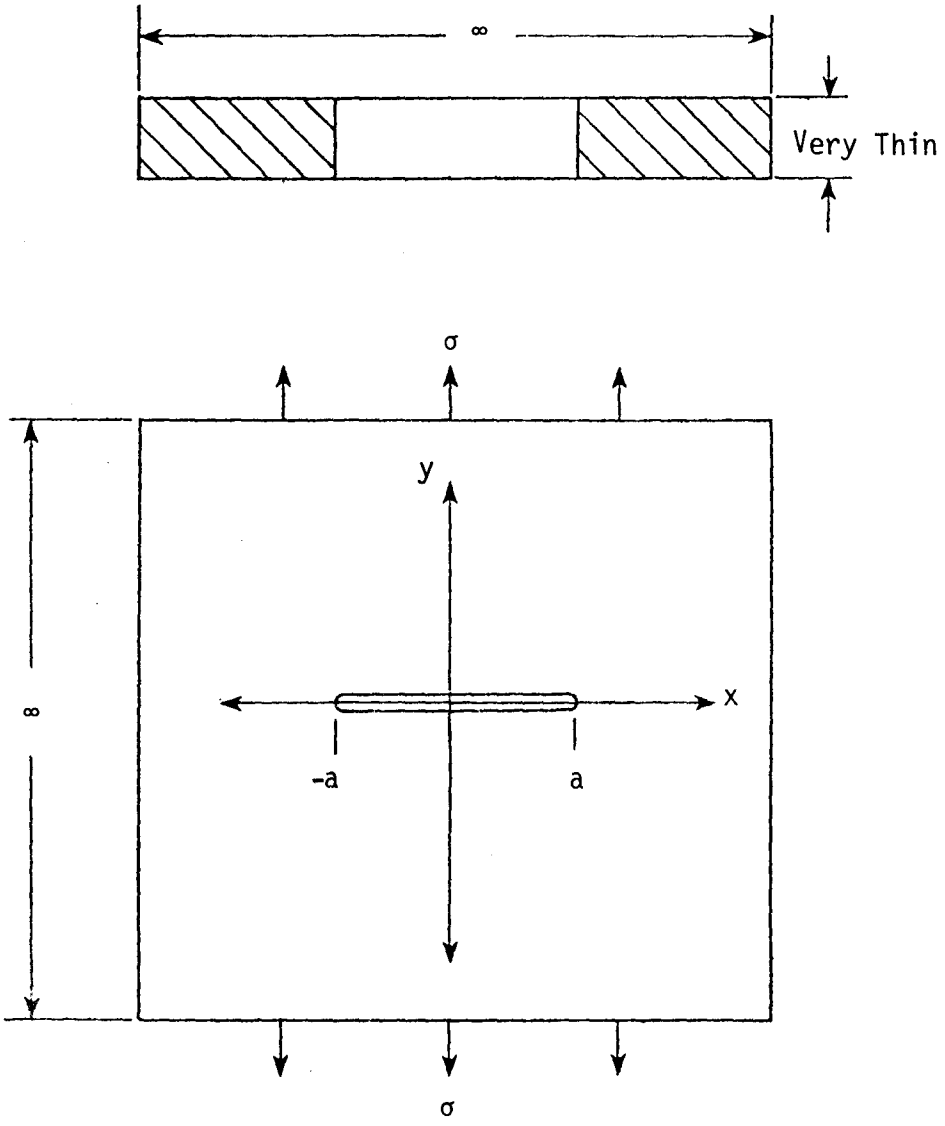

Figure 1. Plate With Infinite Dimensions Used in Griffith's Theory.

$$U_a = \frac{\pi\sigma^2 a^2}{E}$$

U_γ is equal to the product of the surface energy density of the material, γ, and the new surface area of the crack,

$$U_\alpha = 2(2a)\gamma$$

The total elastic energy of the system U is now

$$U = U_o - \frac{\pi\sigma^2 a^2}{E} + 4a\gamma$$

A crack will grow rapidly if more elastic energy is released than can be stored on the crack surfaces. Thus the critical condition for crack growth in Griffith's theory is when the rate of elastic energy release, $\frac{\partial U_a}{\partial a}$, is equal to the rate of surface energy storage, $\frac{\partial U_\alpha}{\partial a}$, and the net rate of change of total energy, $\frac{\partial U}{\partial a}$, is zero. This condition is obtained by setting the first derivative of U with respect to crack length, a, equal to zero:

$$\frac{\partial U}{\partial a} = 0 = -\frac{2\pi\sigma^2 a^2}{E} + 4\gamma$$

which is rearranged to:

$$\frac{\pi\sigma^2 a}{E} = 2\gamma \qquad (2\text{-}1)$$

The left hand side of the above equation has been designated by Irwin (25) to be the "crack extension force" -- "G". It represents the

elastic strain energy per unit crack surface area that is available for infinitesimal crack growth.

For the plate with a crack all the way through its thickness such as Griffith used in his analysis, Irwin defined the stress-intensity factor, K, for that system to be:

$$K \equiv \sigma \sqrt{a \pi} \tag{2-2}$$

Irwin (25) showed the following relationship between G and K:

$$\frac{\pi \sigma^2 a}{E} \equiv G$$

$$\sigma \sqrt{a \pi} = \sqrt{G E}$$

$$K = \sqrt{G E} \tag{2-3}$$

for plane stress and for plane strain conditions:

$$K = \sqrt{GE/(1-\nu^2)} \tag{2-4}$$

with ν being Poisson's ratio.

The energy-balance approach to crack growth, Griffith's theory, defines the conditions necessary for unstable crack growth that is typical in brittle materials. Griffith's theory does not apply to analysis of stable crack growth such as from fatigue loading. The stress-intensity factor, K, is applicable to stable crack growth and has helped in understanding the phenomena of stable crack growth and at what conditions unstable crack growth occurs.

In order to establish a stress analysis for cracks in an elastic solid, Irwin (26) defined three ways in which a crack may grow. Consider an element at the crack tip as shown below:

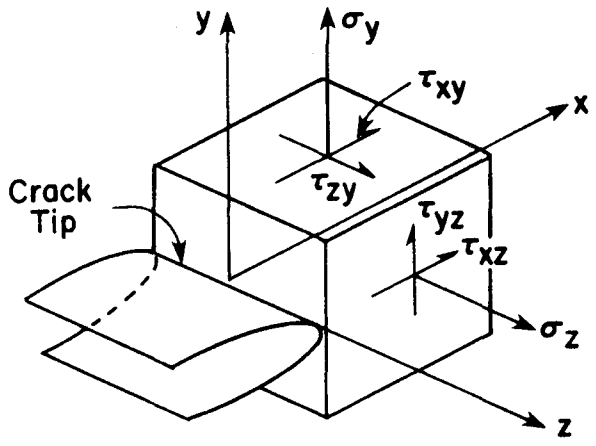

σ_x stress not shown. One way for the crack to extend into the element is if σ_y is the largest stress on the element or when all stresses except σ_y are zero.

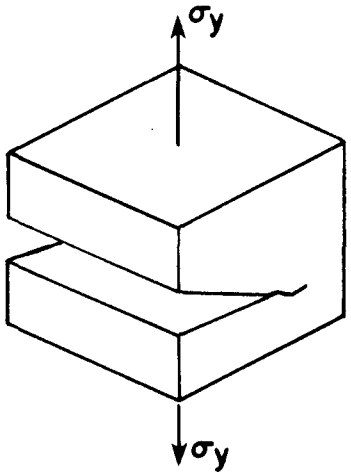

MODE I.

This defines Mode I (or Opening Mode) type crack displacements.

Mode II (or Shearing Mode) type crack displacements occur when τ_{yx} is the largest stress on the element or when the other stresses are zero.

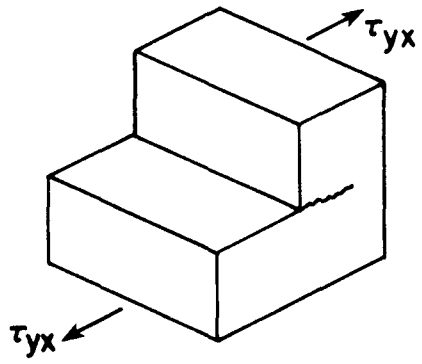

MODE II.

For Mode III crack displacements to take place the τ_{yz} stresses need to be dominant, or all other stresses zero.

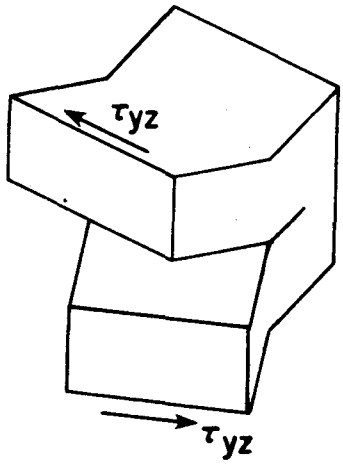

MODE III.

Irwin then set out to find the stresses and displacements in the vicinity of each of the three crack tips that were formed by the above three different modes of crack extension. He accomplished this by using the theory of elasticity and a method developed by Westergaard (54) for representing the Airy's stress function in terms of complex variables which takes into account the boundary conditions of the crack. The stresses and displacements near the crack tip for Mode I along with the coordinate system used are:

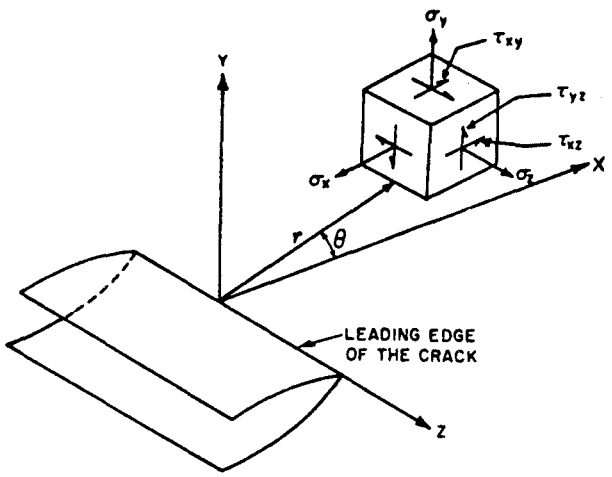

$$\sigma_x = \frac{K_I}{\sqrt{2\pi r}} \cos\frac{\theta}{2} \left[1 - \sin\frac{\theta}{2}\sin\frac{3\theta}{2}\right]$$

$$\sigma_y = \frac{K_I}{\sqrt{2\pi r}} \cos\frac{\theta}{2} \left[1 + \sin\frac{\theta}{2}\sin\frac{3\theta}{2}\right]$$

$$\tau_{xy} = \frac{K_I}{\sqrt{2\pi r}} \sin\frac{\theta}{2}\cos\frac{\theta}{2}\cos\frac{3\theta}{2} \qquad (2\text{-}5)$$

$$\sigma_z = \nu (\sigma_x + \sigma_y) , \quad \tau_{xz} = \tau_{yz} = 0$$

$$u = \frac{K_I}{G} \sqrt{\frac{r}{2\pi}} \cos \frac{\theta}{2} \left[1 - 2\nu + \sin^2 \frac{\theta}{2}\right]$$

$$v = \frac{K_I}{G} \sqrt{\frac{r}{2\pi}} \sin \frac{\theta}{2} \left[2 - 2\nu - \cos^2 \frac{\theta}{2}\right]$$

$w = 0$

ν = Poisson's Ratio

G = Shear Modulus

For a derivation of the above equations refer to Appendix A (p. 114). The Mode II and Mode III stresses and displacements are not shown here; for these equations, see Barsom (22) or Paris and Sih (27).

When θ is equal to zero the stresses for Mode I crack extension Eq. (2-5) reduces to:

$$\sigma_x = \frac{K_I}{\sqrt{2\pi r}} , \quad \sigma_y = \frac{K_I}{\sqrt{2\pi r}} , \quad \tau_{xy} = 0 \qquad (2\text{-}6)$$

This will allow a clear explanation of what a stress-intensity factor is. Consider the infinitely large plate of unit thickness, used in Griffith's theory, shown in Figure 1 (p. 10). The stress-intensity factor for this system was defined in Eq. (2-2). Substituting $\sigma \sqrt{\pi a}$ for K in Eq. (2-6) for the σ_y stresses yields:

$$\sigma_y = \frac{\sigma \sqrt{\pi a}}{\sqrt{2\pi r}}$$

By keeping σ constant and varying a, the behavior of the stress-intensity

factor, K, on the stresses, σ_y, near the crack tip can be seen in Figure 2. In Figure 2 the two curves for the two different crack lengths have an identical shape but different magnitudes of σ_y stresses. The stress-intensity factor tells what the magnitude of these stresses are; it does not have any bearing on the distribution of these stresses. The distribution of these stresses is invariant in all structural components subjected to this type of deformation and the magnitude of these stresses is described by a single parameter, K.

Unstable crack growth occurs when the stress-intensity factor reaches a critical value, K_{Ic}. K_{Ic} represents the ability of a material to withstand a given stress magnitude at the crack tip and to resist unstable crack growth. Also, K_{Ic} is known as the "fracture toughness" of the material and its value depends on the particular material, loading rate, and temperature.

The general relationship among material fracture toughness (K_{Ic}), nominal stress (σ), and crack length (a), for the cracked plate used in Griffith's theory, is shown schematically in Figure 3. Note that there are many combinations of σ and a that will fall on the K_{Ic} curve to cause unstable crack growth.

Barsom (22) made an analogy between the parameters applied load (P), nominal stress (σ), yield stress (σ_{ys}) for a uncracked material, and the parameters for a cracked material, applied load (P), stress-intensity factor (K), and the critical stress-intensity factor (K_{Ic}). In the uncracked material, as the load is increased the nominal stress increases until failure (yielding at σ_{ys}) occurs. For a material with a crack, as the load is increased the stress-intensity factor increases until

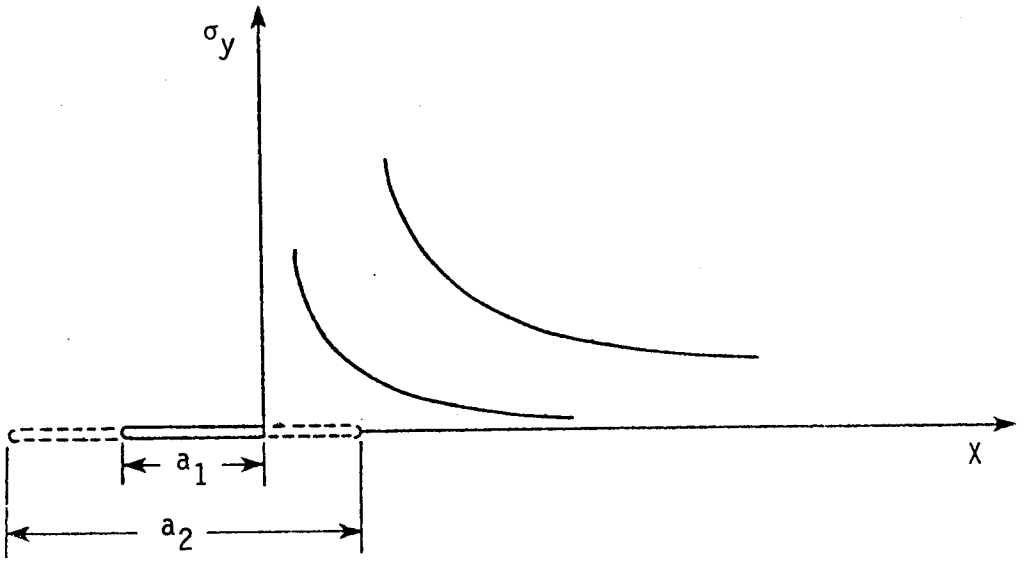

Figure 2. Effects of Crack Length on the Stresses Near the Crack Tip.

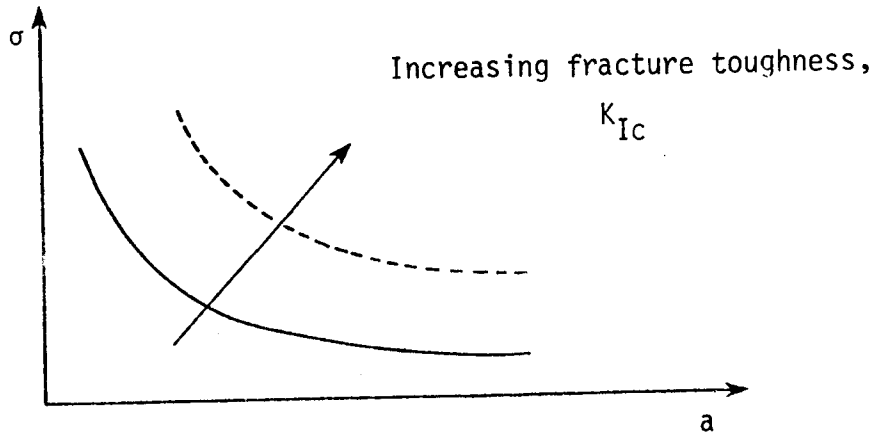

Figure 3. Relationship Between Fracture Toughness (K_{Ic}), Nominal Stress (σ), and Crack Length (a).

$K_I = K_{Ic}$ at which unstable crack growth occurs. As is done in conventional stress analysis, the design stress (σ) is kept below the yield stress (σ_{ys}), the K_I level in a structure should be kept below the K_{Ic} value.

If a structure containing a crack is subjected to several Mode I deformations say by a combination of uniform tensile loads, concentrated tensile loads, and bending loads, then the total stress-intensity factor can be obtained by adding the stress-intensity factors that correspond to each of the loads. For structures that are subjected to loads causing Modes I, II, and III type crack displacements, the stress-intensity factors of these different modes cannot be added. In this case the crack extension force, G, for each mode can be added to obtain the total crack extension force.

The complete useful life of a structure is the time required for the crack to initiate (appear) and the time it takes the crack to grow to critical dimensions at which unstable crack growth occurs. For asphalt concrete pavements crack initiation and stable crack growth may be caused by:

1. cyclic stresses -- traffic loads
2. aggressive environment -- freeze-thaw cycles and large amplitude temperature cycles which drop below the temperature at which stresses in the asphalt concrete will relax to zero during the cycle
3. the combination of cyclic stresses and aggressive environment.

Since the above causes of stable crack growth depend on the magnitude of the stresses at the crack tip, the rate of stable crack growth depends

upon K_I. Therefore fracture mechanics can be used to analyze the behavior of a structure throughout its entire life.

CHAPTER III

FATIGUE CRACK GROWTH

The data from stress versus number of load applications (S - N) curves are not realistic enough to use for predicting the fatigue life of a material, unless the fatigue test specimen and the member it is modeling are identical; they are the same shape, the crack geometries are the same, and the same type of load application and strain history.

The fracture mechanics approach uses fatigue-crack-growth tests performed on samples subjected to constant-amplitude cyclic-load fluctuations or to constant-amplitude cyclic-displacement fluctuations. For a particular number of elapsed load cycles, N, the corresponding crack height, a, is measured. From several test specimens with various initial crack lengths a plot of "a" versus "N" is made as shown in Figure 4 for constant cyclic load tests.

Paris and Erdogan (19) have shown that the curves in Figure 4 reduce to a single curve when the data are represented in terms of crack growth rate per cycle of loading, $\frac{da}{dN}$, and the fluctuation of the stress-intensity factor, ΔK_I. When $\frac{da}{dN}$ and ΔK_I are plotted on log-log paper for the entire life of a material the plot in Figure 5 is obtained.

In Region I the stress-intensity factor is small enough so that no crack growth occurs.

Stable crack growth occurs in Region II. This region is a straight line on log-log paper and is represented by Paris and Erdogan's power law, $\frac{da}{dN} = A(K)^n$.

In Region III the stress-intensity factor is equal to the critical stress-intensity factor and unstable crack growth occurs terminating

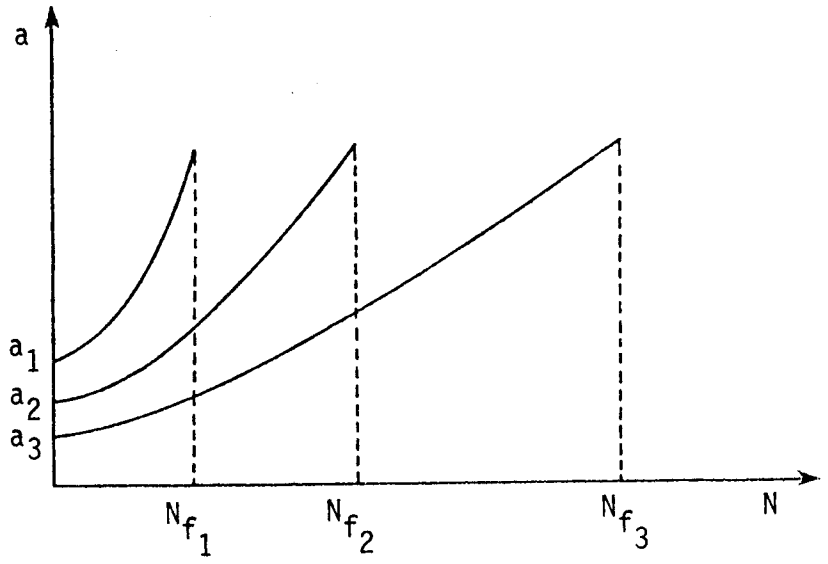

Figure 4. Crack Length (a) Versus Number of Load Applications (N) for Constant Cyclic Load Tests.

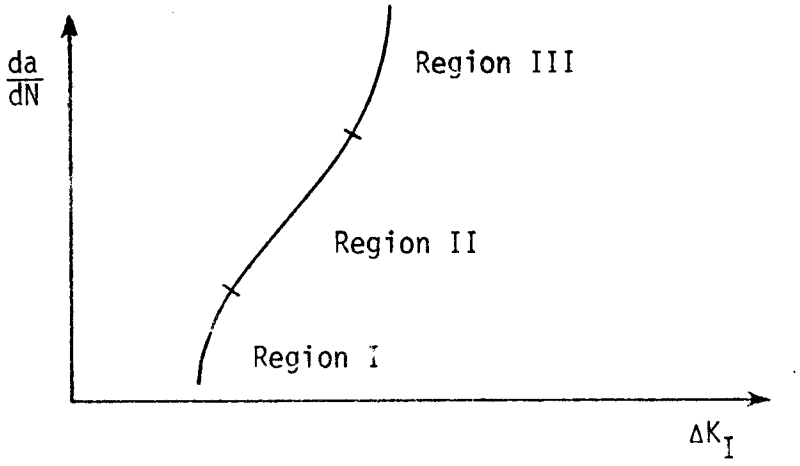

Figure 5. Crack Growth Rate per Cycle (da/dN) Versus Stress-Intensity Factor Fluctuation (ΔK_I) for the Entire Fatigue Life.

the fatigue life of the material.

The number of cyclic load applications a material can withstand is determined from the above power law equation:

$$N = \int_{a_0}^{a_1} \frac{da}{A\left[K(a)\right]^n} \qquad (3\text{-}1)$$

where

a_0 = the crack length at which stable crack growth occurs.

a_1 = that crack length at which unstable crack growth occurs for constant load tests (controlled load tests).

For constant displacement tests (controlled displacement tests), a_1 is the thickness of the material for which the crack has to propagate through to reach a free surface. As will be seen later from the test data, unstable crack growth did not occur for the controlled displacement tests performed on the overlay tester.

CHAPTER IV

SCHAPERY'S THEORY ON CRACK GROWTH IN VISCOELASTIC MATERIALS

Schapery (21) derived an equation relating the velocity of a crack to the material properties of the material in which the crack is propagating due to Mode I type displacements. Basically, Schapery's theory is based on three assumptions (these assumptions will be explained in more detail later):

1. Stresses and displacements very close to the crack tip can be represented by Barenblatt's crack tip model (28).
2. The second derivative of the logarithm of creep compliance with respect to logarithm of time is small for linear viscoelastic materials. This means that the curvature in the master creep compliance curve in Figure 25 (p. 78) is small which will allow certain equations to be simplied and the mathematics required to solve them not rigorous.
3. Failure can be defined by the work done to fail (pull apart) all strands in a region of small cross-sectional area known as the "failure zone" in Barenblatt's crack tip model. The work done in this failure zone to create a unit area of crack surface is termed the "fracture energy" and is designated by "Γ".

Barenblatt's crack tip model is shown graphically in Figures 6 and 7 where

a = crack length

α = length of failure zone

ξ_1 = $x-a$

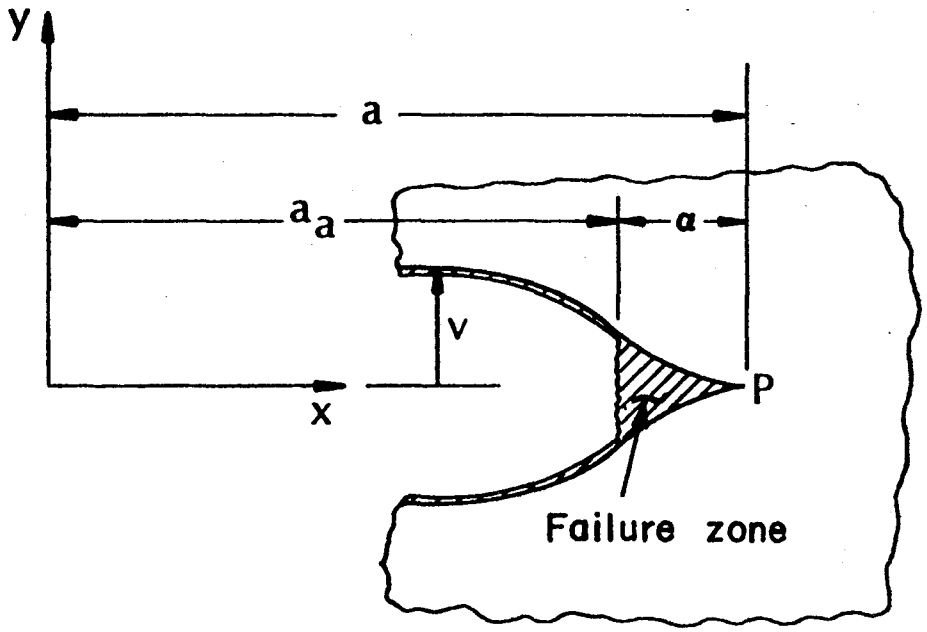

Figure 6. Geometry for Barenblatt's Crack Tip Model.

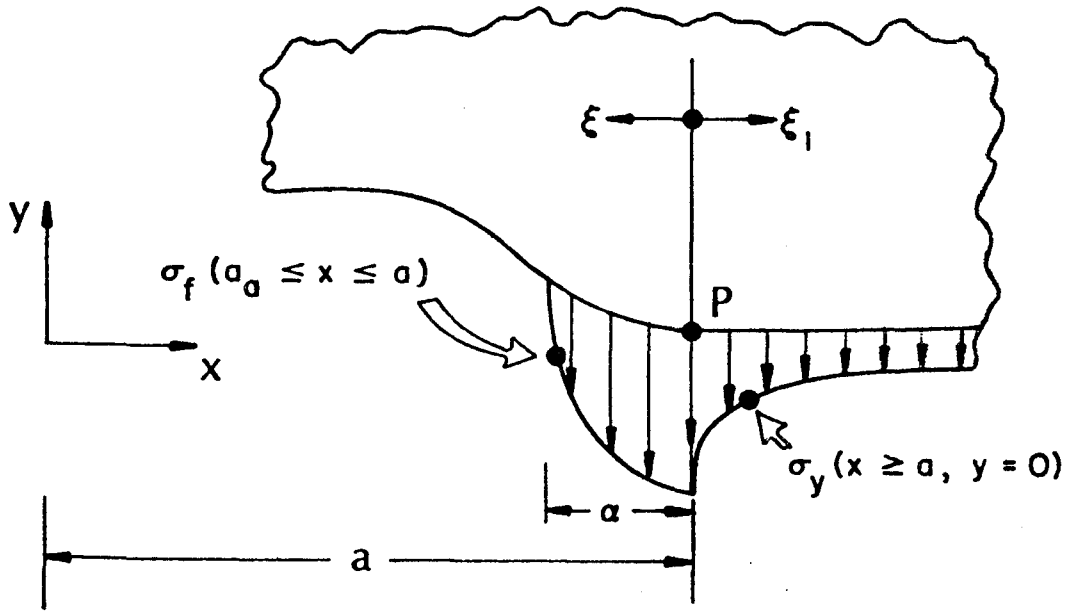

Figure 7. Stress Distribution in Barenblatt's Crack Tip Model

ξ = a-x

σ_f = tensile stresses in the failure zone, failure stress

σ_y = tensile stresses in the material ahead of the failure zone called the linear continuum

Barenblatt (28) showed that the stresses in the linear continuum due to the combined action of the failure stress in the failure zone and the applied loads will be finite if and only if

$$K_I = \sqrt{\frac{2}{\pi}} \int_0^{\alpha} \frac{\sigma_f(\xi)}{\sqrt{\xi}} \, d\xi$$

This will be referred to as the finite stress equation.

Schapery normalized the integrand by letting

$$\eta \equiv \frac{\xi}{\alpha}$$

$$f \equiv \frac{\sigma_f}{\sigma_m}$$

where σ_m is the maximum of σ_f with respect to ξ;

$$I_1 \equiv \int_{0/\alpha}^{\alpha/\alpha} \frac{\sigma_f\left[\frac{\xi}{\alpha} \cdot \alpha\right]}{\sigma_m \sqrt{\frac{\xi}{\alpha}}} \, d\frac{\xi}{\alpha} \equiv \int_0^1 \frac{f(\eta \cdot \alpha)}{\sqrt{\eta}} \, d\eta$$

With another change of integration,

$$\eta' = 2\sqrt{\eta}$$

$$d\eta' = \frac{1}{2}(2)\frac{d\eta}{\sqrt{\eta}} = \frac{d\eta}{\sqrt{\eta}}$$

allows the integrand to be expressed by

$$I_1 \equiv \int_0^2 f\, d\eta'$$

Note that $f \leq 1$, and I_1 will then be less than or equal to 2.

Substituting the normalized integrand into the finite stress equation results in:

$$K_I = \frac{2\alpha}{\pi}\sigma_m I_1$$

From this equation the length of the failure zone can be determined,

$$\alpha = \frac{\pi}{2}\left(\frac{K_I}{\sigma_m I_1}\right)^2$$

The displacement near the crack tip, as a function of creep compliance and failure stress with respect to ξ, will now be defined so that the failure criterion in statement 3 above can be applied.

Williams (29) gave a solution for the displacement v^0 near the crack tip due to loads acting on a linear elastic material for which $\sigma_f \equiv 0$:

$$v^0 = C_e \frac{K_I}{\sqrt{2\pi}}\sqrt{\xi}\; H(\xi)\left(1 + 0\left(\frac{\xi}{\beta}\right)\right)$$

where

$$C_e = \frac{4(1 - \nu^2)}{E}$$

ν = Poisson's ratio

β = distance between crack tip and nearest geometric feature (free surface or opposite crack tip)

$O(\xi/\beta)$ = a term of order (ξ/β)

$H(\xi)$ = the unit step function:

$$H(\xi) \equiv \begin{cases} 0, & (\xi = a\text{-}x) < 0 \\ 1, & (\xi = a\text{-}x) > 0 \end{cases}$$

Barenblatt (28) also gave a solution for the crack tip displacement resulting from the failure stress, σ_f, acting alone on a linear elastic solid:

$$v^f = -\frac{C_e}{2\pi} H(\xi) \int_0^{\alpha} \sigma_f(\xi') \ln \left| \frac{\sqrt{\xi'} + \sqrt{\xi}}{\sqrt{\xi'} - \sqrt{\xi}} \right| d\xi'$$

The resultant displacement, v, of the top crack face near the crack tip due to the applied loads and to σ_f is obtained by adding v^f to v^0 and then use the finite stress equation which yields:

$$v = H(\xi) \frac{C_e}{2\pi} \int_0^{\alpha} \sigma_f(\xi') \left[2\sqrt{\frac{\xi}{\xi'}} - \ln \left| \frac{\sqrt{\xi'} + \sqrt{\xi}}{\sqrt{\xi'} - \sqrt{\xi}} \right| \right] d\xi'$$

For stationary cracks, the above elastic displacement is used to obtain the viscoelastic displacement by applying the classical correspondence principle plus Laplace transform inversion. To obtain the viscoelastic crack tip displacement equation for a moving crack, the extended correspondence principle presented by Graham (30) must be applied to get:

$$v = \frac{1}{2\pi} \int_{t_1}^{t} C_v(t-\tau) \frac{\partial}{\partial \tau} \left\{ \int_0^{\alpha} \sigma_f(\xi') \left[2\sqrt{\frac{\xi}{\xi'}} - \ell n \left| \frac{\sqrt{\xi'} + \sqrt{\xi}}{\sqrt{\xi'} - \sqrt{\xi}} \right| \right] d\xi' \right\} d\tau \tag{4-1}$$

where

τ = variable of integration and ranges from t_1 to t.

t_1 = time when the crack tip first reaches a point x.

t = current time.

Since the time integration is to be evaluated for a constant x, ξ for moving cracks must be expressed in terms of x and τ

$$\xi = \xi(x, \tau) = a(\tau) - x$$

When $a(t_1) = x$, $\xi(x, t_1) = 0$. Let the time required for the crack to propagate an amount α be designated as $(t_2 - t_1)$. For this short period of time, a(t) can be approximated as:

$$a(t) \cong a(t_1) + (t - t_1)\dot{a}$$

with $\dot{a}$ being the crack tip velocity at time t_1.

This allows ξ to be written as:

$$\xi(x,t) = a(t) - x$$

$$\xi(x,t) \cong a(t_1) + (t - t_1)\,\dot{a} - x$$

$$\xi(x,t) \cong (t - t_1)\,\dot{a}$$

$$\xi(x,t) \cong \Delta t\,\dot{a}$$

When the viscoelastic displacement equation, derived from Graham's extended correspondence principle, is evaluated at points near the crack tip ($0 \leq \xi << \alpha$), the following approximation of the crack face displacement equation can be used:

$$v \cong - \frac{2\,\sigma_m\,I_2}{3\pi\sqrt{2}}\,\xi^{3/2}\,C_{ef}(\Delta t)\,H(\xi) \qquad (4\text{-}2)$$

where $C_{ef}(t)$ is defined by Schapery to be the "effective" compliance and is written as:

$$C_{ef}(t) \equiv \frac{3}{2}\,t^{-3/2} \int_0^t C_v(t - \rho)\,\sqrt{\rho}\,d\rho$$

with $\rho \equiv \tau - t_1$

and $$I_2 \equiv \int_0^1 \left(\frac{df}{d\eta}\right) \frac{d\eta}{\sqrt{\eta}}\,.$$

In order to see the behavior of the "effective" compliance, it is rewritten using a logarithmic time scale by letting

$$\rho_v = \frac{\rho}{t}$$

$$L = \log t$$

$$\ell = \log (1 - \rho_v)$$

$$\hat{C_v}(L) \equiv C_v(t)$$

to get

$$C_{ef}(t) = \frac{3}{2} (\ell n\ 10) \int_{\infty}^{0} C_v\ (L+\ell) \left\{ 10^{\ell} \left[1-10^{\ell}\right]^{1/2} \right\} d\ell$$

Schapery plotted the weighting function, $10^{\ell}(1-10^{\ell})^{1/2}$ designated w, against ℓ to show the narrow range for which w differs from zero, and he concluded that $C_{ef}(t)$ depends on only a small part of the total creep compliance curve. He also pointed out that w varies significantly only over a 1.2 decade range from (log t - 1.2) to (log t). Since there is very small curvature of the creep compliance curve over this 1.2 decade range, Schapery represented the creep compliance over this range by the power law:

$$C_v\ (t) = C_1\ t^n$$

He selected the exponent n, the log-log slope of the creep compliance, to be determined at the time, t = L - 0.48, since -0.48 is approximately the centroid of the weighting function, w. Conveniently, 0.48 = log 3 and by definition L = log t, L - 0.48 becomes log(t/3). So now, n is the

slope of a line drawn tangent to the log-log plot of $C_v(t)$ at t/3. The coefficient C_1 is simply the value of the compliance where the tangent line intercepts the log t = 0 axis.

The convolution integral,

$$\int_0^t C_v\,(t-\rho)\,\sqrt{\rho}\;\;d\rho,$$

in the effective compliance equation can now be evaluated by using the power law and treating n and C_1 as constants, with the following result:

$$C_{ef}(t) \cong \lambda_n\, C_1\, t^n$$

Making use of the power law again,

$$C_{ef}(t) \cong C_v(\lambda_n^{\,1/n}\, t)$$

where

$$\lambda_n \equiv \frac{3\sqrt{\pi}\;\;\Gamma(n+1)}{4(n+\frac{3}{2})\;\Gamma(n+\frac{3}{2})}$$

$\Gamma(n)$ is the Gamma function:

$$\Gamma(n) \equiv \int_0^\infty t^{n-1}\, e^{-t}\, dt$$

Now with the convolution integral evaluated, the approximate displacement equation (Eq. 4-2) is now written as:

$$v \cong - \frac{2\,\sigma_m\, I_2}{3\pi\,\sqrt{\alpha}}\ \xi^{3/2}\ C_v(\tilde{t})\ H(\xi)$$

where

$$\tilde{t} \equiv \lambda_n^{1/n}\ \frac{\xi}{\dot{a}}$$

These approximations were applied to the original equation (Eq. 4-1) which gives:

$$v \cong H(\xi)\ \frac{C_v(\tilde{t})}{2\pi} \int_0^{\alpha} \sigma_f(\xi')\ \left\{ 2\sqrt{\frac{\xi}{\xi'}} - \ell n \left| \frac{\sqrt{\xi'} + \sqrt{\xi}}{\sqrt{\xi'} - \sqrt{\xi}} \right| \right\} d\xi' \tag{4-3}$$

Now, the failure criterion that was listed as the third assumption will be applied. As was stated earlier, fracture energy, Γ, is the work done (force · displacement) on a material to increase the surface area of the material a unit area. This allows the fracture energy to be defined by the action of the failure stress, σ_f, on the material inside the failure zone:

$$\Gamma = \int_0^{v_m} \sigma_f\, dv$$

where

v_m = that amount of displacement which causes separation of the material.

Schapery rewrote this equation so that the viscoelastic displacement equation (Eq. 4-3) could be used to evaluate the fracture energy:

$$\Gamma = \int_0^{\alpha} \sigma_f \frac{\partial v}{d\xi} \, d\xi$$

To evaluate the above integral, Schapery defined an auxiliary function v_α,

$$v_\alpha \equiv \frac{C_v(\tilde{t}_\alpha)}{C_v(\tilde{t})} v$$

where

v = displacement in Eq. 4-3

$$\tilde{t}_\alpha \equiv \lambda_n^{1/n} \frac{\alpha}{\dot{a}}$$

Note that $\alpha/\dot{a}$ is the time it takes the crack tip to propagate the length of the failure zone, α. With the aid of the auxilary function, Γ can be divided into two parts by adding and subtracting v_α,

$$\Gamma = \Gamma_a + \Gamma_b$$

$$\Gamma_a \equiv \int_0^{\alpha} \sigma_f(\xi) \frac{\partial v_\alpha}{\partial \xi} \, d\xi$$

$$\Gamma_b \equiv \int_0^{\alpha} \sigma_f(\xi) \frac{\partial}{\partial \xi} (v - v_\alpha) \, d\xi$$

Schapery found that the integral Γ_b is very small compared to Γ_a, and therefore Γ_b can be ignored. By using the auxiliary function defined above along with Barenblatt's finite stress equation and ignoring Γ_b, the fracture energy is defined as:

$$\Gamma = \frac{C_v(\tilde{t}_\alpha)\ K_I^2}{8}$$

$$\text{or} \quad C_v(\tilde{t}_\alpha) = \frac{8\Gamma}{K_I^2} \tag{4-4}$$

$$\text{again} \quad \tilde{t}_\alpha \equiv \lambda_n^{1/n} \frac{\alpha}{\dot{a}}$$

$$\text{and} \quad \dot{a} \equiv \frac{da}{dt}$$

To solve Eq. (4-4) for the tip velocity, $\frac{da}{dt}$, the power law form of $C_v(t) = C_1 t^n$ is used:

$$C_v(\tilde{t}_\alpha) = C_1 \cdot \left(\tilde{t}_\alpha \right)^n$$

$$= C_1 \cdot \left(\frac{\lambda_n^{1/n}\ \alpha}{\dot{a}} \right)^n$$

Substituting $\frac{\pi}{2}\left(\frac{K_I}{\sigma_m\ I_1} \right)^2$ for α which was derived from the finite

stress equation gives:

$$C_v(\tilde{t}_\alpha) = C_1 \lambda_n \left[\frac{\pi}{2} \left(\frac{K_I}{\sigma_m I_1} \right)^2 \right]^n \left(\frac{da}{dt} \right)^{-n}$$

$$\frac{8\Gamma}{(K_I)^2} = C_1 \lambda_n \left[\frac{\pi}{2} \left(\frac{K_I}{\sigma_m I_1} \right)^2 \right]^n \left(\frac{da}{dt} \right)^{-n}$$

$$\left(\frac{da}{dt} \right)^n = \frac{(K_I)^2}{8\Gamma} C_1 \lambda_n \left[\frac{\pi}{2} \left(\frac{K_I}{\sigma_m I_1} \right)^2 \right]^n$$

Taking the n^{th} root and collecting terms gives:

$$\frac{da}{dt} = \frac{\pi}{2} \left(\frac{C_1}{8\Gamma} \right)^{1/n} \lambda_n^{1/n} \left[\frac{(K_I)^{2(1+1/n)}}{\sigma_m^2 I_1^2} \right]$$

Schapery rewrote this equation in the form of Paris and Erdogan's power law equation, $\frac{da}{dN} = AK^n$:

$$\frac{da}{dN} = \frac{\pi}{6\sigma_m^2 I_1^2} \left[\frac{(1-\nu^2) D_2}{2\Gamma} \right]^{1/m} \left[\int_0^{\Delta t} w(t)^{2(1+1/m)} \, dt \right]$$

$$\times \left(K_{I_{max}} \right)^{2(1+1/m)} \qquad (4\text{-}5)$$

where

$C_v(t) = 4(1 - \nu^2)\, D(t)$

$D(t) = D_0 + D_2\, t^m$

D_o is the initial compliance, m and D_2 are respectively the slope and the log t = 0 intercept of a line drawn tangent to a double log plot of $(D(t) - D_0)$ at time t/3; t is the time it takes for the crack tip to propagate the length of the failure zone, α.

Δt = the period of the cycle.

$w(t)$ = the wave shape of the stress-intensity factor.

$K_{I_{max}}$ = the amplitude of the oscillating stress-intensity factor.

Comparing Schapery's power law equation to that of Paris and Erdogan's :

$$A = \frac{\pi}{6\sigma_m^{\,2}\, I_1^{\,2}} \left(\frac{(1 - \nu^2)\, D_2}{2\,\Gamma} \right)^{1/m} \left(\int_0^{\Delta t} w(t)^{2(1+1/m)}\, dt \right)$$

and $n = 2(1 + 1/m)$.

CHAPTER V

STATE OF THE ART

Effect of Mix Variables on Fatigue and Cracking Resistance in Asphalt Concrete Pavements

In an effort to design an asphalt concrete mix that would exhibit a high resistance to cracking and a long fatigue life, many researchers have investigated those parameters in a mix highly resistant to cracking and fatigue. These mix parameters include aggregate characteristics, asphalt content and type, air void content, fibrous and polymeric additives, chemical treatments such as sulfur, and others. In this section only the first three mix parameters listed above will be discussed since this research did not include tests to study the performance of the other mix parameters.

There are conflicting views as to the influence of the aggregate type on the fatigue life of the asphalt mix. From controlled stress tests, Pell and Taylor (21) found that uncrushed gravel compared to crushed rock, for well graded aggregates, has little influence on the fatigue life of the mix. The same results were obtained from tests performed by Epps and Monismith (11) on dense graded asphalt mixes with various types of aggregates such as crushed granite, limestone, and river gravel. These tests showed that aggregate type has little influence on the fatigue life. However, experiments performed by Jimenez and Galloway (31) led to conclusions that the type of aggregate determines the amount of asphalt that can be placed in a mix. These test results showed that mixtures containing rough-textured aggregates

can hold more asphalt and have longer fatigue lives than mixes with smooth textured aggregates.

Results from investigations on the effects of aggregate gradation on fatigue life have led to the follwing views. Based on controlled stress tests performed by Epps and Monismith (11), Pell (14), and Bazin and Saunier (32), for the same asphalt contents, dense graded mixes have longer fatigue lives than the open graded mixes. Pell (13) and Kirk (33) performed controlled strain tests on mixes with various aggregate gradations. Kirk reported aggregate gradation has very little influence on the fatigue life, whereas Pell observed significant influence of gradation on fatigue life.

The effects of asphalt hardness on fatigue life of asphalt mixtures using controlled strain tests were observed by Epps and Monismith (11). They found that as the asphalt hardness is increased, the mixture stiffness increases which results in a lower fatigue life. Santucci and Schmidt (34), also using constant strain tests, reported that the softer the grade of asphalt, the better the fatigue resistance of the mix.

For controlled stress tests the opposite trends that were noted above between asphalt hardness and fatigue life were observed. Jimenez and Galloway (31) found from their controlled stress tests that asphalt mixes made with soft asphalts have a lower endurance under repetitive loads than mixes with harder asphalts. Similar results were obtained from tests conducted by Vallerga, Finn, and Hicks (35) which showed that mixtures with higher stiffnesses related to harder asphalts used in the mixes gave longer fatigue lives than mixes with low stiffnesses.

As for the concern with the effects of air voids in a mix, Pell and Taylor (12) reported that the fatigue life and stiffness of an asphalt concrete mix are reduced when the air void content is increased.

Other researchers such as Saraf (36) and Majidzadeh et al. (37) have taken the route of fracture mechanics to explain the sensitivity of the above various mix parameters to evaluate and explain the fatigue life of asphalt concrete mixes. Particularly they investigated the effects that the different mix parameters have on the material constants A and n used in Paris and Erdogan's power law, $\frac{da}{dN} = AK^n$. In order to obtain the relationship between the rate of crack growth ($\frac{da}{dN}$) and the stress-intensity factor (K), Saraf and Majidzadeh et al. used basically the following procedure:

1. From fatigue experiments, plot a graph of crack length versus the number of load applications (a vs. N) and obtain an exponential form, $a = a_0 e^{(DN)^n}$ where a_0, D, and N are regression constants, and N is the number of load applications.
2. With the aid of a boundary collocation computer program or a finite element program, develop a relationship between crack lengths and the corresponding stress-intensity factors.
3. Obtain the $\frac{da}{dN}$ - K relationship. First differentiate with respect to N the exponential equation that was derived in Step 1. For a specific N, $\frac{da}{dN}$ is calculated. Also, a (crack length) is found from the a-N exponential equation for that particular N. Using this a, K is found using the relationship derived in Step 2. Plot the calculated $\frac{da}{dN}$ and its corresponding K on log-log graph paper.

4. Finally, determine the material constants A and n from the plot of log $\frac{da}{dN}$ versus log K. A will simply be the "y-intercept" and n is the slope of the curve.

From the procedure listed above Saraf found the parameter A to be affected by the viscosity of the asphalt binder used in the mix, a decrease in viscosity gave an increase in A. Increasing A leads to a reduction in the fatigue life for controlled stress tests. Majidzadeh et. al. found that the value for A for open graded slag aggregate mixes was higher than the A value from the design mixes with a dense gradation. Since these were also controlled stress tests, the fatigue life of the open graded mix was shorter than that of the dense graded mix. They also investigated the influence of the asphalt viscosity on A.

They reported that A changes very little for asphalts with penetration grades 60-70 (AC-40) and 85-100 (AC-20), but at higher penetrations of 120-150 (AC-10), softer asphalts, the A values are higher which resulted in a lower fatigue life than those exhibited by the stiffer asphalts.

Majidzadeh et. al. did not investigate to see what effects the mix variables would have on the exponent n. Instead, after the fatigue data were obtained they found by statistical analysis of the data that the best fit, using Paris and Erdogan's power law, with a high coefficient of correlation (r^2) was obtained using n = 1.0 and in some cases n = 2.0. Therefore, they assumed that the mix variables affect A and not n. They also investigated three different regression models for describing the relationship between $\frac{da}{dN}$ and K.

The four term model,

$$\frac{da}{dN} = A_1 K_1 + A_2 K_1^2 + A_3 K_1^4 + A_4 K_1^6$$

had the disadvantage in that the four constants are hard to relate to the mechanical properties of asphalt concrete. However, they found this model to give the best fit to the data out of all the models they considered.

For the three term model, they attempted to use

$$\frac{da}{dN} = A_1 K_1^2 + A_2 K_1^4 + A_3 K_1^6$$

However, they found this to be inconsistent with those data and dropped this equation from their investigation.

The second term model,

$$\frac{da}{dN} = A_1 K_1^2 + A_2 K_1^4$$

was found to be very consistent with the data, but it was still hard to relate the two constants, A_1 and A_2, to the material properties of the asphalt mix.

Majidzadeh et al. then tried to relate Schapery's crack growth theory, Eq. (4-5), to their own experimental data. They reported that the constants A and n determined from Schapery's model did not match the experimentally determined A and n values from their fatigue tests. In their material characterization tests, they performed compressive creep tests and used these results (compressive creep compliance) to calculate the A and n values described by Schapery. However, Schapery

in deriving Eq. (4-5) used the creep compliance found from uniaxial tension creep tests since these tests model the displacements that occur in Mode I type crack extension. This discrepancy may explain the conclusion reached by Majidzadeh et al.

In another study, Majidzadeh (38) investigated the use of Petromat fabric in an asphalt mix to increase its fatigue life. Experimental tests were performed on asphalt beams resting on an elastic support (gum rubber) to simulate the road structure. Asphalt beams with and without fabric were subjected to fatigue testing using dynamic loads of 140, 170, and 200 pounds. The fabric was placed in three different locations, upper third, mid depth, and lower third. For loads of 170 and 200 pounds the position of the fabric had very little effect on the fatigue lives. In other words the fatigue life of beams with fabric in the lower third position was about the same as those beams with fabric in the upper third position. But for the 140-pound load, the effects of fabric position were readily recognized when compared to the fatigue life of beams with no fabric:

1. 400% increase in fatigue life when the fabric was placed in the upper third position,
2. 800% increase when placed at mid-depth, and
3. 1100% to 1300% increase when fabric was placed in the lower third position.

Asphalt beam specimens with two layers of Petromat fabric and a tack coat of asphalt between them were also tested. Test results showed that for loads of 140 pounds the double layer of fabric increased the fatigue life three to four times over the life of asphalt samples with

one layer of fabric.

Further tests were conducted at various temperatures which showed that the fabric's effectiveness increases significantly as the test temperature decreases due to the increase in stiffness of the asphalt mixture and fabric.

Field Performance of Asphalt Overlays with Fabric

The Texas State Department of Highways and Public Transportation (SDHPT) have recently evaluated several different overlay designs that were made to reduce pavement cracking in District 6. Four of these overlay designs were compared by Huffman (39), as follows:

1. Section 1 - the control section which is the usual district design of a one-course surface treatment underseal with two-inch hot mix asphalt concrete (HMAC) followed by a one-inch wearing course.
2. Section 2 consists of HMAC followed by a sealing membrane of Petromat fabric with a one-course surface treatment, and then a one-inch HMAC wearing course.
3. Section 3 is a one-course surface treatment over the existing pavement with a 3/4-inch overlay of plant mix seal.
4. For Section 4 an underseal of Petromat fabric and one course surface treatment overlaid with a 3/4-inch plant mix seal.

The above test sections were part of an actual highway pavement on I-20 and were subjected to a severe winter, hot summer, and at the time of their report, back into winter again. They observed that Sections 1 and 2 have out performed Sections 3 and 4. For Sections 3 and 4 there

is a difference in the amount of cracking between the sections with and without the fabric underseal; sections with the fabric underseal have fewer cracks than the sections without it. Of the four sections tested, Section 1, the control section with no fabric, showed to be the most resistant to cracking.

Donnelly et al. (2) reported on a full scale test with an overlay using Petromat fabric on an Interstate between Eagle and Dowd, Colorado. Prior to the application of the fabric and overlay, the existing pavement's cracks were filled with a cationic asphalt emulsion. After five years since application no cracks have reflected through the fabric.

Test installations of overlays with Petromat on four locations in California show that they are performing better than the adjacent control sections of equal overlay thicknesses without the fabric as reported by Bushey (40). Observations from these tests show that for overlays with fabric, better results are obtained when placed over alligator type cracking instead of over transverse and longitudinal cracks. Also it is more effective in retarding fatigue cracking due to traffic loads than it is in inhibiting thermal cracking. Also the Petromat overlays used in moderate or warm climates appear to perform better than those in cold environments.

In a report by the Federal Highway Administration (FHWA) (1) about reducing reflection cracking in asphalt overlays, it is stated that the Florida Department of Highways observed from cores taken over the cracks in the Petromat overlay that these cracks were not reflected but occurred in the top one-inch course above the fabric. Also in this FHWA report, it was reported that in Wyoming, Petromat helped to reduce reflection

cracking for about two years. About a year's time after the Petromat had been placed, tensile stresses that have built up due to temperature changes resulted in some cracking but less than the cracking in the control section with no fabric. For the next year the low temperatures encountered during January added additional tensile stresses which allowed the Petromat section to catch up to the control section as to the number of cracks. It was also reported that in Wyoming increasing the thickness of the overlay has more influence on reducing reflection cracking than does incorporating Petromat in the overlay. These observations were also made by another field test reported by Gulden (41) where a fabric was placed in three different overlay thicknesses of two, four, and six inches on I-85, 30 miles north of Atlanta, Georgia.

After fifteen months of service the two-inch thick overlays were cracked, but the cracks seem tighter and smaller than the test section with no fabric of the same thickness. The four- and six-inch thick overlays with fabric showed no cracking after the fifteen-month service period.

Summary

Experimental tests performed by Majidazadeh et al. on asphalt concrete beams with fabric tested at various temperatures showed the fatigue life of these beams increased with decreasing temperature. Contrary to the results of the field tests performed in California, Wyoming, and the field test reported by Gulden, these lab experiments showed that overlays with fabrics exhibit a shorter fatigue life due to thermal stresses than the overlays that mainly are subjected to

traffic loads.

Another point that needs to be high-lighted is the difference in test results obtained by performing controlled stress tests as compared to those produced from controlled strain tests. The reason for performing controlled stress tests is to model traffic loads and the reason for conducting controlled strain tests is to model the displacement in pavements. Controlled stress tests usually result in shorter fatigue lives. Neither of these types of fatigue tests directly addresses the problem of reflection cracking, as does the series of tests to be reported subsequently.

CHAPTER VI

MATERIALS AND APPARATUS

Asphalt Concrete Overlay Test Samples

Pertinent information on the materials used in making the test samples and the sample sizes are presented in Tables 1 and 2.

As can be seen from Table 1 three fabrics were tested to see how well they help in resisting fatigue cracking. These fabrics are:

1. a fabric material composed of two fibers: polypropylene and the other is a polypropylene fiber covered with a nylon sheath,
2. a nonwoven polypropylene fabric, and
3. a woven polypropylene fabric.

Asphalt beam control samples with no fabric were made with the same asphalt content, gradation, and aggregate type as those beams with the above fabrics embedded in them. This was done so that the fatigue lives of beams with and without fabric could be compared and the effects of the fabric would then be apparent.

The "overlay samples" in Table 2 were used to determine the effects of thickness and asphalt content on the fatigue life. Also from these test results, the stress-intensity factors determined experimentally are compared to the stress-intensity factors calculated by the computer program developed by Chang et al. (42).

Table 2 also gives results of the tests performed to measure the effects of "hard" and "soft" asphalts with "high" and "low" asphalt contents on open-graded, dense-graded, and hot sand mix overlay materials.

Table 1. Constituents of Fabric Test Samples and the Test Results.

Test Number	u Crack Opening (Inches)	Number of Samples Tested	Samples (Inches)	N_f Cycles to Failure (Average)	Gradation and Aggregate Type	Asphalt Type and Content (By Wt. of Agg.)	Fabric Type
1	0.055	5	3 x 3 x 15	2155	Dense Graded Based On ASTM D-1663 -5A Standard Using River Gravel	AC - 10 3.8%	1
	0.065	5		975			
	0.075	5		500			
2	0.065	4		765			2
3	0.055	4		1241			3
4	0.055	5		750			No Fabric
	0.065	3		115			
	0.075	4		42			

Table 2. Constituents of Test Samples and the Test Results.

TEST NUMBER	u CRACK OPENING (INCHES)	NUMBER OF SAMPLES TESTED	SIZE OF SAMPLES (INCHES)	N_f CYCLES TO FAILURE (AVERAGE)	GRADATION AND AGGREGATE TYPE	ASPHALT TYPE AND CONTENT (BY WT. OF AGG.)	EXPERIMENTAL VALUES		SHAPERY'S THEORY		E(t) - PSI BACK CALCULATED FROM FINITE ELEM. PROGRAM (AVERAGE)	t (SEC)
							A	n	A	n		
5	0.030	2	1 x 3 x 15	5	DENSE GRADED BASED ON ASTM D-1663 -5A STANDARD USING LIMESTONE AGGREGATE	AC - 10 LOW - 3.5%	0.122	0.193	2.88×10^{-7}	4.86	2863.	7×10^{-4}
6	0.030	2	2 x 3 x 15	285			1.49×10^{-6}	2.82	6.42×10^{-8}	4.86		
7	0.030	2	3 x 3 x 15	425			1.20×10^{-6}	2.35	6.42×10^{-8}	4.86		
8	0.030	2	1 x 3 x 15	10		AC - 10 HIGH - 5.5%	0.0291	0.424	1.07×10^{-7}	4.86	1889.	1.4×10^{-3}
9	0.030	2	2 x 3 x 15	2100			2.78×10^{-8}	4.08	5.01×10^{-9}	4.86		
10	0.030	2	3 x 3 x 15	VERY HIGH			1.40×10^{-8}	4.29	5.01×10^{-9}	4.86		
11	0.045	2	3 x 3 x 15	840		AC - 20 MED - 4.5%	1.53×10^{-8}	3.84	7.57×10^{-12}	5.75	3056.	2×10^{-3}
12	0.045	2	3 x 3 x 15	1330		AC - 5 MED - 4.5%	2.14×10^{-8}	4.63	2.31×10^{-8}	4.99	1509.	1×10^{-3}
13	0.045	2	3 x 3 x 15	235	HOT SAND MIX 65% - CONCRETE SAND 30% - FIELD SAND 5 % - FILLER	AC - 20 MED - 5 %	8.46×10^{-6}	2.11	2.68×10^{-10}	5.75	3613.	1.3×10^{-3}
14	0.045	2	3 x 3 x 15	700		AC - 5 MED - 3.5%	2.73×10^{-6}	4.32	3.63×10^{-6}	4.99	832.	2.7×10^{-3}
15	0.045	2	3 x 3 x 15	75	OPEN GRADED LIMESTONE 90% - 3/4" AND 1/2" AGGREGATE 10% - #30 SIEVE SIZE	AC - 20 LOW - 2 %	----	--	----	--	-----	----
16	0.045	2	3 x 3 x 15	852		AC - 20 HIGH - 4 %	----	--	----	--	-----	----
17	0.045	2	3 x 3 x 15	230		AC - 5 LOW - 2 %	----	--	----	--	-----	----
18	0.045	2	3 x 3 x 15	1275		AC - 5 HIGH - 3 %	----	--	----	--	-----	----

To make the asphalt overlay test beams a "Soil Test" model CN-425 kneading compactor machine was used. The beams were compacted in three one-inch lifts at a temperature of 250°F using a constant pressure of 175 psi on a two-by-three inch tamping foot. For the samples with a fabric, the fabric was first saturated with asphalt then applied to the sample after the first one-inch lift was compacted and then the next two one-inch lifts were applied.

For the first overlay sample compacted from each group of samples made with identical asphalt contents, asphalt binder, gradation, etc., the density of each of the three lifts was determined gravimetrically in air and water. If the samples from each lift were not equal in density, the number of tamps per layer, by the kneading compactor, was changed to achieve uniform density.

Overlay Tester

The overlay tester is a fatigue testing machine designed to model displacements caused by thermal stresses in asphalt pavements resulting from cyclic changes in the ambient temperature.

There are two versions of the overlay tester. The original version used a mechanical linkage system driven by an electric motor through a gear box so that various speeds could be used to crack the asphalt overlay beam samples. The overlay samples were epoxied to a split plate making sure that the sample was centered over the split, and then these were bolted down to the two platens of the overlay tester as shown in Figure 8. One platen is fixed, the other is connected to the linkage which is constructed so that the circular motion from the gear box is

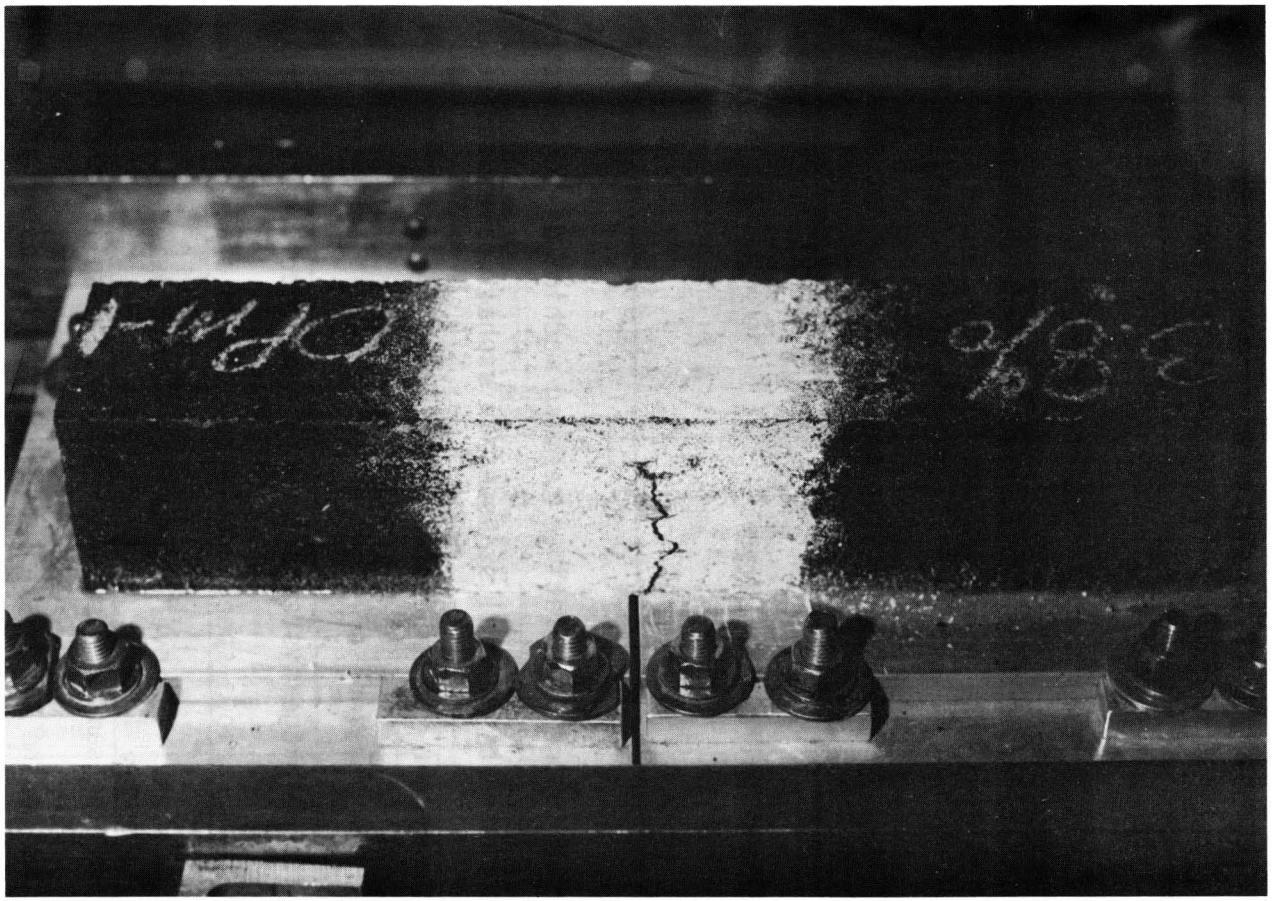

Figure 8. Overlay Sample Epoxied to Plates and Bolted to Overlay-Tester.

transformed into a linear oscillating motion which causes the platen to move back and forth horizontally. The maximum crack opening, the distance between the two platens, could be set for any amount between 0.0 and 0.10 inch.

A strip chart recorder was used to record the load and crack opening which were measured by a load cell and LVDT (linear variable differential transformer) respectively. The crack height was measured on both sides of the overlay samples using a pair of vernier calipers.

Only the overlay samples with fabric embedded in them were fatigue tested on the original overlay tester. After analyzing the data from these tests it was found that the crack opening varied through out the test for each sample; in other words these tests were not controlled strain tests. To correct this problem the overlay tester was modified by substituting a hydraulic servo-control mechanism for the mechanical linkage, gear box, and electric motor. This is the second version of the overlay tester and a picture of it is shown in Figure 9. Along with this change over, the load and crack openings were then recorded on a x-y plotter, see Figure 10, instead of the strip chart recorder. Crack height measurements were still observed and measured visually using a pair of vernier calipers. Those overlay samples listed in Table 2 (p. 50) were tested on this second version of the overlay tester.

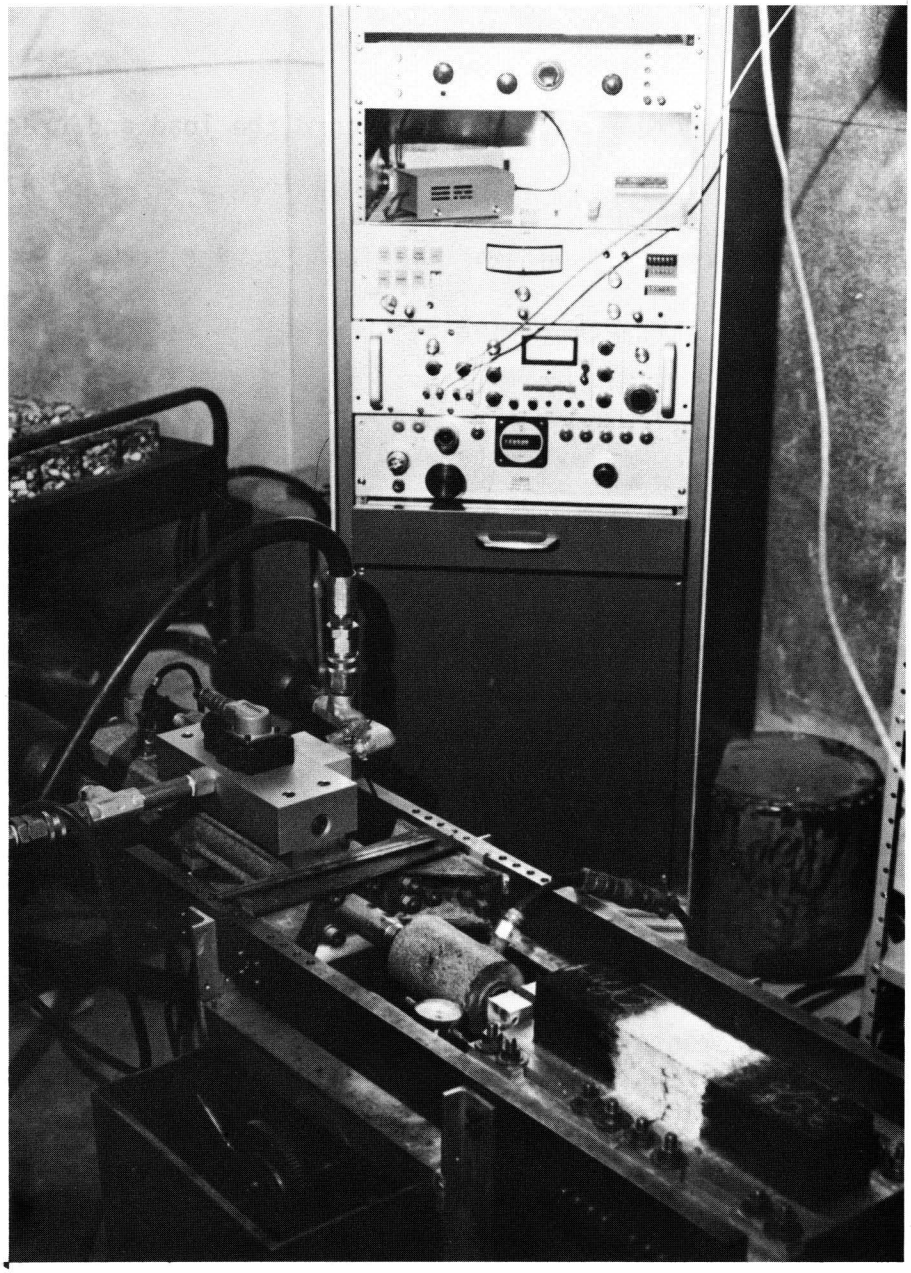

Figure 9. Second Version of the Overlay-Tester.

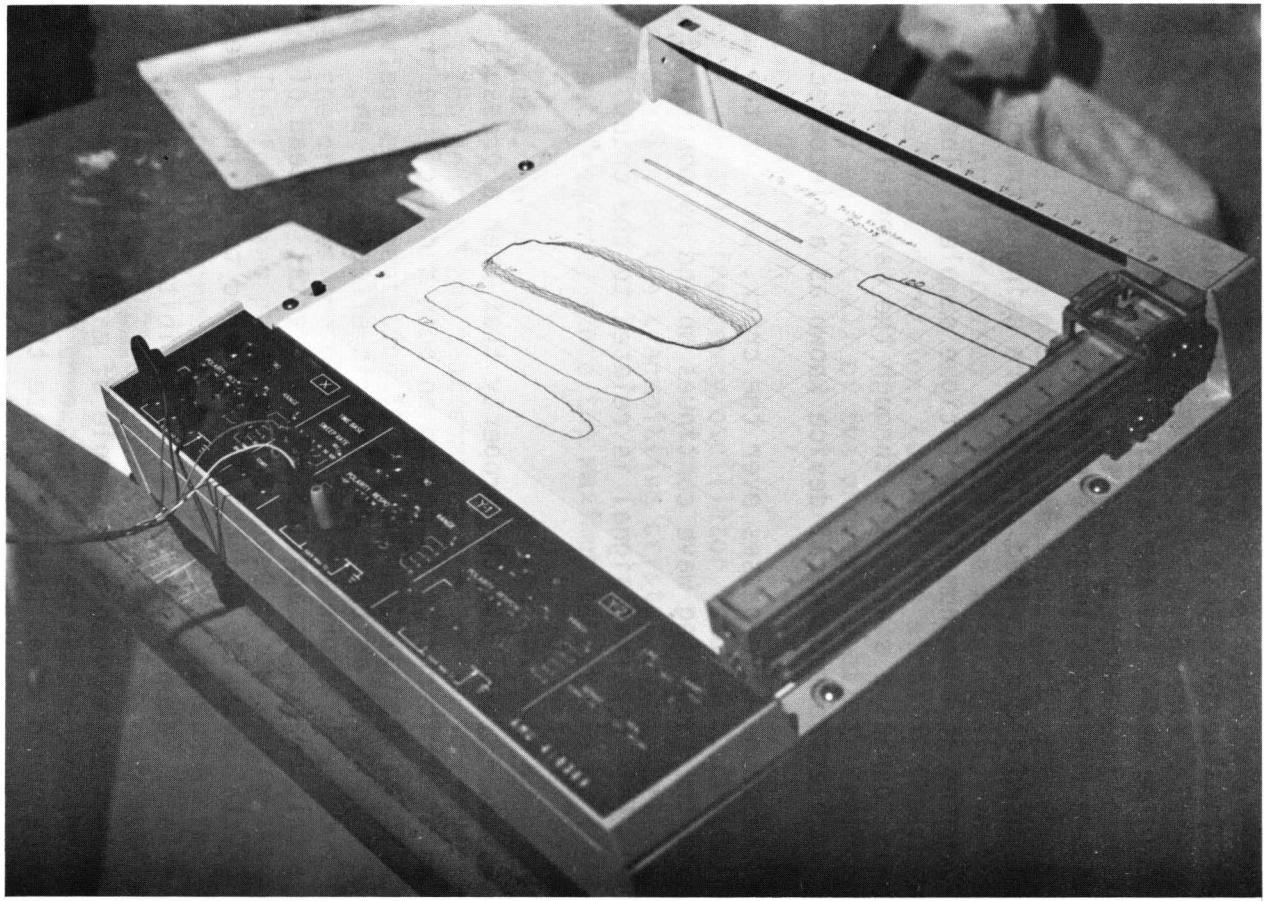

Figure 10. X-Y Plotter Used in Recording Load-Deformation Data.

Measurement of Crack Lengths by Ultrasonic Techniques

As mentioned before the crack lengths were measured visually with a pair of vernier calipers, and to use these calipers accurately the location of the crack tip had to be known but the crack tip was often hard to locate. To alleviate this problem so that accurate crack length measurements could be made, the application of ultrasonics was attempted in order to measure the crack length electronically.

Ho (43) has used and described a procedure using ultrasonics to measure crack lengths in aluminum alloy fatigue samples. The basic procedure used is to pass a sound wave through the material with a crack by using an electro-mechanical device known as a piezoelectric crystal. When the sound wave passes over the crack, part of the wave is attenuated and the remaining wave continues on and is monitored by another crystal. This received signal is related to the crack length determined from calibration tests.

A piezoelectric crystal has the property that when a pressure is applied to it an electric charge is set up on both sides of the crystal and this property is known as the piezoelectric effect. If an oscillating electric charge is applied to the crystal instead of a pressure, the crystal vibrates and this is referred to as the reverse piezoelectric effect. When a crystal which exhibits the reverse piezoelectric effect is mounted on a sample of material, the crystal's vibrations produce sound waves that propagate through the material. These sound waves cause particle movement which results in a force that impinges on the other piezoelectric crystal mounted at the other end of the material sample. This crystal then develops an electric charge

due to the force, and the amount of this charge is read on a voltmeter.

The laboratory setup used to measure the crack lengths in the overlay samples ultrasonically is shown schematically in Figure 11. The crystals are disc-shaped with a two-inch diameter and are made of a ceramic material. These crystals are not epoxied to the asphalt sample, but are encased in a brass housing and this housing is epoxied to the sample for acoustic coupling; a cross sectional view is shown in Figure 12, and a photograph of these parts are shown in Figure 13.

The cap is recessed so that the crystal will be free to vibrate in the vertical direction; however the sides of the crystal are restrained so that all of the energy vibration is directed in the vertical direction.

A variable frequency oscillator is used to control the frequency of vibration of the transmitting crystal. The crystal is operated at resonant frequency since the maximum energy can be transmitted at resonance.

The ends of the test samples are cut at 45° angles since from previous experimentation it was found that best results are obtained when the crystals are placed at these angles, as shown in Figure 14.

The following procedure was used to calibrate the voltage readings of the receiving crystal to the crack lengths. At the start of the calibration test, the transmitting crystal is vibrated at resonant frequency and does so throughout the test. A voltage reading is taken on a sample without a crack, and this voltage reading corresponds to zero crack length. After this a saw cut is made in the sample. For testing purposes the "crack" is a cut made in the sample (see Figure 14)

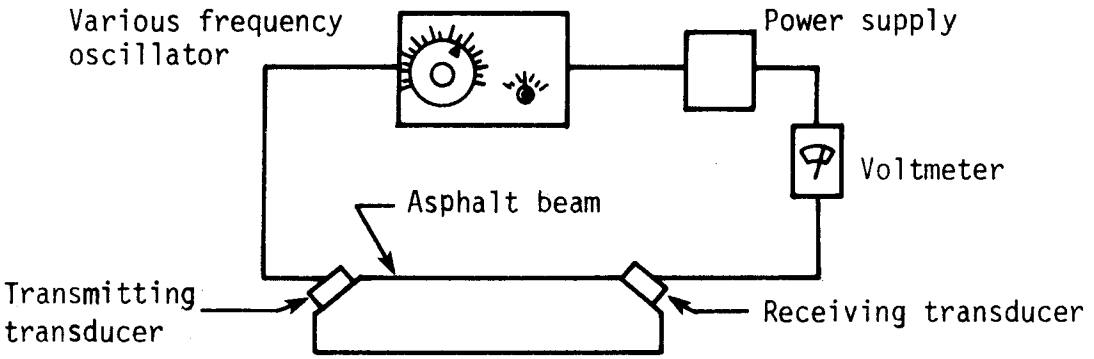

Figure 11. Schematic of the Ultrasonic Crack Length Measurement Apparatus.

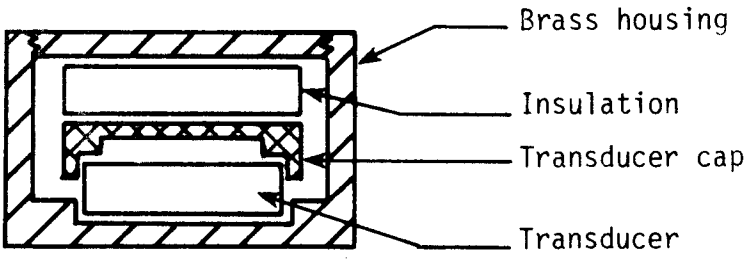

Figure 12. Cross-Section of Ultrasonic Transducers.

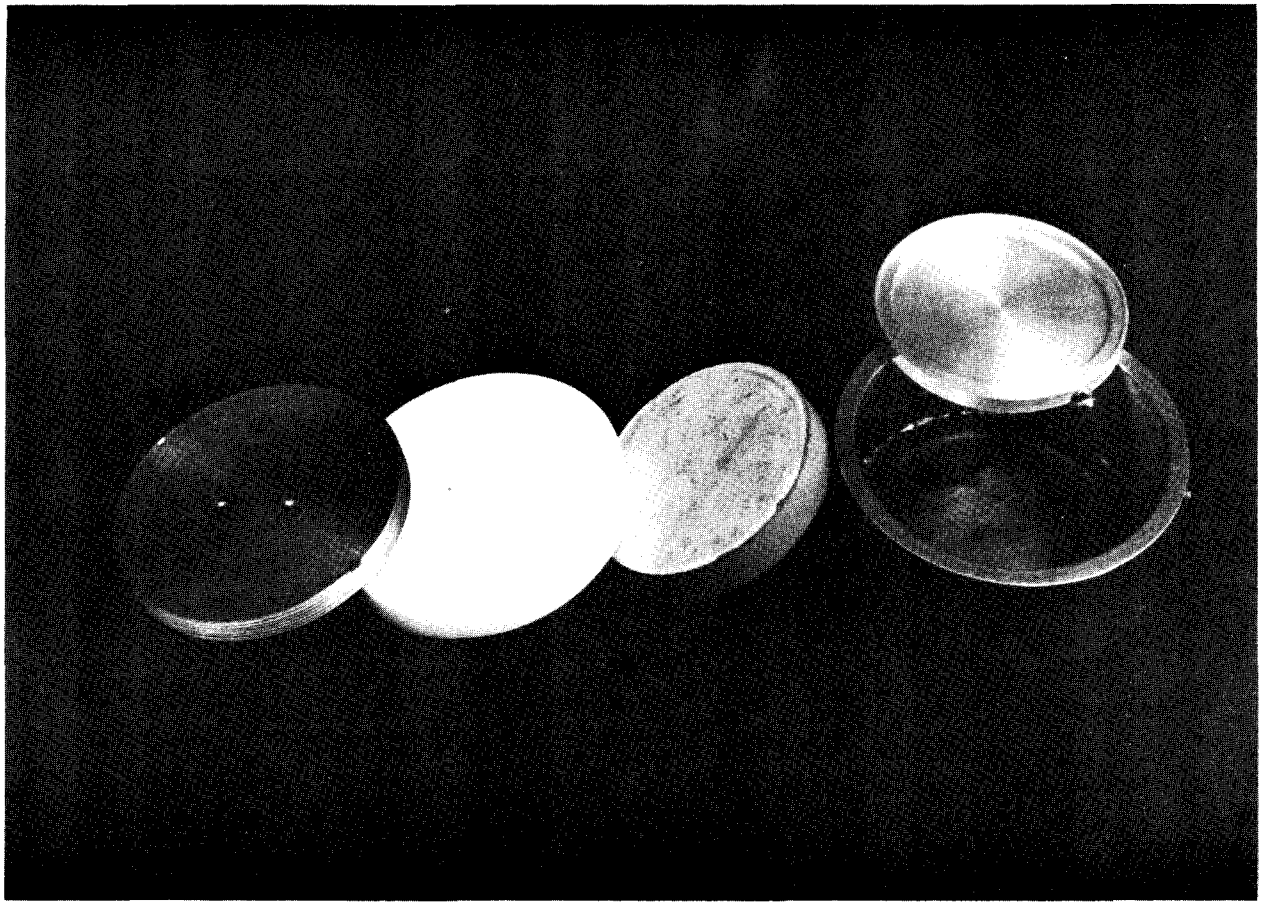

Figure 13. Photograph of Ultrasonic Transducers Taken Apart.

Figure 14. Ultrasonic Transducers Epoxied to Overlay Sample.

by a masonry diamond saw blade since the length of a saw cut can be measured more accurately than an actual crack using a pair of vernier calipers. Another voltage reading is taken which corresponds to the depth of the saw cut measured by the calipers. This is repeated several times until the saw cut is nearly through the sample.

Three asphalt overlay beam samples were tested using the above procedure to compare repeatability of the voltage readings. The voltage readings of the three samples were all normalized by dividing them by the voltage reading taken of the sample without a saw cut. To construct the calibration curve shown in Figure 15, the normalized voltage readings were plotted against their corresponding crack lengths, measured by the calipers.

This calibration curve was then checked by performing a fatigue test on a sample using the overlay tester. The crack lengths determined by ultrasonics were compared to the measurements made visually of the crack with the calipers. Crack lengths found from using the calibration curve did not match the visual measurements and this discrepancy was large; the crack lengths determined from the ultrasonics calibration curve were much smaller than what was visually observed.

The discrepancy might be explained by the method used to construct the calibration curve. Recall that a saw cut was used instead of an actual crack to find the relationship between voltage and crack length. An actual crack forms from forces and displacements applied to the sample and these affect the sound waves propagating through the material by attenuating the waves. This attenuation along with the attenuation caused by the crack itself results in a received voltage output much

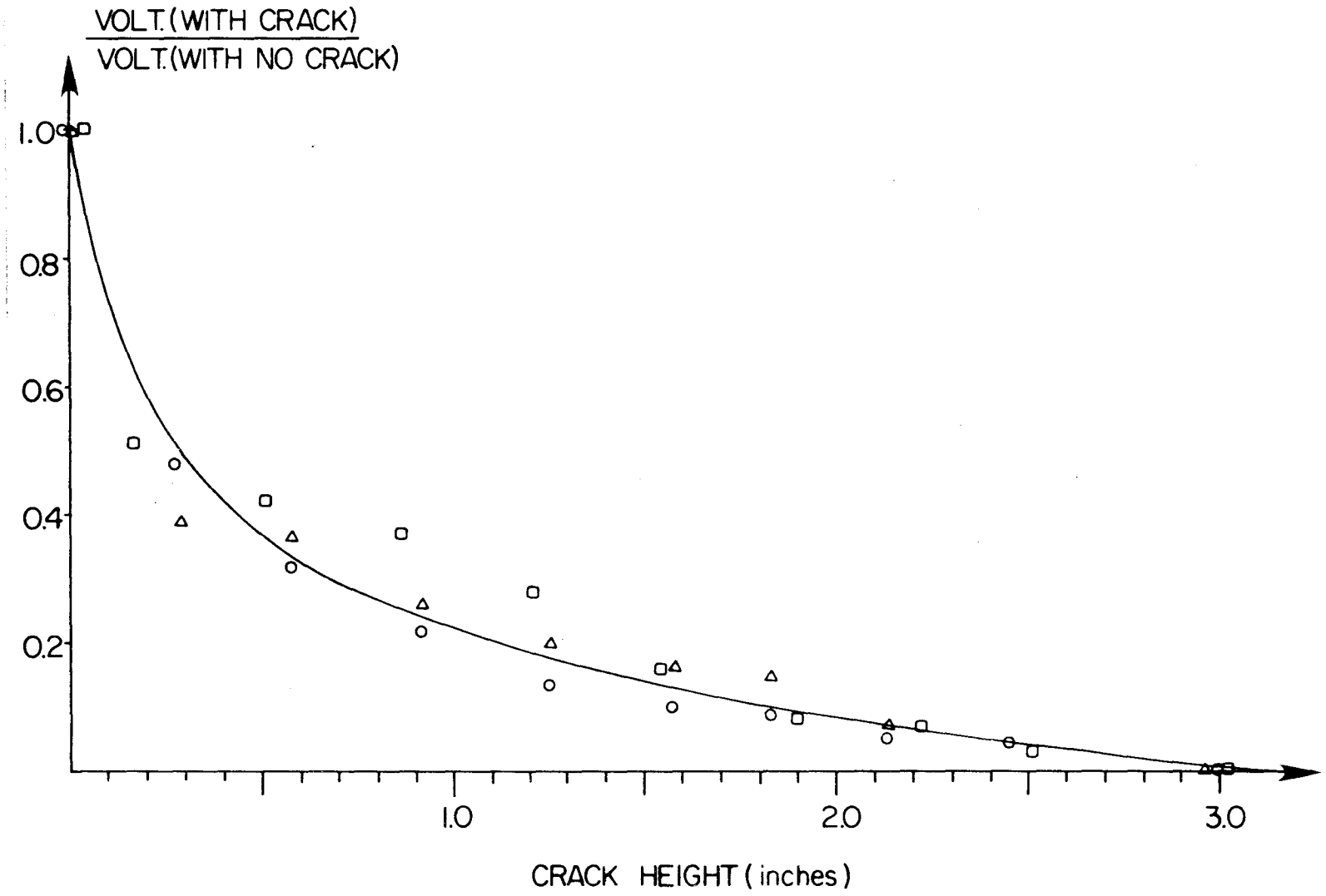

Figure 15. Ultrasonic Calibration Curve-Normalized Voltage Versus Crack Height.

smaller than that voltage output for a saw cut of the same size as that of the crack in the fatigue sample. The small voltage reading used to determine the crack length from the calibration curve results in a crack length smaller than what it actually is.

A calibration curve should therefore be constructed using the loads and displacements causing crack growth and not a saw cut. To record accurate crack lengths for construction of a calibration curve, pictures should be taken of the crack whenever voltage readings are recorded. This may resolve the difference between ultrasonic crack length measurements and those measured visually. If this problem can be resolved then all of the measurements taken from the overlay tester are in the form of voltage output which will then allow complete data acquisition to be done by a micro-processor.

Duomorph

The duomorph is a device used to measure the time dependent modulus, E(t), of the viscoelastic materials such as asphalt. Details of the duomorph apparatus have been presented by Boggess and Noel (44) and others (45, 46), so only a brief and basic description of the apparatus will be given here.

The duomorph consists of two piezoelectric crystals, about the size and shape of a coin, epoxied together in such a way that when excited electrically one crystal will contract and the other will expand to form a spherical dish shape in one direction. When the polarity of the excitation is reversed the bending forms the same shape but in the opposite direction. These crystals are completely embedded

into a material for which the modulus is to be determined, and how much these crystals bend in a material is indicative of the material's modulus.

Strain gages are used to monitor the amount of bending, and a hysteresis plot of excitation versus bending in the shape of an ellipse is produced on an oscilloscope. The shape of the ellipse is an indication of the viscoelastic properties of the material and is recorded by simply taking a picture of it at various frequencies and excitation voltages so that a complete characterization of the material can be made. Figure 16 shows a schematic of the duomorph apparatus, and Figure 17 shows an ellipse that would be viewed on an oscilloscope along with the dimensions required to determine the modulus.

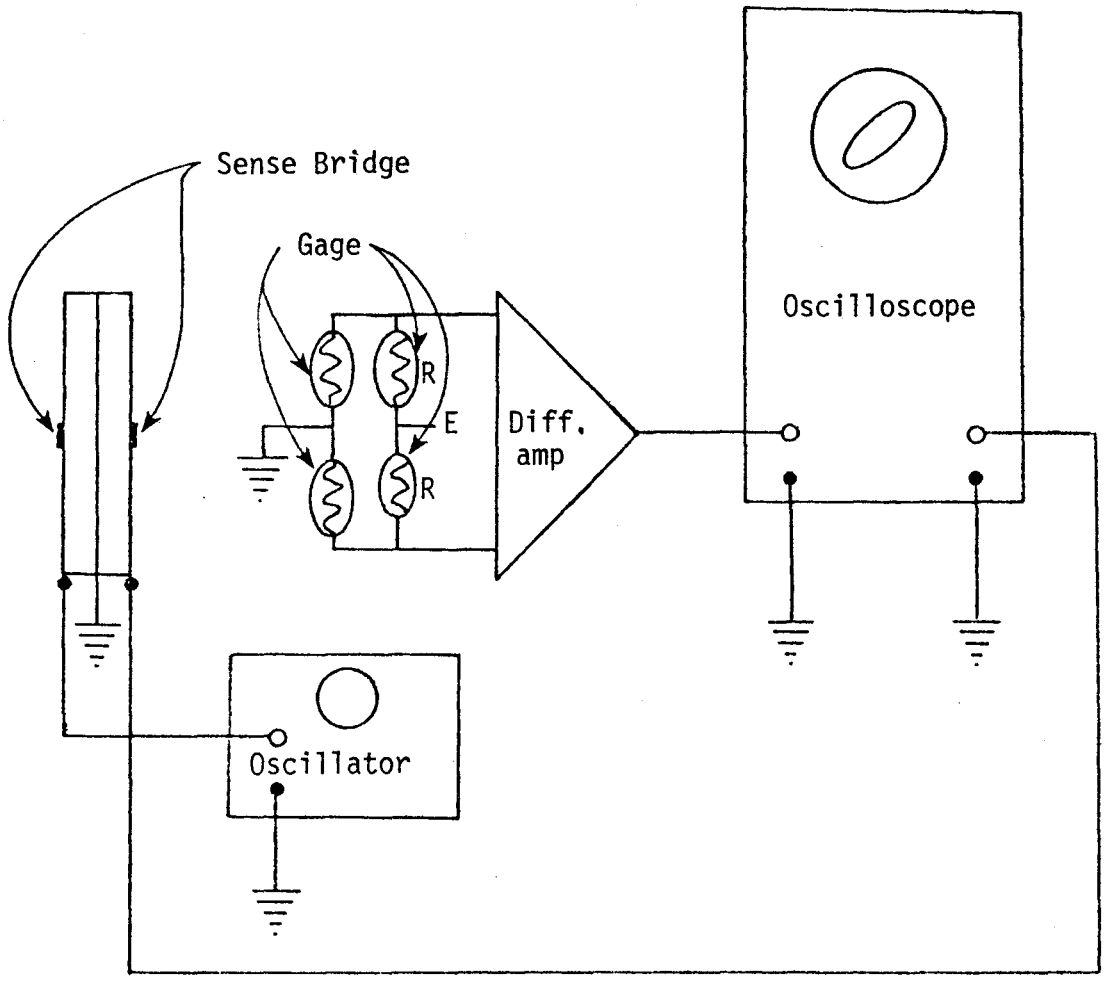

Figure 16. Schematic of duomorph apparatus.

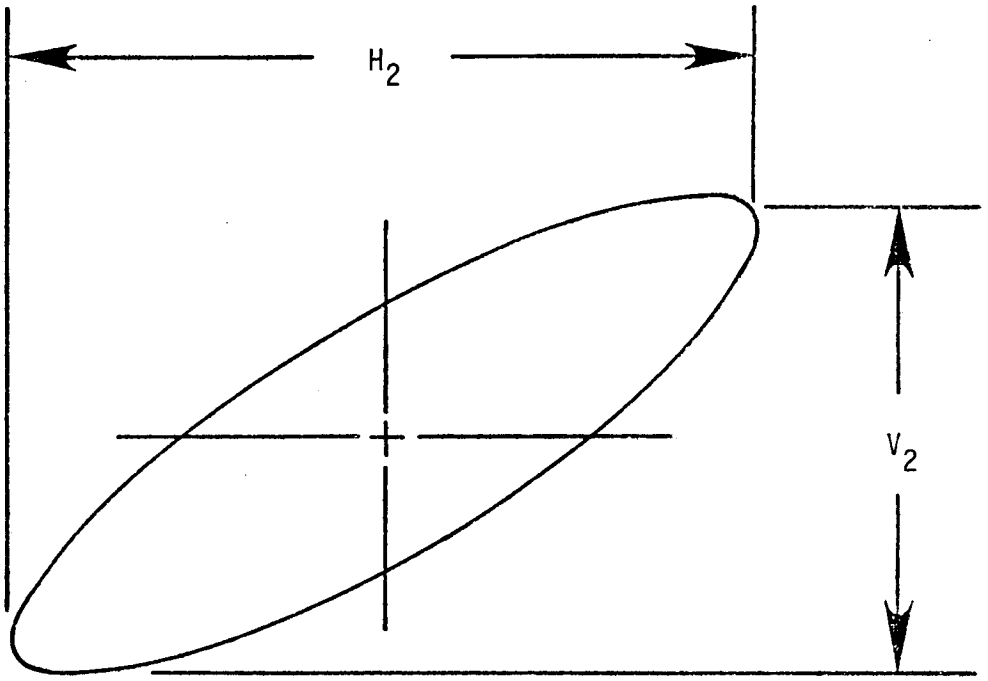

Figure 17. Duomorph Output as Viewed on an Oscilloscope.

CHAPTER VII

PROCEDURE

Material Characterization Using the Duomorph

The method used for reducing the duomorph output to calculate the tensile relaxation modulus, E'(t), relies on the results of an analysis done by Schapery (46). The modulus is found by using the following equation:

$$E' = \frac{M' E_c t^3}{12(1-\nu^2)\, r^3}$$

where

E' = tensile relaxation modulus

E_c = modulus of crystal; for PZT-4 crystal material use 9×10^6 psi, and for PZT-5 material use 12×10^6 psi

t = thickness of duomorph crystal

r = radius of duomorph crystal

ν = Poisson's ratio of the crystal which is 0.33

M' = the value read from Figure 18, entering in with $\frac{V_2 H_A}{H_2 V_A}$ where V_A and H_A are taken from the duomorph output (ellipse) when the crystal was excited in air.

Three different size crystals were used to obtain the moduli at various temperatures as shown in Figure 19. Crystal 1 was used for temperatures ranging from 70°F to 80°F, Crystal 2 for 50° to 70°F and

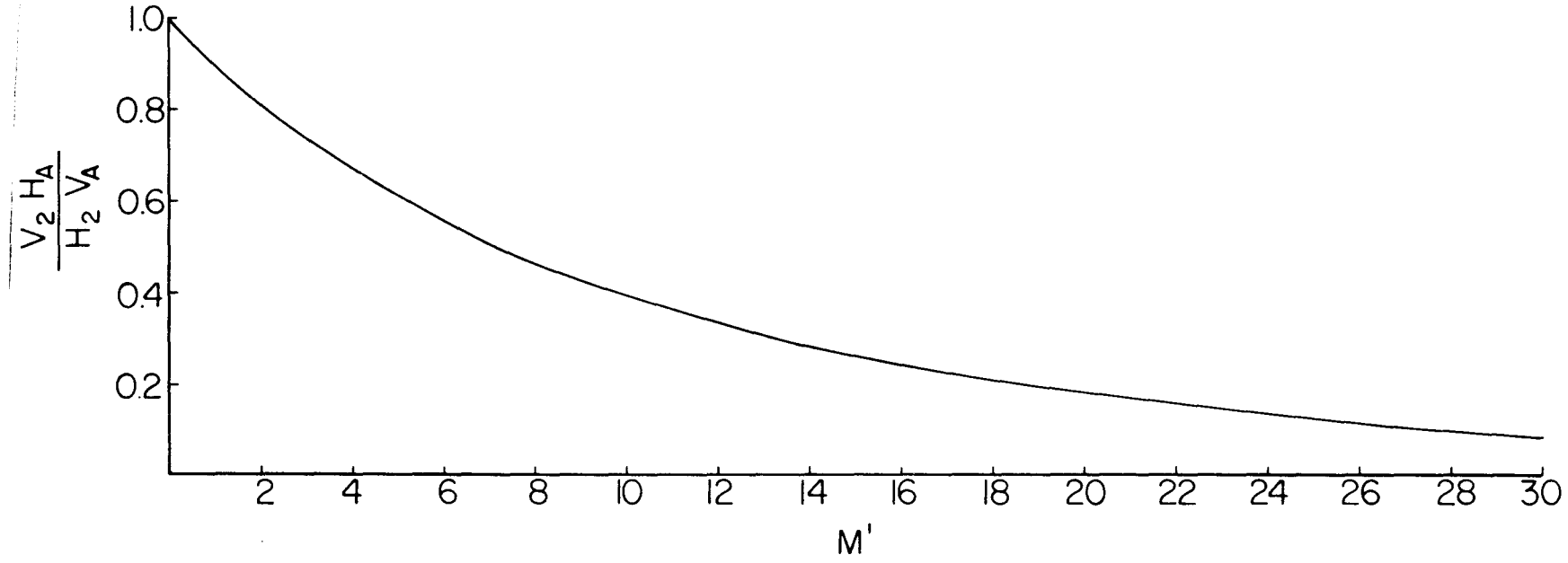

Figure 18. Duomorph Data Reduction Curve.

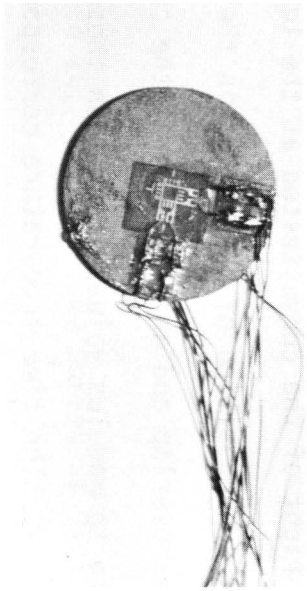

Crystal 1
0.750" O.D. x 0.160" Thick

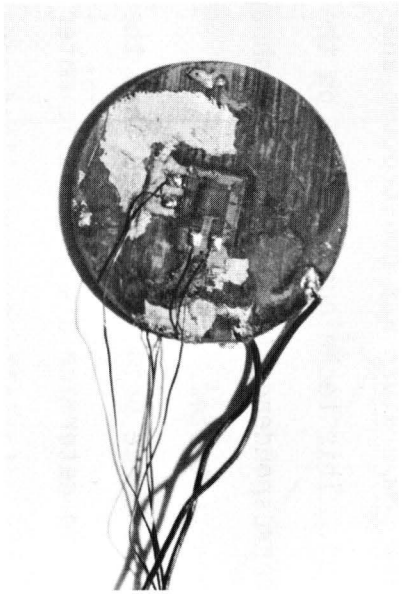

Crystal 2
1.00" O.D. x 0.050" Thick

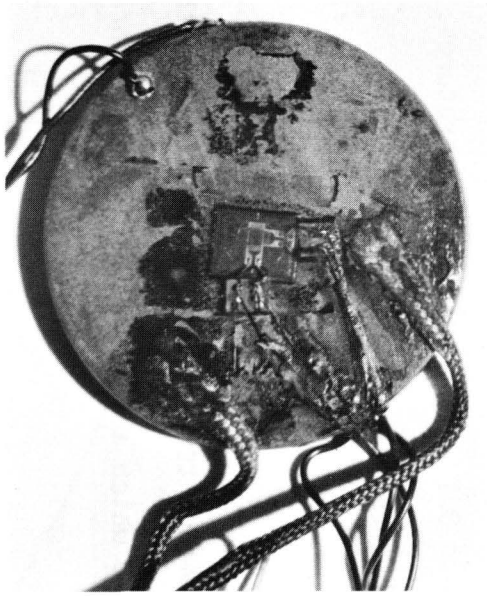

Crystal 3
1.50" O.D. x 0.16" Thick

Figure 19. Duomorph Crystals

Crystal 3 for temperatures between 0°F and 50°F. These crystals were completely submerged into the asphalt to be characterized and excited at frequencies of 100, 10, 1, and 0.1 H_Z for various temperatures. Using Schapery's relationship between time and frequency,

$$\text{time} = \frac{0.1}{\text{frequency}} ,$$

the modulus versus time for constant temperature was plotted for three asphalts, AC-5, AC-10, and AC-20 which are shown in Figures 20 through 22.

By shifting these curves horizontally with respect to one of the curves chosen as reference, for a particular asphalt, a complete modulus-time behavior curve at a constant temperature was constructed and is referred to as the "master curve". This technique is based on the principle of time-temperature correspondence (47). Figure 23 shows the master curves for the three asphalts tested.

The time-temperature correspondence principle states that there are two methods that can be used to determine a viscoelastic material's behavior at long times. First, the material's response (load versus deformation data) can be directly measured at long times which becomes very time consuming. The second method requires raising the temperature of the material and then measuring the material's response. Shifting this curve horizontally to the right of the curve tested at the lower temperature results in an exact superposition of the curves in the regions where the modulus values overlap and an extension of the curve measured at a higher temperature to modulus values lower than those measured at the cooler temperature. The time-temperature correspondence

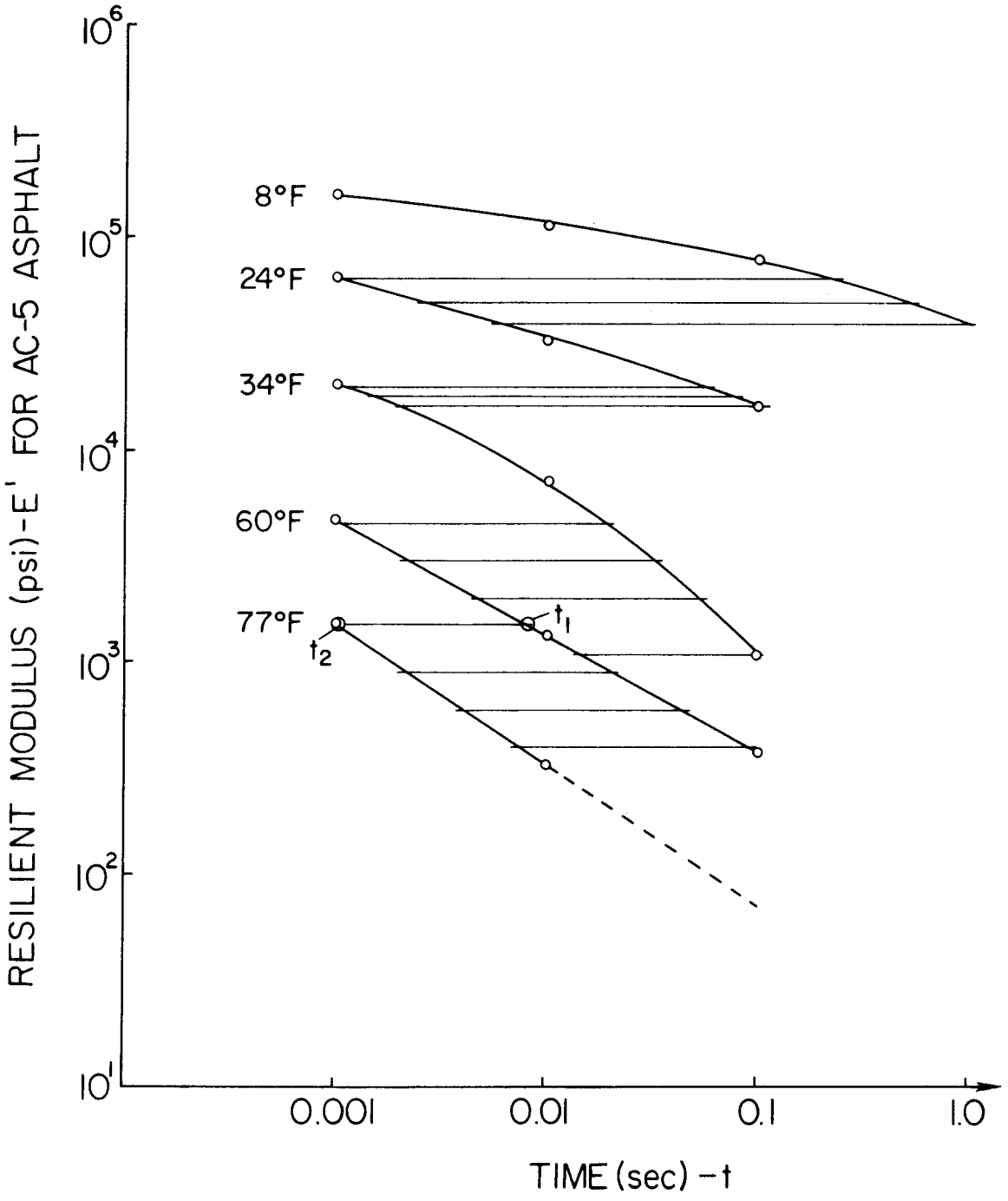

Figure 20. Modulus-Time Curves at Various Temperatures for AC-5 Asphalt.

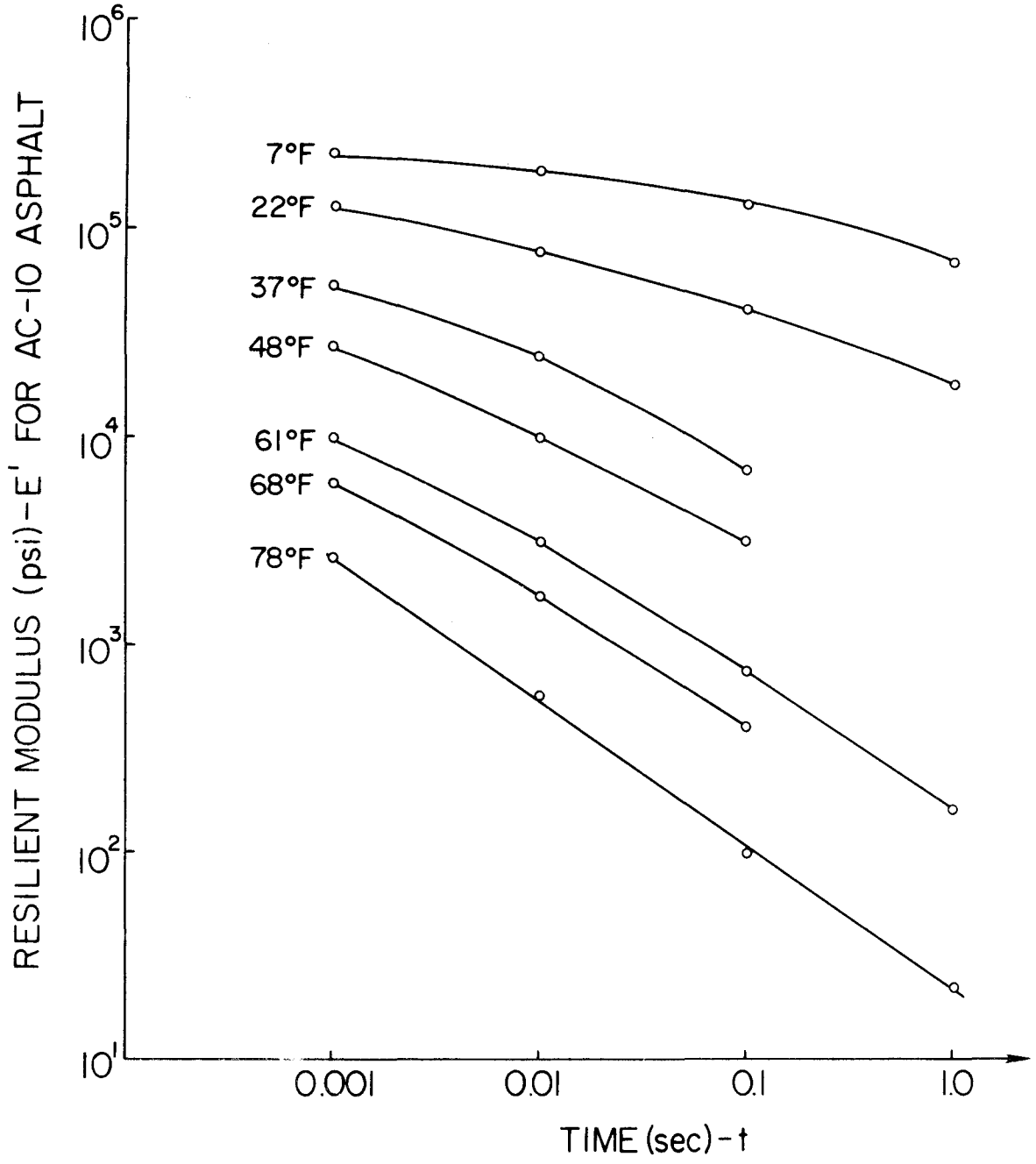

Figure 21. Modulus-Time Curves at Various Temperatures for AC-10 Asphalt.

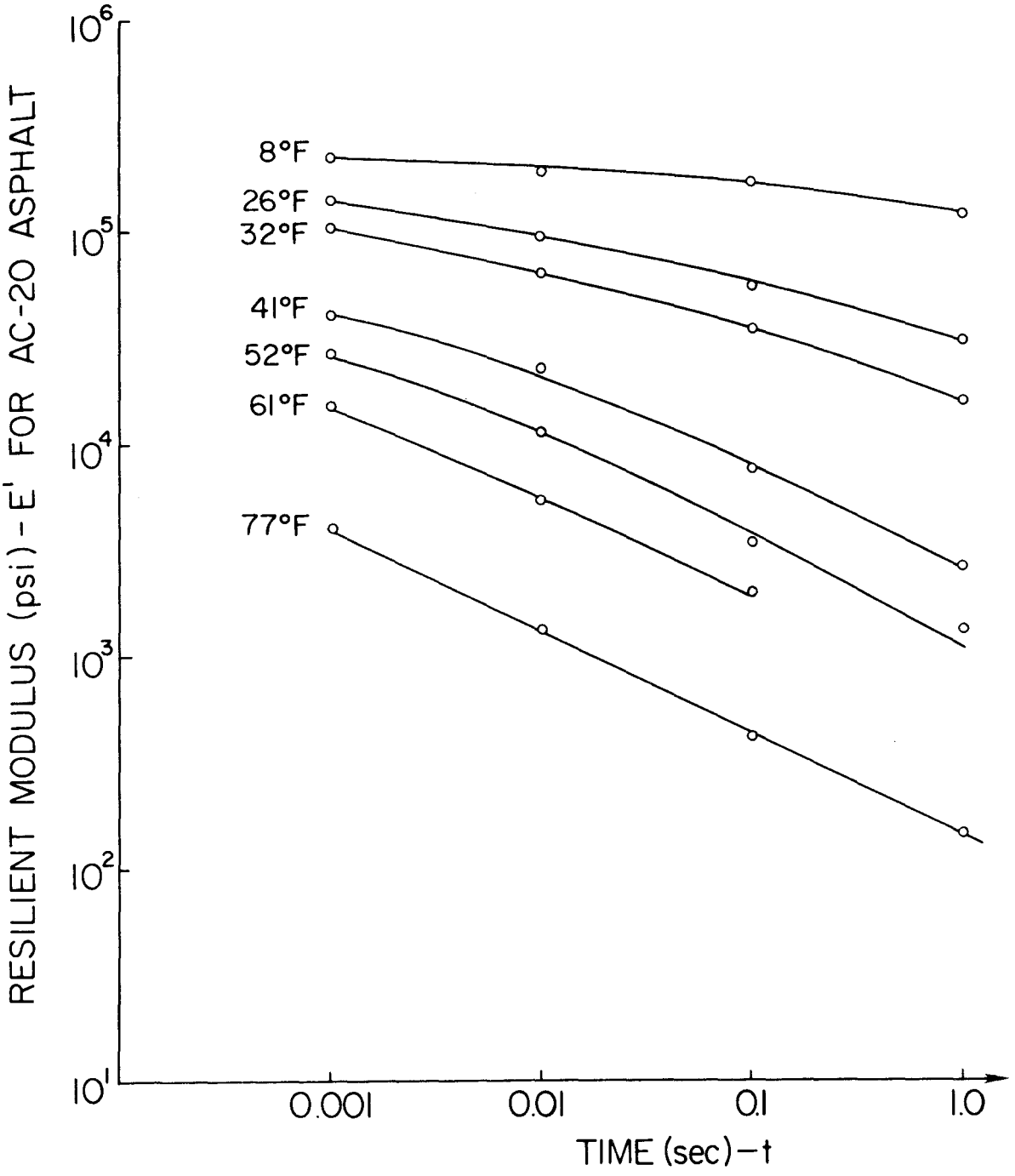

Figure 22. Modulus-Time Curves at Various Temperatures for AC-20 Asphalt.

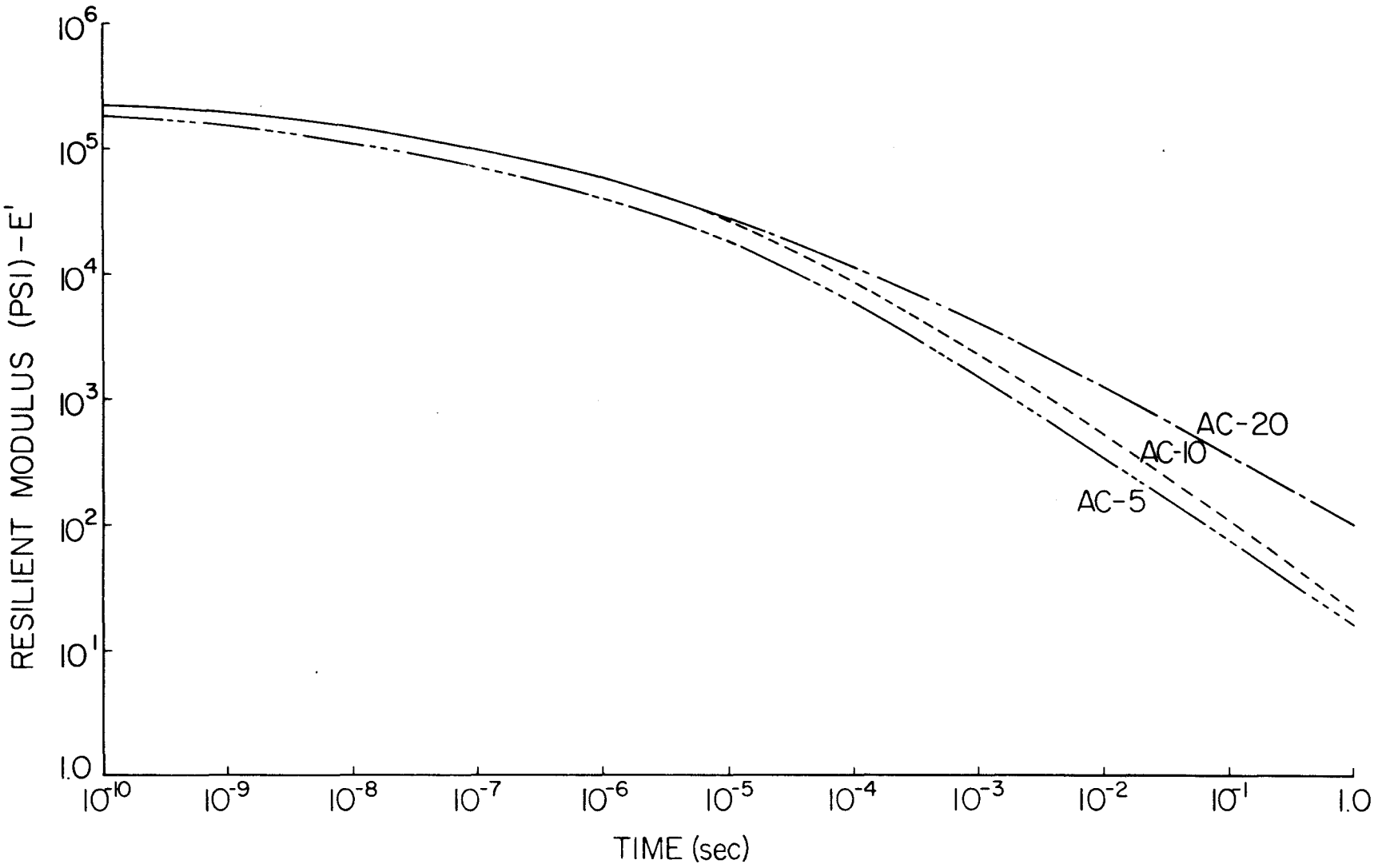

Figure 23, Resilient Modulus ($E'(t)$) Master Curve.

principle states that this extension is identical to that which would be measured at long times.

From the $E'(t)$ master curve, Figure 23 (p. 74), the creep compliance, $D(t)$, master curve was constructed. This was achieved by first fitting a power equation to the $E'(t)$ data:

$$\log E'(t) = \log B + m \log T$$

or

$$E'(t) = B\, t^m$$

Once m is known, the creep compliance for any time, t, used in the $E'(t)$ master curve can be calculated using the relationship:

$$D(t) = \frac{\sin m\pi}{m\pi} \quad \frac{1}{E'(t)}$$

The creep compliance master curves are shown in Figure 24.

The procedure used in constructing the $E'(t)$ and $D(t)$ master curves for the AC-5 grade asphalt is shown in Appendix B (p. 121).

Stress-Intensity Factors for the Asphalt Overlay Samples

Determined from finite element program. Stress functions of the types suggested by Westergaard provide a large number of solutions for two-dimensional crack problems. One such function shown in Appendix A is $K = \sigma \sqrt{\pi a}$. For three-dimensional crack problems, exact solutions in closed form are few in number. In general, unless the crack can be regarded as in a material with infinite dimensions, compact analytical solutions of the crack stress fields are not available, and numerical

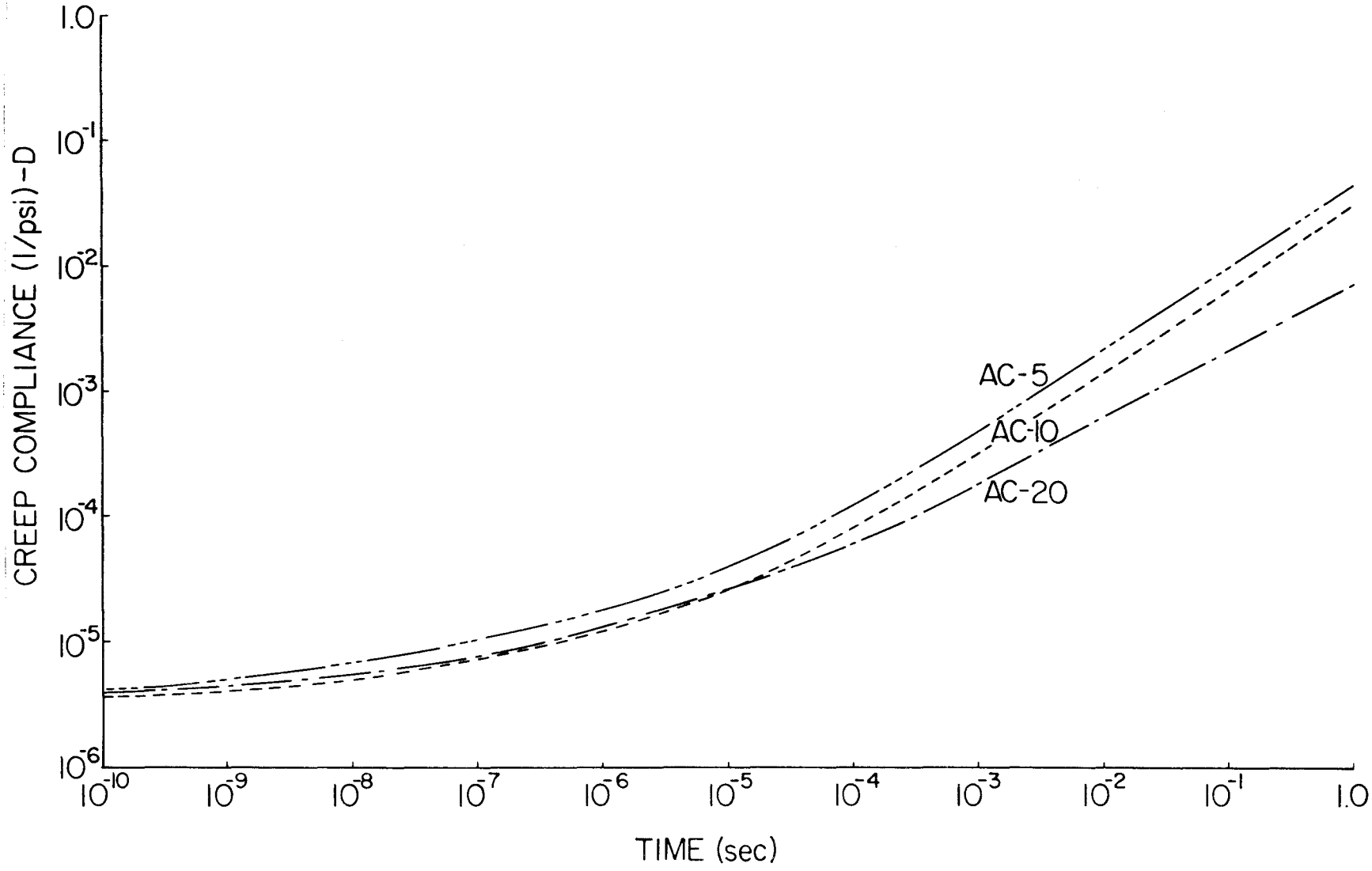

Figure 24. Creep Compliance (D(t)) Master Curve.

methods are required to determine the stress-intensity factors.

One such numerical method, that was described by Chang (42) is a constant strain finite element program which incorporates a hybrid crack-tip element for calculating stress-intensity factors. This program was used in determining the K-values of the asphalt overlay samples for various crack lengths. Two values were found that, at a constant depth of sample, are invariant for various moduli, crack openings, and loads. One of these, K/P, is found by dividing the stress intensity factor by the load remaining in the uncracked area. The other, 2K/Eu, is found by dividing twice the stress-intensity factor by the product of the modulus, E', and the crack opening, u. These values are plotted against the crack lengths normalized by the depth of the overlay sample, a/d, as shown in Figures 25 and 26 for one-inch, two-inch, and three-inch thick samples.

Determined experimentally. From experimental observations, Irwin (25) found that crack growth could be regarded as a rate-controlled process driven by a force which he termed the "crack extension force". Irwin assumed that this crack extension force was Griffith's strain-energy-release rate which Irwin designated as "G", see Eq. (2-1). The crack extension force, G, was further described by Irwin to be the irreversible strain-energy loss per unit of crack extension. Figure 27 will help to explain what is meant by "irreversible strain energy loss". Figure 27 is a typical plot of load versus crack opening made by x-y plotter of an overlay sample being fatigued on the overlay tester. The area bounded by the load-crack opening curve for cycle N and the x-axis is the work done (strain energy) on the sample to extend the crack a certain amount. For the cycle, N + 1, the area bounded by this curve

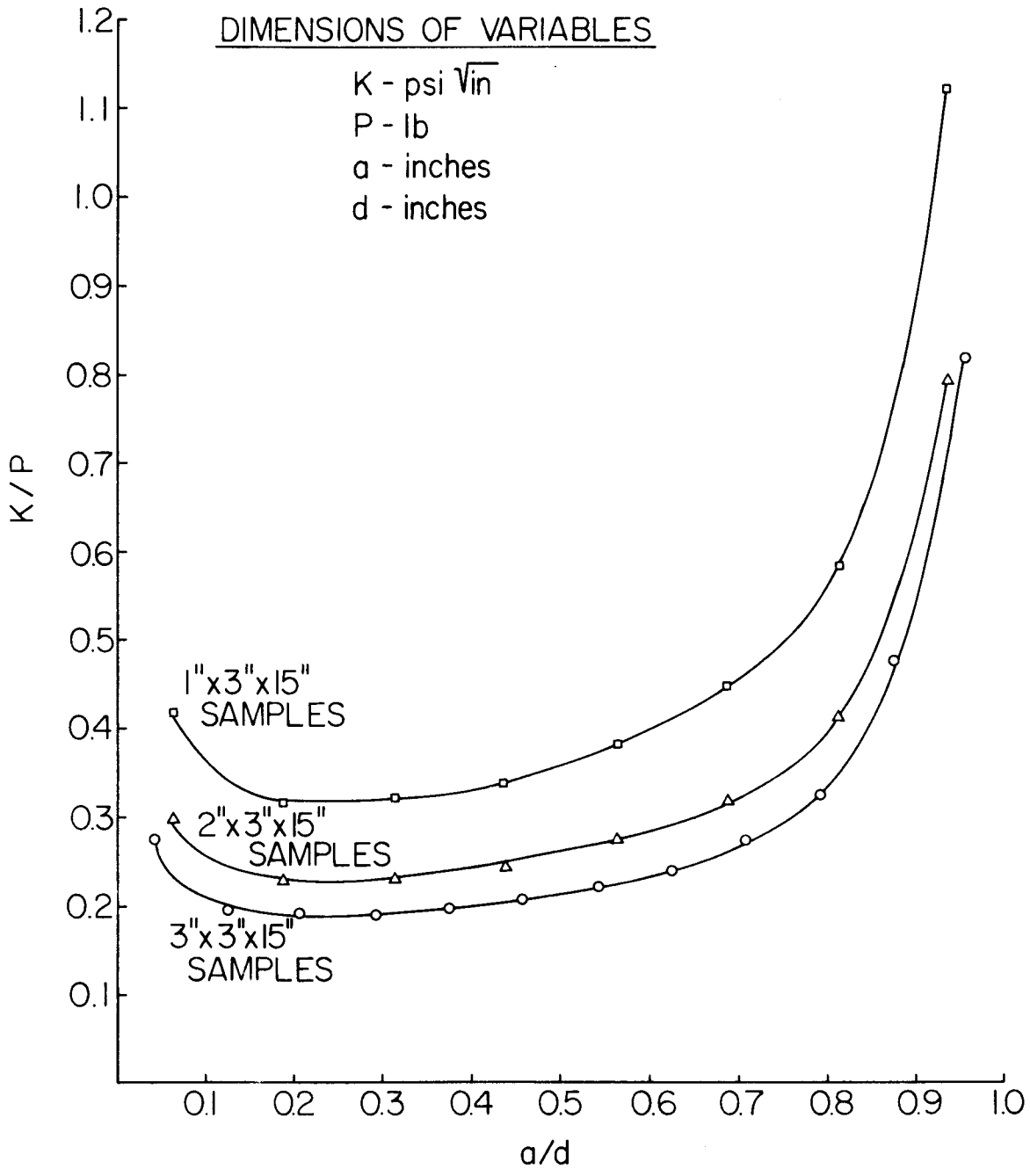

Figure 25. K/P Versus a/d.

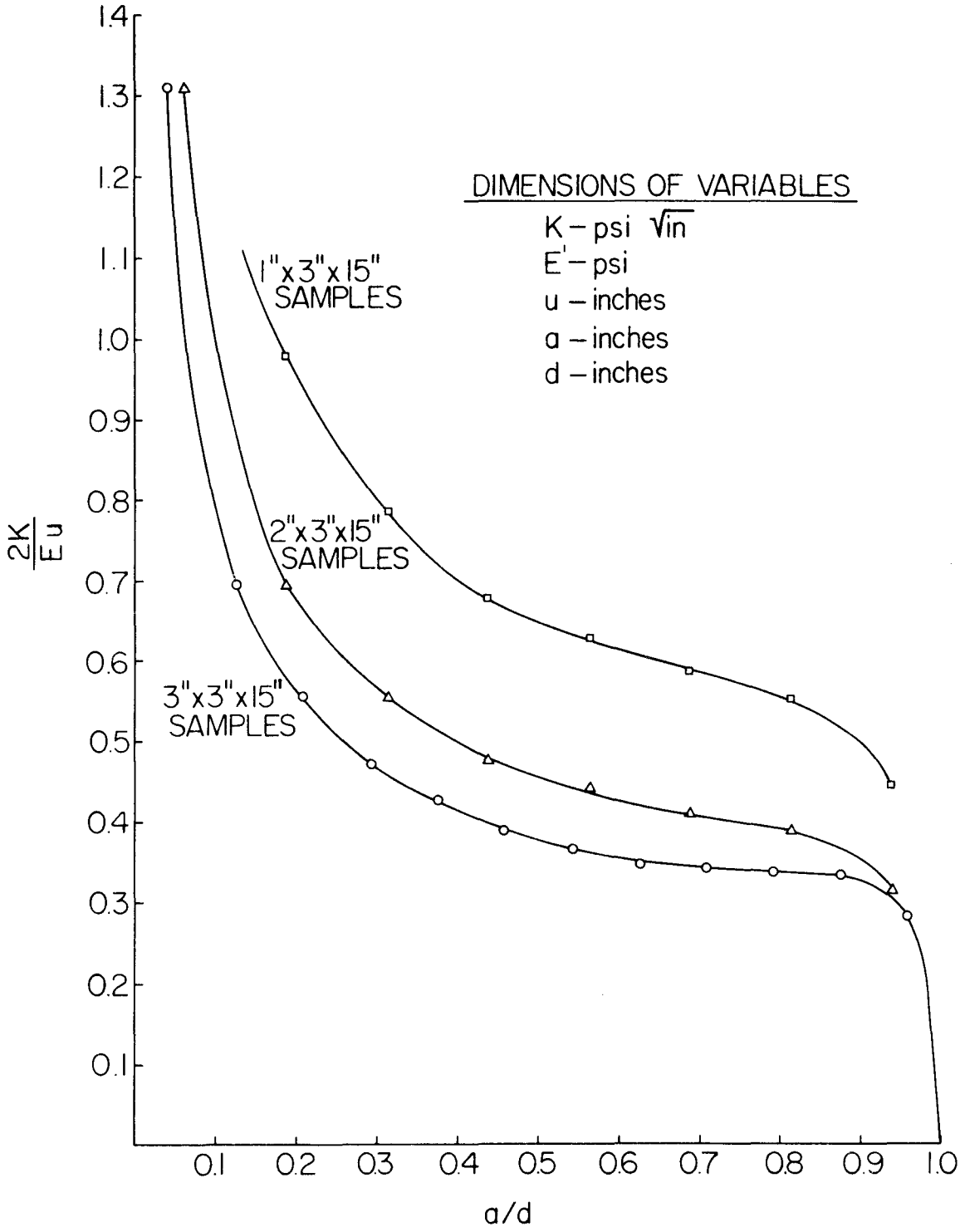

Figure 26. 2K/E'u Versus a/d.

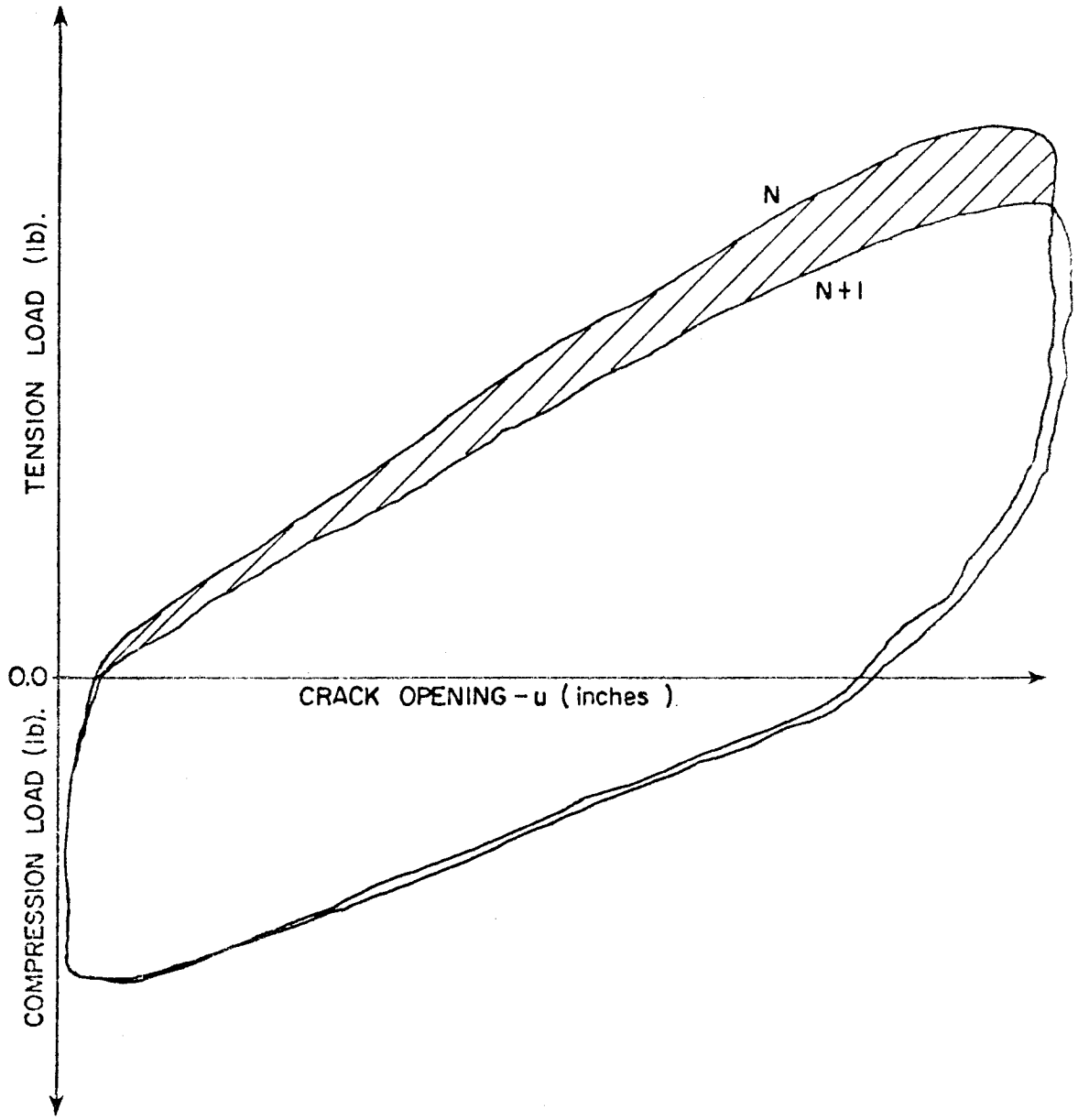

Figure 27. Typical Recording of Load Versus Deformation to Determine the Crack Extension Force - G.

and the x-axis is less than the area associated with the previous cycle, and the resulting crack extension is less than what it was for cycle N. The difference in areas under these two curves, the shaded region in Figure 27 (p. 80), is the "irreversible strain energy loss" associated with the area of crack extension which is found by subtracting the two crack heights measured at the end of cycles N and N + 1 and multiplying this difference by twice the width of the sample.

A simple mathematical representation of the crack extension force is:

$$G = \frac{\partial U}{\partial A}$$

where

$\frac{\partial U}{\partial A}$ = the rate of change of strain energy with respect to the cracked surface area.

The procedure used to find G is as follows. U is first found, from the recordings of load versus crack opening made by the x-y plotter, by using a planimeter to determine the area bounded by the curves and the x-axis, and the cycle, N, at which the recordings were taken were noted. Then a simple power equation was fitted through the U-N data which gave an equation of the form

$$U = aN^b \tag{7-1}$$

where both a and b are regression coefficients. This power equation was differentiated with respect to N to give:

$$\frac{\partial U}{\partial N} = a \cdot b\, N^{b-1} \tag{7-2}$$

The next step taken was to find the relationship between the cracked surface area, A, and the number of cycles, N. The cracked surface area was found from the crack length measurements, made by the vernier calipers, and multiplying this by twice the width of the asphalt overlay sample. A power equation was used again to find the relationship between the N-A data which gave:

$$N = c\,A^{d}$$

This equation was differentiated with respect to A:

$$\frac{\partial N}{\partial A} = c \cdot d\,A^{d-1} \tag{7-3}$$

The final step to find G is to multiply the two differentiated equations, Eq. (7-2) and Eq. (7-3), together:

$$G = \frac{\partial U}{\partial N} \cdot \frac{\partial N}{\partial A} = \frac{\partial U}{\partial A} \tag{7-4}$$

By substituting a power relationship of cracked surface area to the number of cycles,

$$A = e\,N^{f}$$

into Eq. (7-3) to give

$$\frac{\partial N}{\partial A} = c \cdot d \left(e\,N^{f}\right)^{d-1}$$

allowed G, Eq. (7-3), to be evaluated at any cycle, N.

The power equations that were used in fitting curves to the data, to find the above relationships, resulted in good correlations based on their coefficients of determination (r^2) values which were usually above 0.900. Since good correlations were obtained with these simple power equations no other regression models were tried.

Once the G is found, the stress-intensity factor can be determined by using Eq. (2-4) for plane strain conditions. As can be seen from this equation, the material's modulus must be known. To choose the correct modulus Schapery's theory needs to be used; the modulus is that value read from the master curve, Figure 23 (p.74), for some time, t, which the crack requires to propagate over the length of the failure zone, α, divided by three. Recall that $t = \alpha / (3\dot{a})$ where $\dot{a}$ is the velocity of the crack. To use this procedure for determining t requires a measurement of α to be made during the fatigue test which is a very formidable task. Another approach had to be used to determine the modulus.

The following method was used to determine the modulus. Knowing the crack height and the thickness of the overlay sample, a K/P value was found using Figure 25 (p. 78). From the load versus crack opening recordings made during the fatigue test, the load for that particular crack height was determined and multiplied by the K/P value to calculate the stress-intensity factor. Entering into Figure 26. (p. 79) with the same a/d ratio used before, a $2K/E'u$ value was obtained. Since K has already been determined and u is the crack opening which is also known, the modulus, E', was easily solved for.

The modulus found by using the above procedure is assumed to be equal to that modulus determined by Schapery's crack growth theory. This assumption is reasonable since all of the E's, determined from Figure 26 (p. 79) were found to fall on the straight line region of the master curve, Figure 23 (p. 74), and therefore also Figure 24 (p. 76), which was used in deriving Eq. (4-5).

Using these E' values, the crack extension forces, G, were obtained by using the stress-intensity factors found from Figure 25 (p. 78) and the equation:

$$G = \frac{K^2 (1-\nu^2)}{E'} \qquad (7\text{-}5)$$

where ν, Poisson's ratio, was taken to 0.400. The G values based on Eq. (7-5) will be referred to as G_{fe}, that is the crack extension force found from Chang's finite element program as opposed to G_{exp} which is the crack extension force determined experimentally. These values, G_{fe} and G_{exp}, were compared to one another by computing the percent difference:

$$\% \text{ Diff.} = \frac{G_{exp} - G_{fe}}{G_{fe}}$$

Relationship of Crack Growth Rates and Stress-Intensity Factors, $\frac{da}{dN} - K$

The rate of crack growth per cycle was obtained by first fitting a power equation to the crack height (c) - cycle (N) data:

$$c = gN^h \qquad (7\text{-}6)$$

and then differentiated with respect to N which yielded:

$$\frac{dc}{dN} = g \cdot h \; N^{h-1} \tag{7-7}$$

For a particular cycle, N, Eq. (7-6) was used to determine the crack height, then Figure 25 (p. 78) was used to get K/P value for that crack height. From a graph of load, P, versus N, the load for that particular cycle was determined and multiplying it by the K/P value, the stress-intensity factor was found. Using Eq. (7-7) the rate of crack growth, for the cycle of interest, corresponding to the stress-intensity factor found for the same cycle. This procedure was repeated for various other cycles throughout the fatigue life of the sample and then these values were plotted on logarithmic paper as shown in Appendix C (p. 127) for test numbers 5 through 14.

The coefficients A and n used Paris and Erdogan's power law equation were obtained by fitting a power equation to the $\frac{dc}{dN}$ - K values. Values of A and n are presented in the power law equation itself as shown in Appendix C and also in Table 2 (p. 50) for those samples which $\frac{dc}{dN}$ - K plots could be made.

Determination of the Parameters Used in Schapery's Theory

As was shown by Schapery, the coefficients A and n in Paris and Erdogan's power law for crack growth were related to the material properties in which the crack propagates:

$$A = \frac{\pi}{6 \sigma_m^{\,2} I_1^{\,2}} \left[\frac{(1-\nu^2) D_2}{2 \Gamma} \right]^{1/m} \left[\int_0^{\Delta t} w(t)^{2(1+1/m)} \, dt \right] \tag{7-8}$$

$$n = 2(1 + 1/m) \tag{7-9}$$

The maximum stress that the samples can withstand before failure, σ_m, was found by taking the largest load recorded by the x-y plotter for the first or second cycle of loading, and dividing this by the area occupied by the aggregate in a cross-sectional plane of the sample. The area of aggregate was found by taking the volume of aggregate, used in making the asphalt overlay sample, and dividing it by the length of the sample. Values of σ_m ranged from 20 psi to 65 psi depending upon the constituents of the asphalt concrete mix. These values were compared with tensile strengths of some asphalt samples obtained from direct tension tests performed on the Instron Machine and close agreement was observed.

Reasonable values of I_1 can be taken to be any value between one and two. For the analysis done here, I_1 was arbitrarily assigned a value of 1.5.

Poisson's ratio, ν, was taken to be 0.400.

The fracture energy, Γ, is defined as the work done on a material to produce a unit area of crack surface. Values of Γ were found from the early portions of the fatigue tests. The load-crack done on the material which was determined by finding the area between the curve and the crack opening axis using a planimeter. Using Eq. (7-6) to find the crack heights at the beginning and the end of the cycle for which the work done on the sample was determined from, and then taking the difference of these two crack heights and multiplying by twice the width of the sample gave the cracked surface area associated with the

work done on the sample for that cycle. Γ was then found by dividing the work done for that cycle by the cracked surface area produced during that cycle.

From the compliance curve in Figure 24. (p. 76), D_2 and m are found; D_2 is the compliance at the time equal to one second and m is the slope of the straight line portion of the curve which extends from t = 1 sec. to about $t = 10^{-4}$ sec.

Values of D_2 and m are shown below for the three asphalts tested:

Asphalt Grade	$D_2 \left(\frac{1}{psi}\right)$	m
AC-5	4.66×10^{-2}	0.669
AC-10	3.44×10^{-2}	0.700
AC-20	7.65×10^{-3}	0.533

For the integral in brackets in Eq. (7-8), w(t) is the wave shape of the stress-intensity factor which is sinusoidal as shown in Figure 28, and the equation of this sine curve is:

$$w(t) = \begin{cases} \sin \frac{2\pi t}{10} , & 0 \leq t \leq 5. \text{ sec.} \\ 0 , & 5 < t \leq 10 \text{ sec.} \end{cases} \qquad (7\text{-}10)$$

This equation was integrated over the period of the cycle, Δt, which is ten seconds:

$$\int_0^5 \left[\sin \frac{2\pi t}{10}\right]^{2(1+1/m)} dt + \int_5^{10} \left[0\right]^{2(1+1/m)} dt \qquad (7\text{-}11)$$

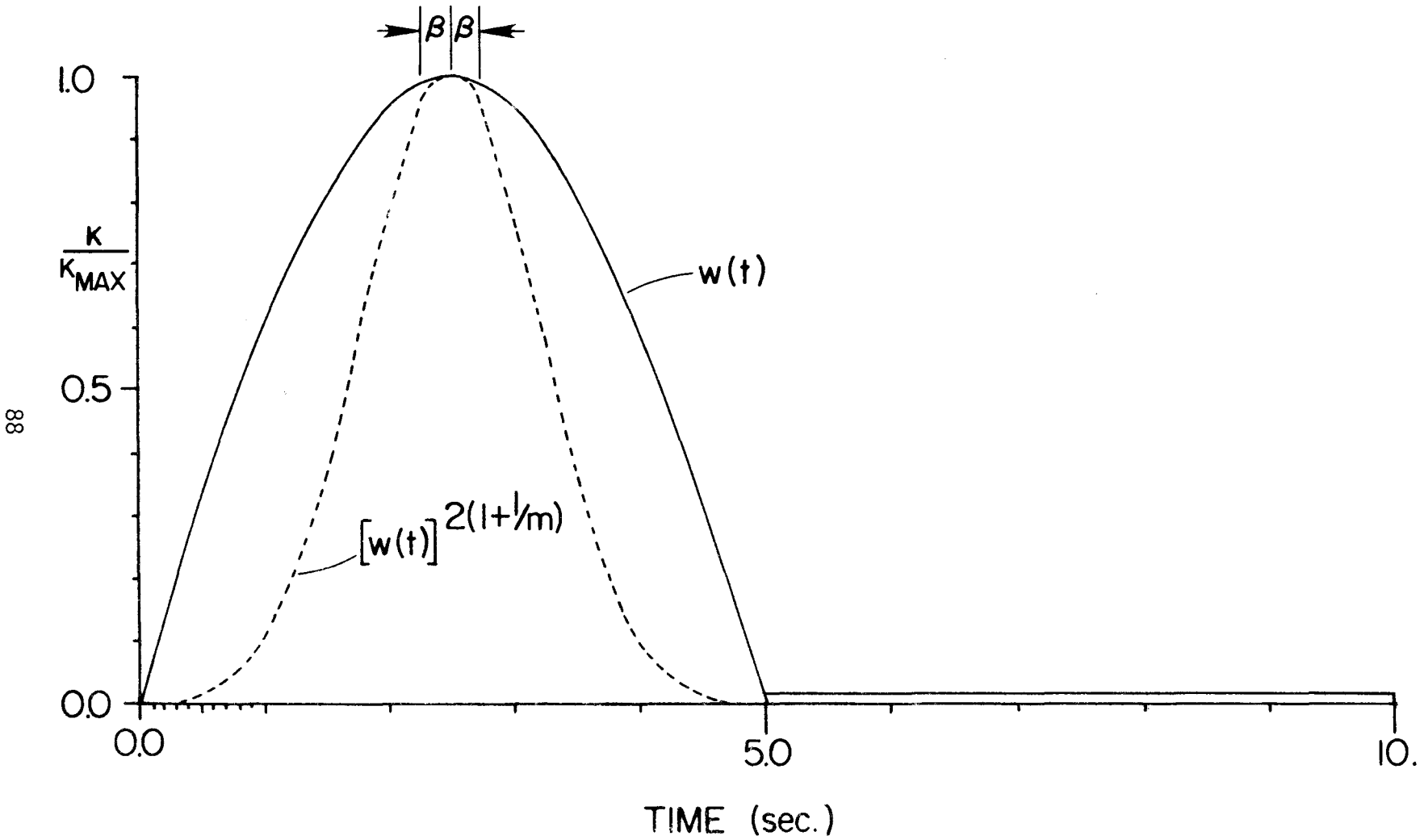

Figure 28. Wave Shape of the Stress-Intensity Factor Applied to the Samples in the Overlay Tester.

The above integral was evaluated numerically using Simpson's rule and the results are presented below for the three asphalts:

Asphalt Grade	Eq. (7-11)
AC-5	1.72
AC-10	1.72
AC-20	1.59

Values of the parameters used to evaluate the equations derived from Schapery's theory, Eqs. (7-8) and (7-9), are shown in Table 3.

Table 3. Values of the Parameters Used in Schapery's Theory.

Test Number	σ_m (psi)	I_1	Γ $\left(\frac{lb - in}{in^2}\right)$	D_2 $\left(\frac{1}{psi}\right)$	m	$\frac{1}{m}$	$2\left(1 + \frac{1}{m}\right)$ Eq. (7-9)	$\int_0^{\Delta t} w(t)^{2\left(1+\frac{1}{m}\right)}$	A Eq. (7-8)
.5	57		1.0						2.88×10^{-7}
6	57		10.0						6.42×10^{-8}
7	57		10.0	3.44×10^{-2}	0.700	1.43	4.86	1.72	6.42×10^{-8}
8	57		2.0						1.07×10^{-7}
9	57	1.5	17.0						5.01×10^{-9}
10	57		17.0						5.01×10^{-9}
11	60		20.0	7.65×10^{-3}	0.533	1.88	5.76	1.59	7.57×10^{-12}
12	40		10.0	4.66×10^{-2}	0.669	1.49	4.99	1.72	2.31×10^{-8}
13	60		3.0	7.65×10^{-3}	0.533	1.88	5.76	1.59	2.68×10^{-10}
14	20		0.85	4.66×10^{-2}	0.669	1.49	4.99	1.72	3.63×10^{-6}

CHAPTER VIII

RESULTS AND DISCUSSION

Performance of Fabric Materials

As seen from Table 1 (p. 49), asphalt overlay samples with Fabric 1 have the longest fatigue life of the three fabrics tested. Fabric 2 overlay samples have the second longest fatigue life and Fabric 3 samples have the lowest life of the fabric samples. The control samples, those with no fabric, failed sooner than the samples with fabric.

For the samples with Fabric 1 and 2 tested at a crack opening set for 0.065 inch or more, when the crack reached the fabric it began to propagate horizontally for a short distance while a crack would initiate at the top of the sample and propagate downwards to the crack at the fabric. This behavior was observed in the field by the Florida Department of Transportation as mentioned before. Overlay samples made with Fabric 3 did not exhibit the above trends, and there is only a small amount of difference between the fatigue lives of the Fabric 3 samples and the control samples.

In all of the fatigue tests performed, these fabrics did not tear apart for the crack openings (displacements) they were subjected to. This can be attributed to the fact that the fabric material can sustain those displacements that cause cracking to occur in the asphalt concrete. The rate of crack growth is much slower in the samples with fabric than the control samples since the fabric prevents the asphalt concrete from opening up to those displacements causing faster crack growth. The crack was noted to stop momentarily at the fabric until the fabric was

stretched enough to allow the displacements in the surrounding asphalt concrete to cause crack growth immediately above the fabric. This permitted the crack to propagate to the top of the sample as was observed in Fabric 3 samples or meeting the crack propagating down from the top as was the case with Fabrics 1 and 2 samples.

Majidzadeh (38) concluded that for the best performance (longest fatigue life), the fabric should be placed in the lower third portion of the sample where the stress-intensity factors are a minimum. Recall that Majidzadeh et al. modeled traffic induced loads; whereas, in this report loading due to thermal changes was being modeled and the region where the stress-intensity factors are a minimum are in the top third of the sample as was done for the tests performed on the overlay-tester.

Bushey (40) reported that overlay sections in the field with fabric performed best in moderate or warm climates, and field tests performed in Wyoming (1) showed that after two years time the overlays with fabric caught up with the overlays without fabric of the same thickness as to the number of cracks. The tests performed on the samples listed in Table 1 (p. 49) were conducted at a temperature of 77°F, so no comparison between the field observations and the results from the overlay tester on the effects of temperature can be made.

Effects of Thickness and Asphalt Content on the Behavior of Cracking in the Overlay Samples

Looking at Table 2 (p. 50) for test identification numbers 5 through 10 shows that thicker overlay samples have longer fatigue lives and increasing the asphalt contents also results in longer fatigue

lives for the various thicknesses. The effects of thickness on the constants A and n used in Paris and Erdogan's power law are very small for the two- and three-inch thick samples, but for the one-inch thick samples they differ considerably from the others. The values of A and n, for the one-inch thick samples are not sound because the crack propagated so rapidly during the tests making the crack height measurements inaccurate. So, for a particular asphalt content, thickness does not affect A and n based on the results from the two and three inch thick samples.

When the asphalt content is increased the parameter A decreases and n increases. The trend which A takes is consistent with the findings made by Majidzadeh (37); they kept n constant in the power law equation using values of 1 and 2 for n to determine A. This makes A solely dependent upon the material properties, so they could not report upon the effects of the mix variables on n. Also from Table 2 (p. 50), low values of A and high values of n are associated with long fatigue lives.

The values of A and n determined from Schapery's theory are seen to be in close agreement with those found experimentally for the samples with high asphalt contents. When the asphalt content is decreased, the difference between theory and experiment become significant.

Effects of "Hard" and "Soft" Asphalts With "High" and "Low" Asphalt Contents in Various Graded Mixes on the Cracking Behavior in the Overlay Samples

Referring to Table 2 (p. 50) and test identification numbers 11 and 18 the effects of asphalt grade on the fatigue lives of these samples show that the stiffer the asphalt the lower the fatigue life. These trends also occurred in the hot sand mixes and in the open graded mixes. Santucci and Schmidt (34), Epps and Monismith (11) all reported the same observations, as was just described, for controlled strain tests; however Majidzadeh et al. found that the samples made with softer asphalts, such as with AC-5, had short fatigue lives, but these results were obtained from controlled stress tests.

The effects of "high" and "low" asphalt contents on the open graded mixes, test numbers 15 through 18, show again that the higher the asphalt content the longer the fatigue life. The open graded mixes and the hot sand mixes exhibited shorter fatigue lives than the dense graded mixes. No comparison can be made between the hot sand mixes and the open graded mixes since these samples did not have identical asphalt contents.

Epps and Monismith (11) and others (13, 14, 32) have also found that for the same asphalt contents dense graded mixes have longer fatigue lives than the open graded mixes.

Experimental values of A show that they are affected by aggregate gradation and not by the grade of asphalt used in the mixes made with the same asphalt content, and the experimental values of n are affected only by the asphalt grade for these samples. Schapery's A and n values

agree fairly closely with the experimental values for those samples made with the soft asphalt, AC-5.

Crack Extension Forces - G ; Experimental and From the Finite Element Program

The percent difference between the experimentally and numerically determined crack extension forces have a range of 90% to 0% for all the samples tested in Table 2 (p. 50) except the open graded samples. The difference between the G_{exp} and G_{fe} values are the largest in the early portion of the fatigue tests, where the stress-intensity factors are large. Toward the end of the fatigue tests when the stress-intensity factors become small, the differences between G_{exp} and G_{fe} also become small.

For the majority of the fatigue tests performed, the crack extension forces found from experiment are larger than those values determined numerically. This means that the rate of the irreversible strain-energy loss per unit crack area is larger than what the numerical values suggest. The heat generated in the crack tip region could probably be the cause of this larger rate of energy loss. There is convincing evidence that in viscoelastic materials, such as in asphalts, the heat buildup in the crack tip region under cyclic loading cannot be ignored (48, 49). Researchers (50, 51) have reported that these materials can undergo such extensive softening, as a result of heat generated due to cyclic loading, that failure occurs by excessive deformation and crack propagation becomes virtually impossible because the material flows rather than fractures. Therefore the difference

between G_{exp} and G_{fe} might be reduced significantly if the rate of cyclic loading is reduced, from 0.1 H_z say to 0.01 H_z or something even lower, so that the heat generated at the crack tip will be kept to a minimum.

CHAPTER IX

DESIGN EXAMPLE FOR PREDICTING THE REFLECTION CRACKING LIFE OF AN ASPHALT OVERLAY

Two methods will be used to predict the average fatigue life of the overlay samples with the test identification number 12. One method uses A and n values found from the fatigue tests and the other method uses A and n values calculated from Schapery's theory. The method using the experimental A and n values will be performed first.

Paris and Erdogan's power law based on the experimental values is:

$$\frac{da}{dN} = 2.14 \times 10^{-8} K^{4.63}$$

and solving for dN gives:

$$dN = \frac{da}{2.14 \times 10^{-8} K^{4.63}}$$

To find the number of cycles to failure, N_f, the above equation has to be integrated between crack length limits a_0, the initial crack size, and a_f, the crack size at which the sample completely separates in two which is the sample's thickness (3 inches):

$$\int_1^{N_f} dN = \int_{a_0}^{a_f = 3"} \frac{da}{2.14 \times 10^{-8} K^{4.63}}$$

This integral was solved numerically using Simpson's Rule and also by replacing da/dN with $\Delta a/\Delta N$:

$$\Delta N = \frac{\Delta a}{2.14 \times 10^{-8} K^{4.63}}$$

The latter numerical method is shown in Table 4, and its procedure is as follows:

1. Assume the following:
   a. a_0 = 0.300 inch
   b. u = crack opening which is 0.45 inch
   c. E' = relaxation modulus which is about 1500 psi. This value was found using the method described earlier by calculating the asphalt tensile modulus, E'(t), for various crack lengths over the fatigue lives of the samples and then averaging them to get 1500 psi.
   d. a_f = 3 inches
   e. d = thickness of sample which is 3 - inches.
2. Assume an increment of crack growth, Δa. For this example Δa = 0.1. Note that the accuracy would be increased slightly by using smaller increments of crack growth.
3. Determine K by using the 2K/Eu - a/d relationship in Figure 26 (p. 79).
4. Calculate N for the increment of crack growth.
5. Repeat the above steps until a_f = 3 inches.

The total life to propagate a crack from 0.3 to 3.00 inches as shown in Table 3 (p. 90) is 1820 cycles. Using Simpson's Rule gave a total life of 1440 cycles which is closer to the average fatigue life of 1330 cycles.

Table 4. Fatigue-Crack-Growth Calculations Based on Experimental Results.

$$\Delta N = \frac{\Delta a}{2.14 \times 10^{-8} K^{4.63}}$$

a_1 (in)	a_2 (in)	a_{avg} (in)	a_{avg}/d	$\frac{2K}{Eu}$	K (psi $\sqrt{in}$)	ΔN (cycles)	ΣN (cycles)
0.3	0.4	0.35	0.12	0.71	23.2	2.2	2.2
0.4	0.5	0.45	0.15	0.64	20.9	3.6	5.8
0.5	0.6	0.55	0.18	0.59	19.2	5.3	11.2
0.6	0.7	0.65	0.22	0.54	17.6	8.0	19.2
0.7	0.8	0.75	0.25	0.51	16.6	10.5	29.7
0.8	0.9	0.85	0.28	0.48	15.7	13.6	43.2
0.9	1.0	0.95	0.32	0.45	14.7	18.4	61.6
1.0	1.1	1.05	0.35	0.43	14.2	21.6	83.2
1.1	1.2	1.15	0.38	0.42	13.7	25.5	108.7
1.2	1.3	1.25	0.42	0.41	13.2	30.3	139.
1.3	1.4	1.35	0.45	0.39	12.7	36.2	175.2
1.4	1.5	1.45	0.48	0.38	12.4	40.5	215.7
1.5	1.6	1.55	0.52	0.37	12.1	45.3	261.0
1.6	1.7	1.65	0.55	0.365	11.9	49.0	310.0
1.7	1.8	1.75	0.58	0.358	11.7	53.0	362.9
1.8	1.9	1.85	0.62	0.35	11.5	57.4	420.3
1.9	2.0	1.95	0.65	0.348	11.4	59.7	480.0
2.0	2.1	2.05	0.68	0.342	11.3	62.2	542.2
2.1	2.2	2.15	0.72	0.34	11.2	64.8	607.0
2.2	2.3	2.25	0.75	0.339	11.1	67.6	674.6
2.3	2.4	2.35	0.78	0.338	11.0	70.5	745.1
2.4	2.5	2.45	0.82	0.335	10.9	73.5	818.6
2.5	2.6	2.55	0.85	0.333	10.8	76.7	895.3
2.6	2.7	2.65	0.88	0.330	10.7	80.1	975.4
2.7	2.8	2.75	0.92	0.316	10.3	95.5	1070.9
2.8	2.9	2.85	0.95	0.292	9.5	138.9	1209.8
2.9	3.0	2.95	0.98	0.213	6.9	610.5	1820.

The same procedure was used to find the life of the samples using Schapery's values of A and n. From Table 5 a life of 750 cycles was obtained and then using Simpson's Rule a fatigue life of 573 cycles was found.

To use the above procedure for actual overlays in the field, in Step 1 of the above procedure, the crack opening, u, would have to be determined from the coefficient of thermal expansion or from previous observations and experience. To determine a value of the resilient modulus, E', engineering judgement is required. Reasonable values of E'(t) might be obtained by using the following procedure based on Schapery's theory. Referring to the dashed line curve in Figure 28 (p. 88), there is a narrow region of time, $|t_1 - t_2|$, at which the stress-intensity factor has values large enough to cause crack growth. By multiplying the abscissa scale by $\frac{2\pi}{\Delta t}$ (Δt is the period of the cycle) allows it to be represented in terms of radians, i.e. the t(sec) scale is converted to the $\emptyset$ (radians) scale. This enabled a relationship to be established between t, Δt, and β:

$$\frac{2\pi}{\Delta t}\ t_1 = \frac{\pi}{2} - \beta$$

$$\frac{2\pi}{\Delta t}\ t_2 = \frac{\pi}{2} + \beta$$

Subtracting these equations from one another gives:

$$\frac{2\pi}{\Delta t}\ |t_1 - t_2| = 2\beta$$

Table 5. Fatigue-Crack-Growth Calculations Based on Schapery's Theory.

$$\Delta N = \frac{\Delta a}{2.31 \times 10^{-8} K^{4.99}}$$

a_1 (in)	a_2 (in)	a_{avg} (in)	a_{avg}/d	$\frac{2K}{Eu}$	K (psi $\sqrt{in}$)	ΔN (cycles),	ΣN (cycles)
0.3	0.4	0.35	0.12	0.71	23.2	.7	.7
0.4	0.5	0.45	0.15	0.64	20.9	1.1	1.8
0.5	0.6	0.55	0.18	0.59	19.2	1.7	3.5
0.6	0.7	0.65	0.22	0.54	17.6	2.6	6.1
0.7	0.8	0.75	0.25	0.51	16.6	3.5	9.7
0.8	0.9	0.85	0.28	0.48	15.7	4.7	14.3
0.9	1.0	0.95	0.32	0.45	14.7	6.5	20.8
1.0	1.1	1.05	0.35	0.43	14.2	7.7	28.5
1.1	1.2	1.15	0.38	0.42	13.7	9.2	37.7
1.2	1.3	1.25	0.42	0.41	13.2	11.1	48.8
1.3	1.4	1.35	0.45	0.39	12.7	13.4	62.2
1.4	1.5	1.45	0.48	0.38	12.4	15.1	77.4
1.5	1.6	1.55	0.52	0.37	12.1	17.1	94.5
1.6	1.7	1.65	0.55	0.365	11.9	18.6	113.1
1.7	1.8	1.75	0.58	0.358	11.7	20.2	133.3
1.8	1.9	1.85	0.62	0.35	11.5	22.1	155.4
1.9	2.0	1.95	0.65	0.348	11.4	23.0	178.4
2.0	2.1	2.05	0.68	0.342	11.3	24.1	202.5
2.1	2.2	2.15	0.72	0.34	11.2	25.2	227.7
2.2	2.3	2.25	0.75	0.339	11.1	26.3	254.0
2.3	2.4	2.35	0.78	0.338	11.0	27.5	281.5
2.4	2.5	2.45	0.82	0.335	10.9	28.8	310.3
2.5	2.6	2.55	0.85	0.333	10.8	30.2	340.5
2.6	2.7	2.65	0.88	0.33	10.7	31.6	372.1
2.7	2.8	2.75	0.92	0.316	10.3	38.2	410.3
2.8	2.9	2.85	0.95	0.292	9.5	57.2	467.6
2.9	3.0	2.95	0.98	0.213	6.9	282.2	750.

and assuming that $\tilde{t}_\alpha = |t_1 - t_2|$:

$$\frac{2\pi}{\Delta t}\ \tilde{t}_\alpha = 2\beta \qquad (9\text{-}1)$$

where $\tilde{t}_\alpha$ is the time it takes the crack to propagate over the failure zone divided by three ($\tilde{t}_\alpha = \alpha/3\dot{a}$). As seen in Table 2 (p. 50) the t's, corresponding to the moduli back calculated using the finite element program, have a narrow range and the average value of these t's is 1.52×10^{-3} seconds. Substituting this average time value in for $\tilde{t}_\alpha$ and 10 seconds for Δt in Eq. (9-1) allows β to be solved for:

$$\beta = \frac{\pi}{6575}\ \frac{\text{cycles}}{\text{radians - cycle}}$$

This permits Eq. (9-1) to be rewritten as:

$$t = \frac{\Delta t \left(\frac{\text{sec}}{\text{cycle}}\right)}{6575\left(\frac{1}{\text{cycle}}\right)} \qquad (9\text{-}2)$$

Knowing any period, Δt, for the wave shape of the stress-intensity factor (K/K_{max}), t is calculated from Eq. (9-2) and entering into Figure 26 (p. 79) with this value the modulus is found which corresponds to a temperature of 77°F to which an overlay can be subjected.

For temperatures other than 77°F which an overlay can be subjected to, Eq. (9-2) needs to be adjusted. This is accomplished by dividing t by some "horizontal shift factor", a_T, associated with the ambient temperature of the overlay. The value of a_T is found from

a plot of log a_T versus temperature as shown in Figure 29 (p. 104) for the three asphalt grades. Now the time, t, and the modulus, E'(t), can be found for any temperature by using the following equation:

$$t = \frac{\Delta t}{6575} \cdot \frac{1}{a_T} \qquad (9\text{-}3)$$

along with Figures 26 and 29 (pp. 79 and 104). This equation should be verified by performing fatigue tests on the overlay tester at various temperatures and cyclic periods (Δt).

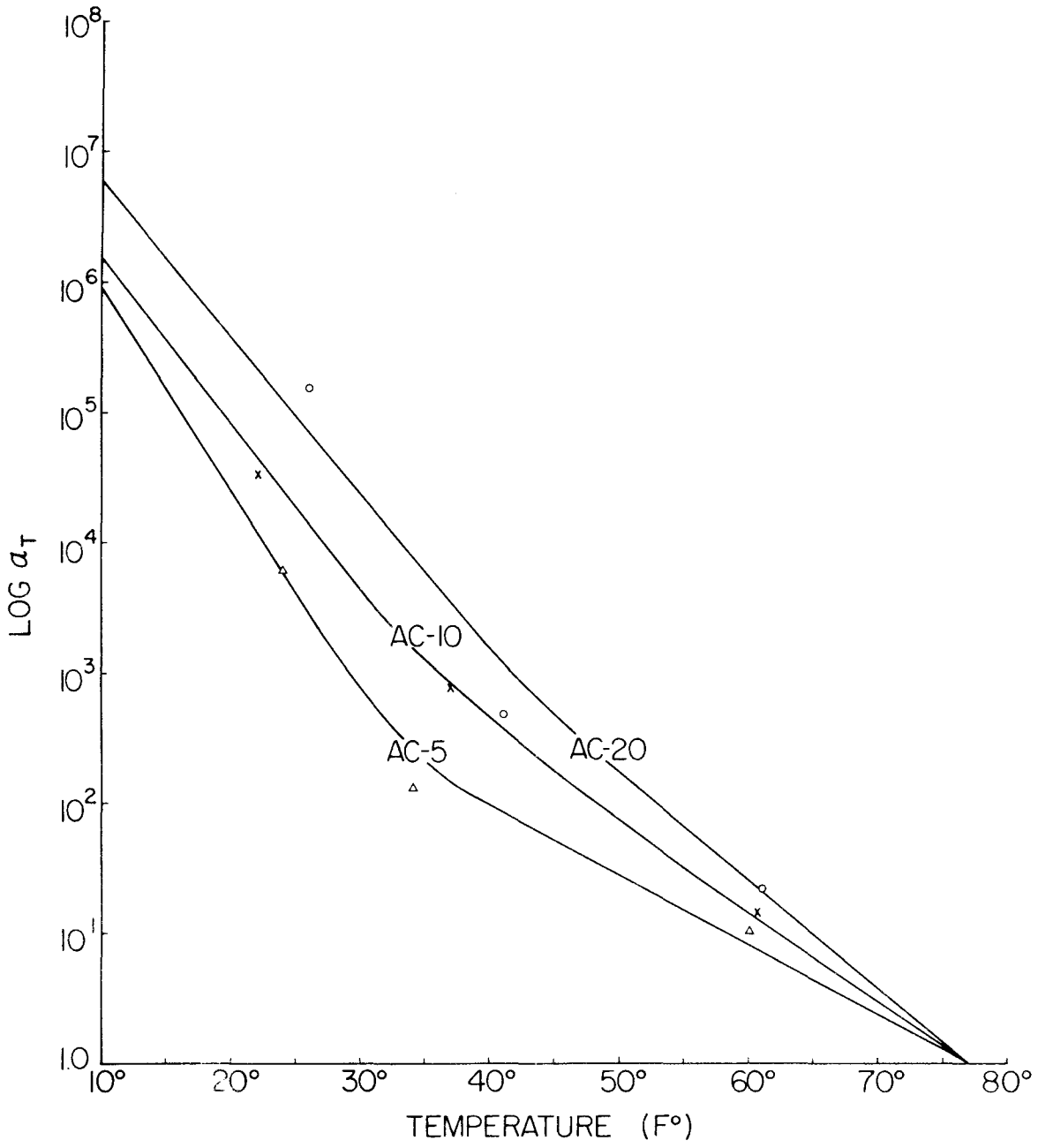

Figure 29. Log a_T Versus Temperature.

CHAPTER X

CONCLUSIONS AND RECOMMENDATIONS

Agreement between the crack extension forces G_{exp} and G_{fe} may be improved by using the procedure developed by Irwin and Wells (52). Applying this procedure to asphaltic concrete entails using several asphalt concrete samples of the same dimensions with various size "cracks". These "cracks" are actually saw cuts of various depths similar to that shown in Figure 14 (p.60). Each sample is loaded until a certain displacement (crack opening) is achieved, and the load-displacement data are recorded by an x-y plotter. The area under each load-displacement curve is found to determine the strain-energy, U, and the corresponding crack surface area, A, which is height of the saw cut times the sample's width. A power law equation is fitted to the U-A data and differentiated with respect to A to obtain the crack extension force. This procedure should reduce the effects of the heat generated at the crack tip since the samples are loaded monotonically instead of cyclic.

A more concentrated effort should be made to use ultrasonics in measuring crack lengths since this will allow a micro-processor to gather all the data and perform the necessary calculations for determining the experimental values of A and n expediently, so that the overlay scheme most resistant to cracking in the field can be determined rapidly. Using the calibration procedure by taking photographs of an actual crack instead of using saw cuts should result in an improvement.

Fatigue tests performed on the samples imbedded with various fabrics should be done again using the new version of the overlay tester that was used in testing those samples listed in Table 2 (p. 50). From these tests the effects of the fabric on the material constants A and n would be seen, and possibly, from the results of such a study, Schapery's theory could be modified to take into account the material properties of these fabrics so that values of A and n can be numerically determined.

The experimental values of A were found to be affected by asphalt content and aggregate gradation but invariant to the thickness of the sample and the grade of asphalt used. Asphalt content and the grade of asphalt used in the samples seem to be the only variables affecting n; the thickness of the samples and their gradation have very little influence upon n, if any. Previous observations of Table 2 (p. 50) revealed that samples with large values of A and small n values had shorter fatigue lives than the samples with smaller A values and larger n values.

Numerical predictions of the fatigue life of overlays can be made reliably using experimental values of A and n. Even the values of A and n derived from Schapery's theory can predict overlay life reasonably well. The numerical procedure is simple to program even on a hand-held calculator as were the Simpson's Rule computations reported herein. The fatigue lives found by using Simpson's Rule results in smaller values compared to those determined from the trapezoidal rule as presented in Tables 4 and 5 (pp. 99 and 101).

A more accurate procedure for determing the maximum stress, σ_m, and the fracture energy, Γ, can be obtained by performing direct tension tests on tensile specimens of the overlay samples using the Instron Machine. The tensile strength of the specimens can be taken to be σ_m, and during a tensile test the Instron has the capability of recording the applied load and resulting displacement from which Γ can be found. Tensile specimens of the proposed overlay from which σ_m and Γ are to be determined should have dimensions of one-by-one-by-six inches, and the rate at which these specimens are loaded on the Instron should be the same as the rate of loading at which the overlay samples will be subjected to on the overlay tester. This procedure is an attempt to reduce the effects of the heat generated at the crack tip on σ_m and Γ.

The experimental testing procedure for quantitative analysis developed and reported herein is capable of determining material properties for overlays. From this investigation, the values of A and n based on Schapery's theory agree well with the experimentally determined values for asphalt mixtures using a high asphalt content and soft grades of asphalt such as AC-5. Better agreement between experiment and theory, for mixtures using lower asphalt contents and stiffer asphalts, may be achieved by performing the fatigue tests at a slower cyclic rate to minimize heat generation at the crack tip. These slower rates are felt to be more representative of the conditions and behavior of cracking occurring in the field. Schapery's theory appears to work well in predicting the reflection cracking life of an overlay. The material properties used in Schapery's theory are

considerably easier to measure than a series of overlay fatigue tests and they can be extended to predict reflection cracking life of overlays in the field. It was for this purpose that this study attempted to see how well Schapery's theory works in predicting cracking life.

REFERENCES

1. Federal Highway Administration, "Interim Report - National Experimental and Evaluation Program (NEEP) Project No. 10 - Reducing Reflection Cracking in Bituminous Overlays," FHWA HHO-31, January 19, 1976.

2. Donnelly, Denis E., McCabe, Philip J., Swanson, Herbert N., "Reflection Cracking in Bituminous Overlays," FHWA-CO-RD-76-6.

3. Carpenter, S. H., Lytton, R. L., Epps, J. A., "Pavement Cracking in West Texas Due to Freeze-Thaw Cycling," paper presented at the annual meeting of the Transportation Research Board, January 1975, Washington, D.C.

4. Monismith, C. L., "Flexibility Characteristics of Asphaltic Paving Mixtures," Proceedings, Association of Asphalt Paving Technologists, Vol. 27, 1958.

5. Monismith, C. L., Sicor, K. E., and Blackmer, E. W., "Asphalt Mixture Behavior in Repeated Flexure," Proceedings, Association of Asphalt Paving Technologists, Vol. 30, 1961.

6. Monismith C. L., "Asphalt Mixture Behavior in Repeated Flexure," Report No. TE 64-2, University of California, Berkeley, 1964.

7. Monismith, C. L., "Asphalt Mixture Behavior in Repeated Flexure," Report No. TE 65-9, University of California, Berkeley, 1965.

8. Monismith, C. L., "Asphalt Mixture Behavior in Repeated Flexure," Report No. TE 66-6, University of California, Berkeley, 1967.

9. Monismith, C. L., "Asphalt Mixture Behavior in Repeated Flexure," Report No. TE 67-4, University of California, Berkeley, 1967.

10. Monismith, C. L., Epps, J. A., and Kasianchuk, D. A., "Asphalt Mixture Behavior in Repeated Flexure," Report No. TE 68-8, University of California, Berkeley, 1969.

11. Monismith, C. L., and Epps, J. A., "Asphalt Mixture Behavior in Repeated Flexure," Report No. TE 69-6, University of California, Berkeley, 1969.

12. Pell, P. S. and Taylor, I. F., "Asphalt Road Materials in Fatigue," Proceedings, Association of Asphalt Paving Technologists, Vol. 38, 1969.

13. Pell, P. S., "Fatigue Characteristics of Bitumen and Bituminous Mixes," Proceedings, First International Conference on the Structural Design of Asphalt Pavements," University of Michigan, 1962.

14. Pell, P. S., "Fatigue of Asphalt Pavement Mixes," Proceedings, Second International Conference on the Structural Design of Asphalt Pavements, University of Michigan, 1967.

15. Ramsamooj, D. V., "Analysis and Design of the Flexibility of Pavements," Ph.D. Thesis, The Ohio State University, 1970.

16. Majidzadeh, K., Buranarom, C., and Karakouzian, M., "Application of Fracture Mechanics for Improved Design of Bituminous Concrete," Report No. FHWA-RD-76-91, Vol. 1, June 1976.

17. Majidzadeh, K., Ramsamooj, D. F., and Fletcher, T. A., "Analysis of Fatigue of a Sand Asphalt Mixture," Proceedings, Association of Asphalt Paving Technologists, Vol. 30, 1969.

18. Majidzadeh, K., and Ramsamooj, D. V., "Development of Testing Procedures and a Method to Predict Fatigue Failures of Asphalt Concrete Pavement Systems," The Ohio State University Research Foundation Final Report, Project R.F. 2873, March 1971.

19. Paris, P. C., and Erdogan, F., "A Critical Analysis of Crack Propagation Laws," Transactions of the ASME, Journal of Basic Engineering, Series D, 85, No. 3, 1963.

20. Paris, P. C., Gomez, M. P. and Anderson, W. E., "A Rational Analytic Theory of Fatigue," Trend in Engineering (University of Washington), Seattle, Washington, Vol. 13, No. 1, 1961.

21. Schapery, R. A., "A Theory of Crack Growth in Viscoelastic Media," Mechanics and Materials Research Center, Texas A&M University, College Station, Texas, 1973.

22. Rolfe, S. T., Barson, J. M., Fracture and Fatigue Control in Structures - Applications of Fracture Mechanics, Englewood Cliffs, New Jersey: Prentice-Hall, Inc., 1977.

23. Griffith, A. A., "The Phenomena of Rupture and Flow in Solids," Transactions, Royal Society of London, A-221, 1920.

24. Inglis, C. E., "Stresses in a Plate Due to the Presence of Cracks and Sharp Corners," Proceedings, Institute of Naval Architects, 60, 1913.

25. Irwin, G. R., "Analysis of Stresses and Strains Near the End of a Crack Traversing of Plate," Transactions, ASME, Journal of Applied Mechanics, Vol. 24, 1957.

26. Irwin, G. R., "Fracture Mechanics," Proceedings First Symposium on Naval Structures Mechanics, MacMillan Press, 1958.

27. Paris, P. C. and Sih, G., "Stress Analysis of Cracks," Fracture Toughness Testing and Its Applications - ASTM STP No. 381, June 1964.

28. Barenblatt, G. I., "The Mathematical Theory of Equilibrium Cracks in Brittle Fracture," Advances in Applied Mechanics, Vol. VII, Academic Press, 1962.

29. Williams, M. L., "On the Stress Distribution at the Base of a Stationary Crack," Journal of Applied Mechanics, Vol. 24, 1957.

30. Graham, G. A. C., "The Correspondence Principle of Linear Viscoelasticity Theory for Mixed Boundary Value Problems Involving Time-Dependent Boundary Regions, " Q. Applied Math., Vol. 26, 1968.

31. Jimenez, R. A. and Gallaway, B. M., "Behavior of Asphaltic Concrete Diaphragms to Repeated Loadings," Proceedings, First International Conference on the Structural Design of Asphalt Pavements, University of Michigan, 1962.

32. Bazin, P. and Saunier, J. B., Proceedings, Second International Conference on the Structural Design of Asphalt Pavements, University of Michigan, 1967.

33. Kirk, J. M., Proceedings, Second International Conference on the Structural Design of Asphalt Pavements, University of Michigan, 1967.

34. Santucci, L. E. and Schmidt, R. J. "The Effect of Asphalt Properties on the Fatigue Resistance of Asphalt Paving Mixtures," Proceedings, Association of Asphalt Paving Technologists, Vol. 38, 1969.

35. Vallerga, B. A., Finn, F. N., and Hicks, R. G., Proceedings, Second International Conference on the Structural Design of Asphalt Pavements, University of Michigan, 1967.

36. Saraf, C. L., "Effect of Mix Variables in the Fatigue Response of Asphalt Mixes," Ph.D. Dissertation, The Ohio State University, Columbus, Ohio, 1973.

37. Majidzadeh, K., Buranarom, C., and Karakouzian, M., "Application of Fracture Mechanics for Improved Design of Bituminous Concrete," Report No. FHWA-RD-76-92, Vol. 2, June 1976.

38. Majidzadeh, K., "A Laboratory Investigation of the Use of Petromat for Optimization of Pavement Performance," A private study sponsored by Phillips Petroleum Company, October 1975.

39. Huffman, M., "Comparison of Reflective Crack Retardation by Fabric Material (Petromat), Open-Graded Friction Courses, and Conventional Hot Mix," Texas State Department of Highways and Public Transportation, FHWA TX 78-606-3, February 1978.

40. Bushey, R. W., "Experimental Overlays to Minimize Reflection Cracking," FHWA-CA-TL-3167-76-28.

41. Gulden, W., "Rehabilitation of Plain Portland Cement Concrete Pavements With Asphaltic Concrete Overlays," Presented at the Annual Meeting of the Association of Asphalt Paving Technologists, February 13-15, 1978.

42. Chang, H., Lytton, R. L., Carpenter, S. H., "Prediction of Thermal Reflection Cracking in West Texas," Report No. TTI-2-8-73-18-3, Texas A&M University, March 1976.

43. Ho, C. L., "Ultrasonic Surface-Wave Detection Technique," Experimental Techniques in Fracture Mechanics, 2; Society for Experimental Stress Analysis, Westport, Connecticut, 1975.

44. Boggess, R., and Noel, J., "The Duomorph - A Complex Modulus Transducer," Civil Engineering Department, Texas A&M University.

45. Briar, H. P. and Bills, K. W., Jr., "Development of an In-Situ Transmitter for Solid Rocket Propellant Surveillance," Final Report AFRPL-TR-72-93, Air Force Rocket Propulsion Laboratory, Edwards Air Force Base, California, December, 1972.

46. Briar, H. P., Bills, K. W., Schapery, R. A., "Design and Test of the Operational In-Situ Gage for Solid Propellant Surveillance," Final Report AFRPL-TR-76-36, Air Force Rocket Propulsion Laboratory, Edwards Air Force Base, California, June, 1972.

47. Aklonis, J. J., MacKnight, W. J., and Shen, M., Introduction to Polymer Viscoelasticity, John Wiley & Sons, Inc., 1972.

48. Regel, V. R., and Leksovsky, A. M., "A Study of Fatigue Within the Framework of the Kinetic Concept of Fracture," International Journal of Fracture Mechanics, 3, 1967.

49. Constable, I., Williams, J. G., and Burns, D. J., "Fatigue and Cyclic Thermal Softening of Thermo-Plastics," Journal of Mechanical Engineering Science, Vol. 12, 1970.

50. Tormey, J. F., and Britton, S. C., "Effect of Cyclic Loading on Solid Propellant Grain Structures," AIAA Journal, 1, 1963.

51. Schapery, R. A., "Thermomechanical Behavior of Viscoelastic Media With Variable Properties Subjected to Cyclic Loading," Journal of Applied Mechanics, Vol. 32, 1965.

52. Irwin, G. R., and Wells, A. A., "A Continuum Mechanics View of Crack Propagation," Metallurgical Review, 10, 1965.

53. Higdon, A. and Stiles, W. B., Mechanics of Materials, John Wiley & Sons, Inc., New York, 1960.

54. Westergaard, H. M., "Bearing Pressures and Cracks," Transactions, American Society of Mechanical Engineers, Journal of Applied Mechanics, 1939.

APPENDIX A

CRACK TIP STRESS ANALYSIS

Starting first with the differential equations of equilibrium for plane stress as can be found in any text on the theory of elasticity (see Higdon and Stiles (53)):

$$\frac{\partial \sigma_x}{\partial x} + \frac{\partial \tau_{xy}}{\partial y} = 0$$

$$\frac{\partial \tau_{xy}}{\partial x} + \frac{\partial \sigma_y}{\partial y} = 0$$

$$\tau_{xy} = \tau_{yx}$$

Using the strain displacement equations for plane stress,

$$\varepsilon_x = \frac{\partial u}{\partial x}$$

$$\varepsilon_y = \frac{\partial v}{\partial y}$$

$$\gamma_{xy} = \frac{\partial v}{\partial x} + \frac{\partial u}{\partial y}$$

and using Hooke's Law, the compatability equation is obtained

$$\nabla^2 (\sigma_x + \sigma_y) = \left(\frac{\partial^2}{\partial x^2} + \frac{\partial^2}{\partial y^2} \right) (\sigma_x + \sigma_y) = 0$$

The solution to any given problem (solving for σ_x, σ_y, and τ_{xy}) must satisfy both the compatability equation and the equations of equilibrium.

By writing the stresses as derivatives of an Airy stress function, the equations of equilibrium are automatically satisfied:

$$\sigma_x = \frac{\partial^2 \psi}{\partial y^2} \quad , \quad \sigma_y = \frac{\partial^2 \psi}{\partial x^2} \quad , \quad \tau_{xy} = - \frac{\partial^2 \psi}{\partial x \, \partial y} \tag{A-1}$$

Solving a problem in plane elasticity entails finding an Airy stress function, ψ, that represents the loading of the structure (boundary conditions) and satisfies the compatibility equation. The chosen Airy stress function will satisfy compatibility if it is harmonic, that is, it must satisfy Laplace's equation, $\nabla^2 \psi = 0$.

To solve for the stresses in a structure containing a crack, Irwin used an Airy stress function in terms of complex variables, $z = x + iy$, developed by Westergaard (54),

$$\psi_I = \text{Re } \bar{\bar{Z}}_I + y \text{ Im } \bar{Z}_I$$

for Mode I type crack displacements, where

$$\bar{Z} = \frac{d\bar{\bar{Z}}}{dz} \quad , \quad Z = \frac{d\bar{Z}}{dz} \quad , \quad Z' = \frac{dZ}{dz}$$

and

$$\frac{\partial(\text{Re } \bar{Z})}{\partial x} = \frac{\partial(\text{Im } \bar{Z})}{\partial y} = \text{Re } Z \tag{A-2}$$

$$\frac{\partial(\text{Im } \bar{Z})}{\partial y} = - \frac{\partial(\text{Re } \bar{Z})}{\partial y} = \text{Im } Z \tag{A-3}$$

Substituting ψ_I into Eq. (A-1) and using Eq. (A-2), the stresses resulting from ψ_I are

$$\left.\begin{aligned} \sigma_x &= \text{Re } Z_I - y \text{ Im } Z_I' \\ \sigma_y &= \text{Re } Z_I + y \text{ Im } Z_I' \\ \tau_{xy} &= -y \text{ Re } Z_I' \end{aligned}\right\} \qquad \text{(A-4)}$$

The next step is to define a function Z_I so that it satisfies the boundary conditions of the problem of interest. For example, consider the plate used in Griffith's theory with a crack of length of 2a and a uniform stress applied at opposite ends of the plate, as in Figure 1 (p. 10). The function

$$Z_1 = \frac{\sigma z}{\left[(z - a)(z + a)\right]^{1/2}} \qquad \text{(A-5)}$$

solves this problem of a stress free crack at $-a < x < a$, $y = 0$. This function reduces to the boundary conditions of uniform biaxial stress, σ, at very large distances away from the crack tip. It should be noted that any function, Z_1, which is analytic in a region except for a particular branch cut along a portion of the x-axis, will have the general form

$$Z_1 = \frac{g(z)}{\left[(z + b)(z - a)\right]^{1/2}}$$

Returning now to the stress function, Eq. (A-5), and letting $\xi = z-a$ yields:

$$Z_1 = \frac{1}{\sqrt{\xi}} \cdot \frac{\sigma(\xi+a)}{\sqrt{\xi+2a}} = \frac{1}{\sqrt{\xi}} \cdot f(\xi) \qquad \text{(A-6)}$$

$$\lim_{|\xi| \to 0} f(\xi) = \lim_{|\xi| \to 0} \left[\frac{\sigma(\xi+a)}{\sqrt{\xi+2a}}\right]$$

$$f(0) = \frac{\sigma\sqrt{a}}{\sqrt{2}}$$

Recall that Irwin defined $K_I = \sigma\sqrt{a\pi}$ for the Griffith crack problem so that

$$f(0) = \frac{K_I}{\sqrt{2\pi}}$$

Eq. (A-6) may now be written as,

$$Z_I \Big|_{|\xi| \to 0} = \frac{K_I}{\sqrt{2\pi\xi}} \qquad \text{(A-7)}$$

This form of Eq. (A-7) is found for all stress functions for crack problems near the crack tip. The stress-intensity factor is readily solvable from Eq. (A-7) if the stress function Z_1 can be determined:

$$K_I = \lim_{|\xi| \to 0} (2\pi\xi)^{1/2} Z_1$$

The crack tip stress field for all crack problems is obtained by substituting Eq. (A-7) into Eq. (A-4). Before doing this Eq. (A-7) is rewritten in polar coordinates,

$$\xi = re^{i\theta} = r(\cos\theta + i\sin\theta)$$

and noting the following relationships:

$$\frac{1}{\sqrt{\xi}} = \frac{1}{\sqrt{re^{i\theta}}} = \frac{1}{\sqrt{r}}\left(\cos\frac{\theta}{2} - i\sin\frac{\theta}{2}\right)$$

$$\frac{1}{\sqrt{\xi^3}} = \frac{1}{\sqrt{r^3 e^{i3\theta}}} = \frac{1}{\sqrt{r^3}}\left(\cos\frac{3\theta}{2} - i\sin\frac{3\theta}{2}\right)$$

and $$y = r\sin\theta = 2r\sin\frac{\theta}{2}\cos\frac{\theta}{2}$$

which gives values of Z_I and Z_I' of

$$Z_I = \frac{K_I}{\sqrt{2\pi r}}\left(\cos\frac{\theta}{2} - i\sin\frac{\theta}{2}\right)$$

and $$Z_I' = \frac{dZ_I}{d\xi} = \frac{K_I}{\sqrt{2\pi}}\left(-\frac{1}{2}\right)\frac{1}{\sqrt{\xi^3}}$$

$$= \frac{K_I}{2\sqrt{2\pi}\, r^{3/2}}\left(\cos\frac{3\theta}{2} - i\sin\frac{3\theta}{2}\right)$$

Now substitute Z_I and Z_1' into Eq. (A-4)

$$\sigma_x = \frac{K_I}{\sqrt{2\pi r}} \cos\frac{\theta}{2} - 2r \sin\frac{\theta}{2}\cos\frac{\theta}{2}\left[-\frac{1}{2}\frac{K_I}{\sqrt{2\pi}\, r^{3/2}}\left(-\sin\frac{3\theta}{2}\right)\right]$$

After collecting like terms, σ_x reduces to:

$$\sigma_x = \frac{K_I}{\sqrt{2\pi r}} \cos\frac{\theta}{2}\left(1 - \sin\frac{\theta}{2}\sin\frac{3\theta}{2}\right)$$

Similarly

$$\sigma_y = \frac{K_I}{\sqrt{2\pi r}} \cos\frac{\theta}{2}\left(1 + \sin\frac{\theta}{2}\sin\frac{3\theta}{2}\right)$$

$$\tau_{xy} = \frac{K_I}{\sqrt{2\pi r}} \sin\frac{\theta}{2}\cos\frac{\theta}{2}\cos\frac{3\theta}{2}$$

The crack surface displacements near the crack tip are obtained from the strains and the application of Hooke's law:

$$\varepsilon_y = \frac{\partial v}{\partial y} = \frac{\sigma_y}{E} - \frac{\nu}{E}(\sigma_x + \sigma_z)$$

where for plain strain condition, $\sigma_z = \nu(\sigma_x + \sigma_y)$, and the strain now becomes

$$\varepsilon_y = \frac{1 - \nu^2}{E}\sigma_y - \frac{\nu(1+\nu)}{E}\sigma_x$$

Substituting Eq. (A-4) for σ_y and σ_x,

$$v = \frac{(1+\nu)(1-2\nu)}{E} \int \text{Re } Z_I \, dy + \frac{1+\nu}{E} \int y \text{ Im } Z_I' \, dy$$

Then using Eq. (A-2) and Eq. (A-3):

$$v = \frac{1+\nu}{E} \left[2(1-\nu) \text{ Im } \bar{Z}_I - y \text{ Re } Z_I\right]$$

with $$Z_I = \frac{K_I}{\sqrt{2\pi r}} \left(\cos \frac{\theta}{2} - i \sin \frac{\theta}{2}\right)$$

and $$\bar{Z}_I = 2 K_I \left(\frac{r}{2\pi}\right)^{1/2} \left(\cos \frac{\theta}{2} + i \sin \frac{\theta}{2}\right)$$

Finally,

$$v = \frac{\frac{K_I}{E}}{2(i+\nu)} \sqrt{\frac{r}{2\pi}} \sin \frac{\theta}{2} \left(2 - 2\nu - \cos \frac{2\theta}{2}\right)$$

Note $G = \frac{E}{2(1+\nu)}$ can be substituted for the denominator.

Similarly,

$$u = \frac{1+\nu}{E} \left[(1-2\nu) \text{ Re } \bar{Z}_I - y \text{ Im } Z_I\right]$$

Then

$$u = \frac{K_I}{G} \sqrt{\frac{r}{2\pi}} \cos \frac{\theta}{2} \left(1 - 2\nu + \sin^2 \frac{\theta}{2}\right)$$

APPENDIX B

CONSTRUCTION OF THE MASTER RESILIENT MODULUS AND MASTER CREEP COMPLIANCE CURVES

The procedure used to construct a master resilient modulus curve and a master compliance curve will be presented in this appendix for the AC-5 grade asphalt. This procedure was also used in constructing the master curves for the two other grade asphalts, and can be applied to any viscoelastic material that is thermo-rheologically simple (the time-temperature correspondence principle can be applied to that material).

As shown in Figure 20 (p. 71), duomorph tests were performed at various temperatures but at constant frequencies of 100, 10, 1, and 0.1 Hz. which corresponds to times of 0.001, 0.01, 0.1, and 1.0 second respectively. Since the fatigue tests performed on the overlay tester were conducted in an environment of 77°F, the material response with respect to this temperature for times smaller than 0.001 second are needed. This response is found by shifting all of the curves, those above the curve marked 77°F, horizontally to the left until they overlap one another resulting in one curve known as the "master curve".

The amount that which each of these curves are to be shifted horizontally to construct the master curve is known as the "horizontal shift factor" which is designated "a_T". This shift factor was determined as follows. Referring first to Figure 20 (p. 71), three or four horizontal lines are drawn connecting each pair of curves. For each of these horizontal lines the times at which the line

intersects the lower temperature curve, t_1, and the higher temperature curve, t_2, were found and recorded in Table 6. Once this is done for each pair of curves, t_1 was divided by t_2 and the average quotient was determined. This quotient is the horizontal shift factor, a_T, for the 60°F curve immediately above the reference temperature curve of 77°F. For the remaining lower temperature curves, a_T was found by multiplying the average of t_1/t_2 for the temperature in question by the a_T value found for the immediate higher temperature shown in Table 6. A plot of a_T versus temperature was made as shown in Figure 29 (p.104).

The times used to construct the master curve were found by dividing the times used in the duomorph tests (0.001, 0.01, 0.1, and 1.0 sec.) by a_T determined for each temperature. This procedure is shown in Table 7, and the master curve is plotted in Figure 23 (p. 74) using the (t/a_T) values.

To construct the master creep compliance curve, the following procedure was used. A power law equation of the form:

$$\log E'(t) = \log B + m \log t$$

was fitted to the master resilient modulus data in Table 7, and the regression coefficients were found to be:

$$B = 55.73$$

$$m = 0.410$$

Then using the relationship

$$D(t) = \frac{1}{E'(t)} \quad \frac{\sin m\pi}{m\pi}$$

Table 6. Horizontal Shift Factor (a_T) Calculations for AC-5 Asphalt.

T_1	T_2	t_1 (sec)	t_2 (sec)	t_1/t_2	Average a_T for T_1	
60°F	77°F	0.008	0.001	8.00		
		0.02	0.0022	9.09		
		0.435	0.004	10.88		
		0.09	0.0074	12.2		
			Avg t_1/t_2 = 10.03		10.03	60°F
34°F	60°F	0.019	0.00108	17.59		
		0.033	0.00225	14.67		
		0.053	0.0045	11.78		
		0.1	0.014	7.14	10.03 x 12.79 =	
			Avg t_1/t_2 = 12.79		128.33	34°F
24°F	34°F	0.06	0.0014	52.63		
		0.08	0.0015	53.33		
		0.1	0.00205	48.78		
			Avg t_1/t_2 = 51.58		6619.5	24°F
8°F	24°F	0.24	0.001	240.0		
		0.56	0.00265	211.3		
		1.0	0.0062	161.3		
			Avg t_1/t_2 = 204.2		1,351,724.3	9°F

Table 7. Reduced Times (t/a_T) for AC-5 Asphalt.

Temperature (°F)	t (sec)	t / a_T (sec)	E'(t) (psi)
77°F (Reference Temperature)	0.001	0.001	1,657.
	0.01	0.01	329.
	0.1	0.1	102.
	1.0	1.0	----
60°F	0.001	9.97×10^{-5}	4,790.
	0.01	9.97×10^{-4}	1,362.
	0.1	9.97×10^{-3}	375.
	1.0	9.97×10^{-2}	75.
34°F	0.001	7.79×10^{-6}	20,640.
	0.01	7.79×10^{-5}	7,080.
	0.1	7.79×10^{-4}	1,080.
	1.0	7.79×10^{-3}	-----
24°F	0.001	1.51×10^{-7}	65,000.
	0.01	1.51×10^{-6}	33,100.
	0.1	1.51×10^{-5}	16,300.
	1.0	1.51×10^{-4}	2,450.
8°F	0.001	7.40×10^{-10}	160,000.
	0.01	7.40×10^{-9}	114,000
	0.1	7.40×10^{-8}	80,100.
	1.0	7.40×10^{-7}	33,500.

the master creep compliance values were found as shown in Table 8 and are plotted in Figure 24 (p. 76).

Table 8. Creep Compliance Calculations for AC-5 Asphalt.

t/a_T (sec)	$E'(t)$ (psi)	$D(t) = \frac{1}{E(t)} \frac{\sin(0.410\ \pi)}{0.410\ \pi}$ (1/psi)
10^{-10}	181,000.	4.12×10^{-6}
10^{-9}	155,000.	4.81×10^{-6}
10^{-8}	107,000.	6.97×10^{-6}
10^{-7}	70,000.	1.07×10^{-5}
10^{-6}	40,000.	1.86×10^{-5}
10^{-5}	18,500.	4.03×10^{-5}
10^{-4}	6,100.	1.22×10^{-4}
10^{-3}	1,500.	4.97×10^{-4}
10^{-2}	350.	2.13×10^{-3}
10^{-1}	75.	9.94×10^{-3}
1.0	16.	4.66×10^{-2}

APPENDIX C

CRACK GROWTH RATES, $\frac{da}{dN}$, VERSUS STRESS-INTENSITY FACTORS, K.

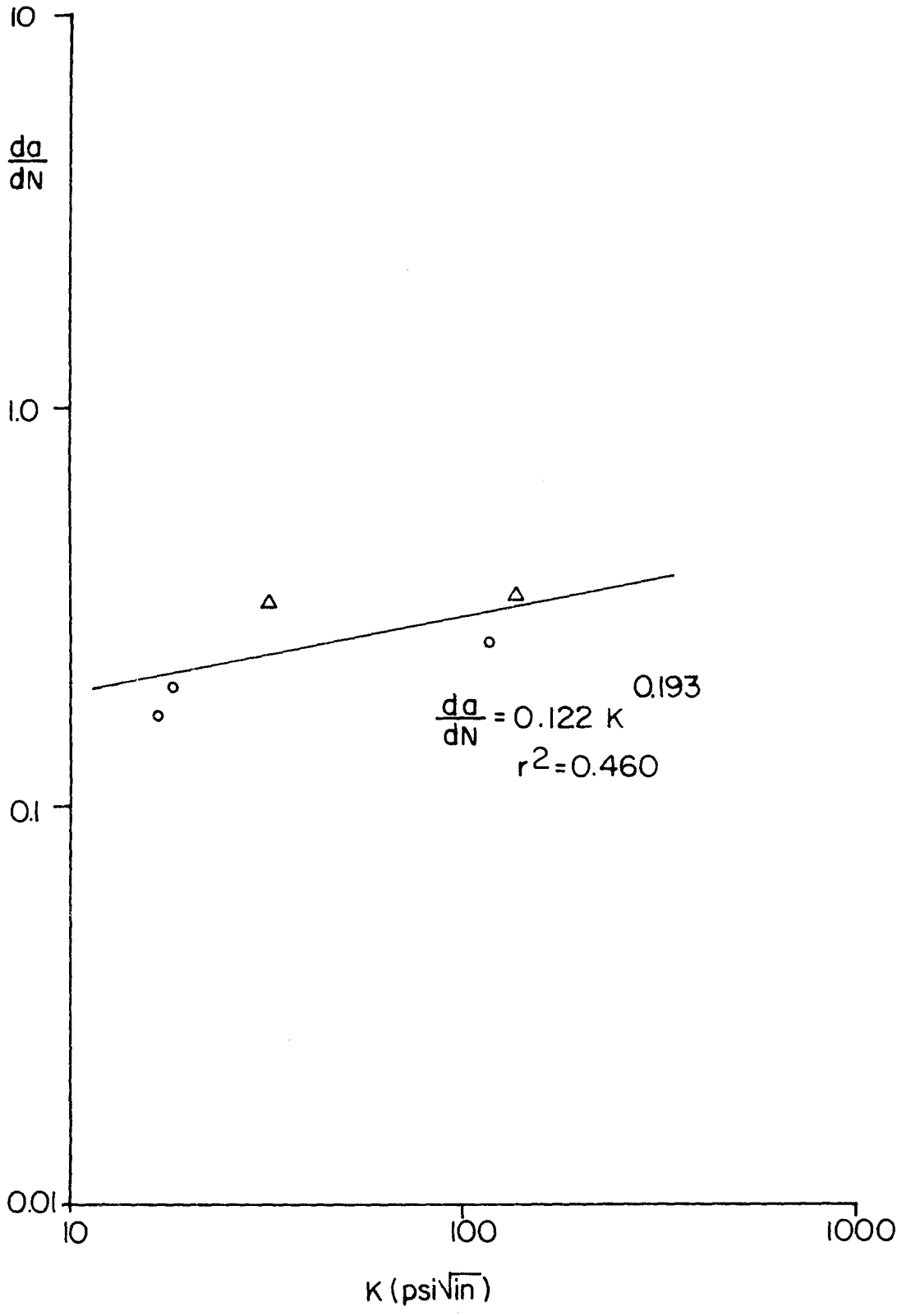

Figure 30. Log $\frac{da}{dN}$ Versus Log K for Test No. 5.

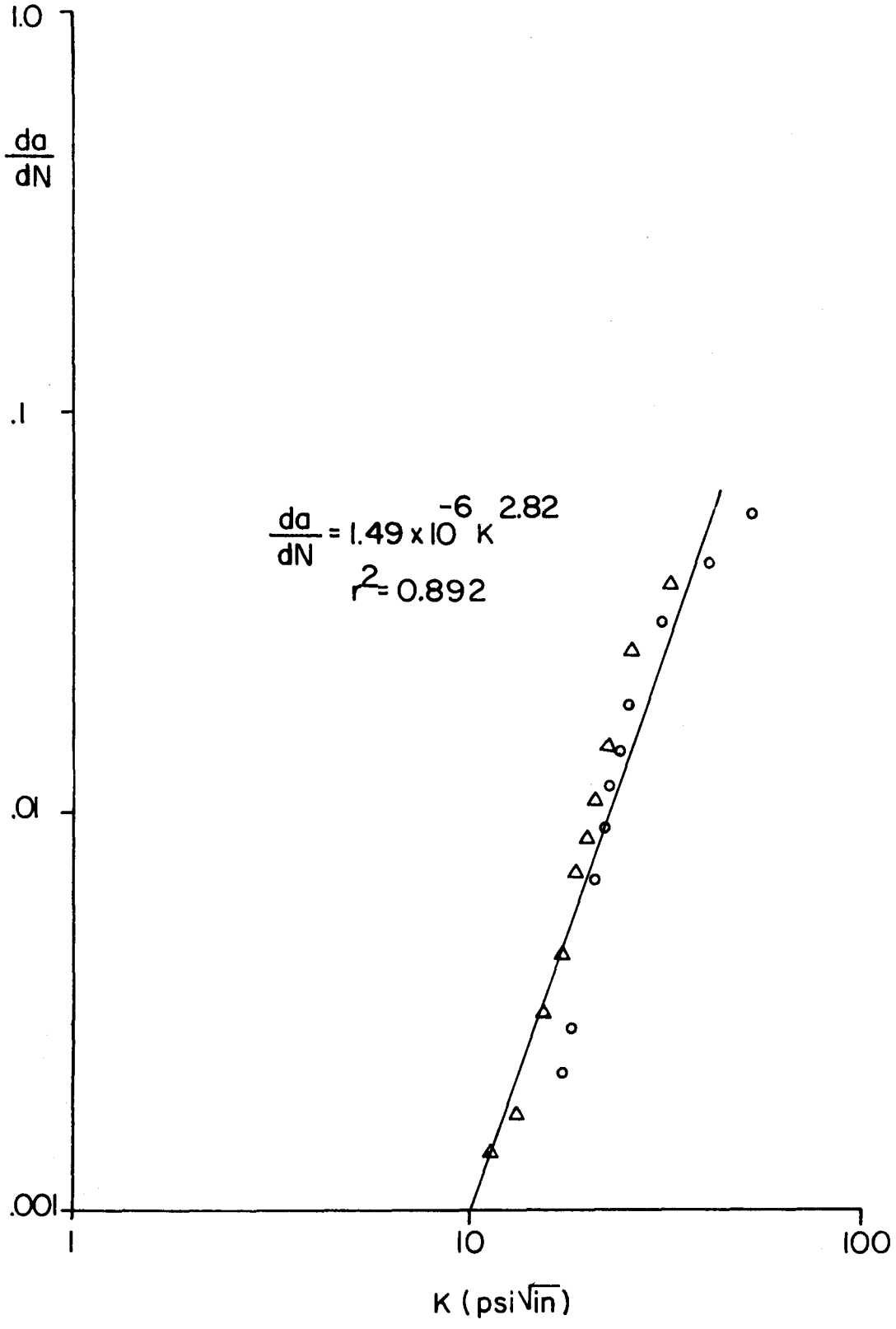

Figure 31. Log $\frac{da}{dN}$ Versus Log K for Test No. 6.

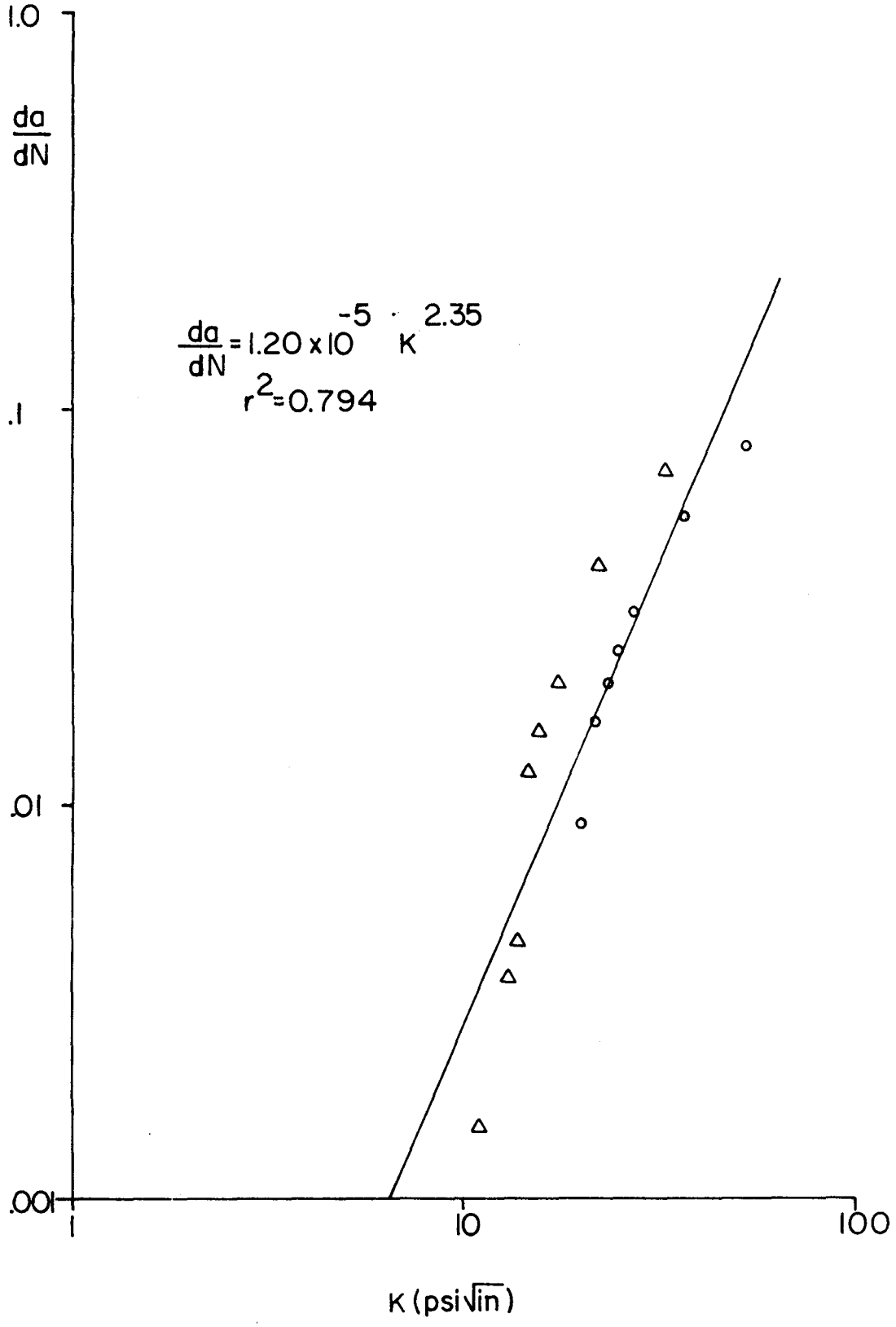

Figure 32. Log $\frac{da}{dN}$ Versus Log K for Test No. 7.

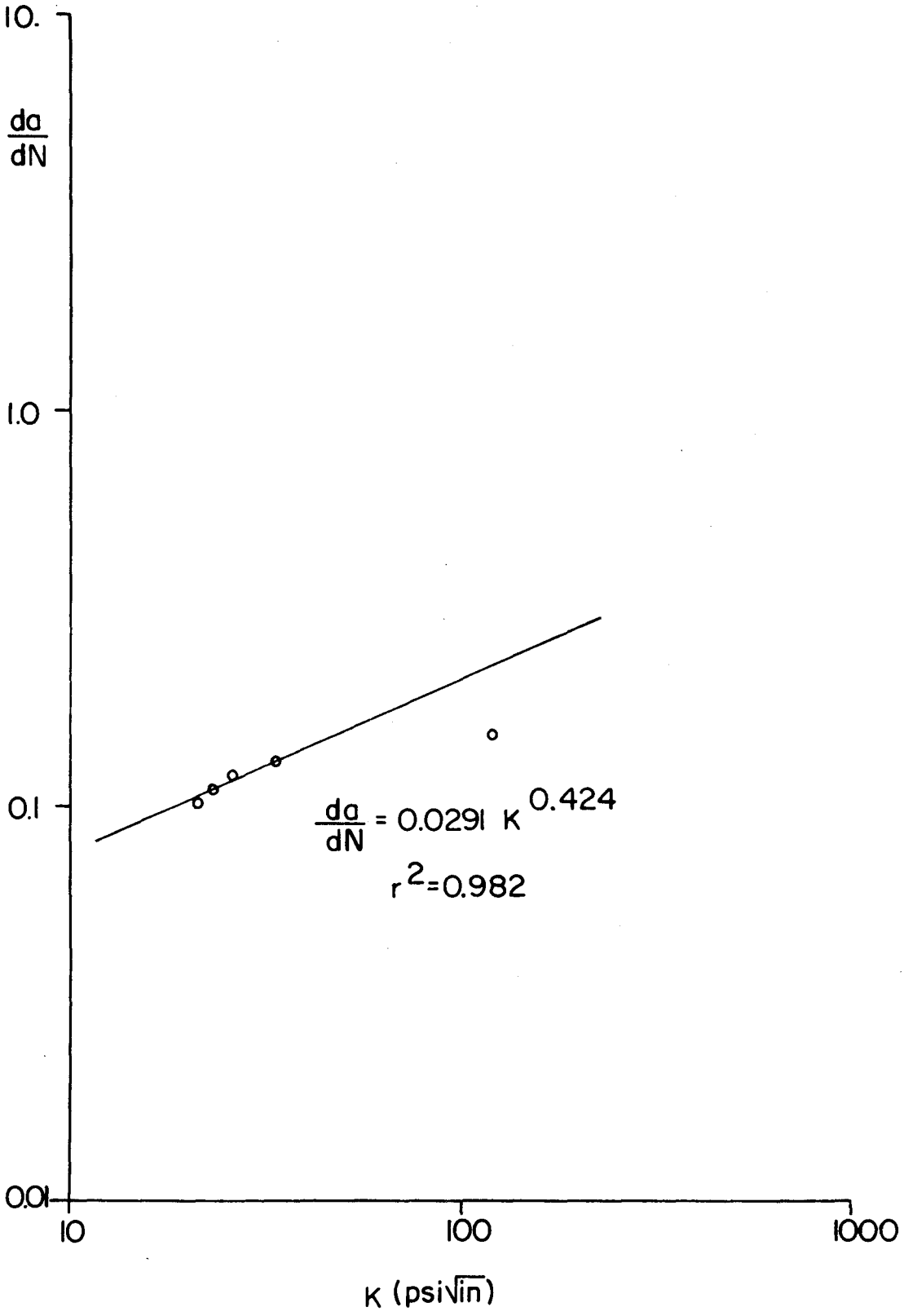

Figure 33. Log $\frac{da}{dN}$ Versus Log K for Test No. 8.

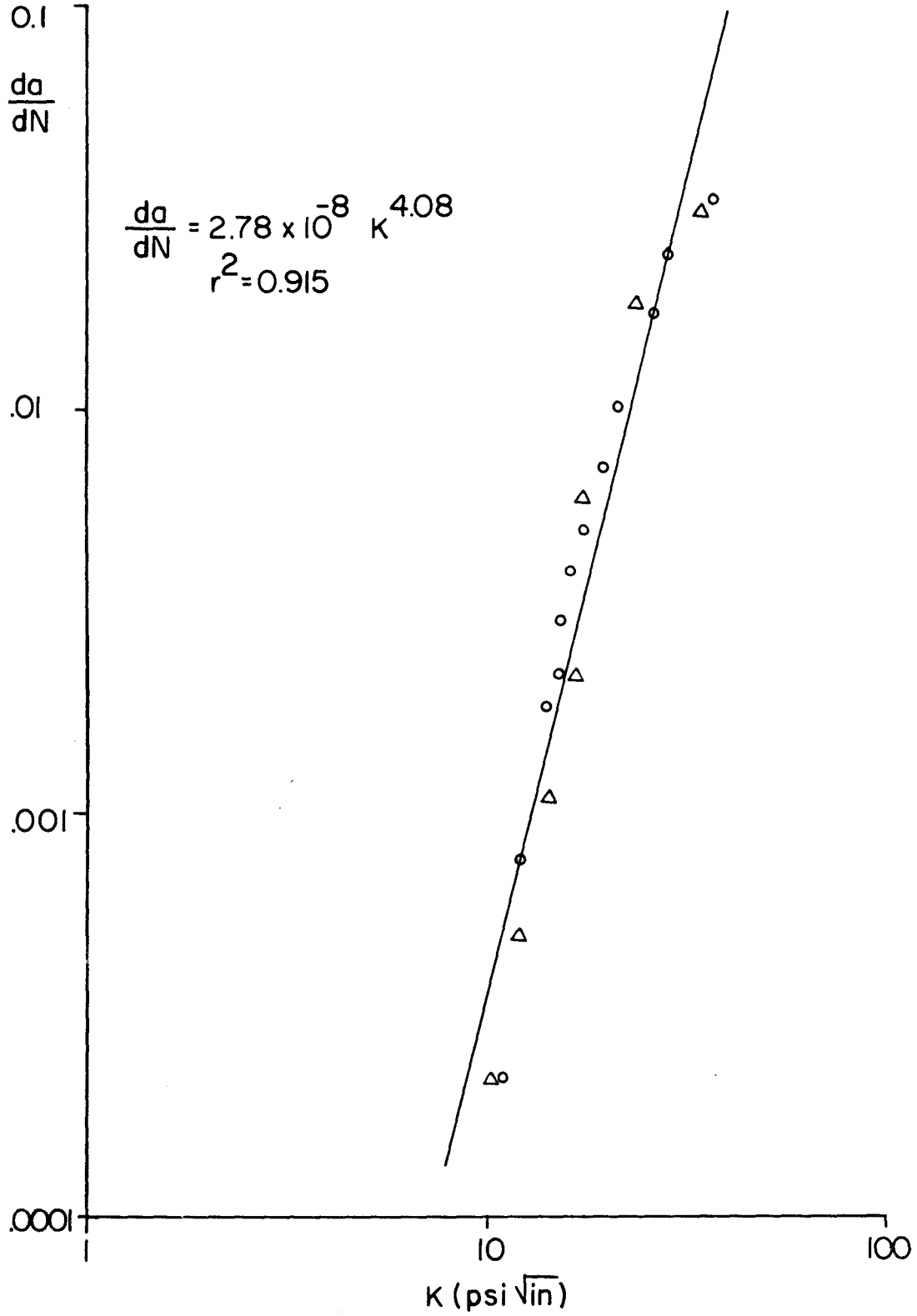

Figure 34. Log $\frac{da}{dN}$ Versus Log K for Test No. 9.

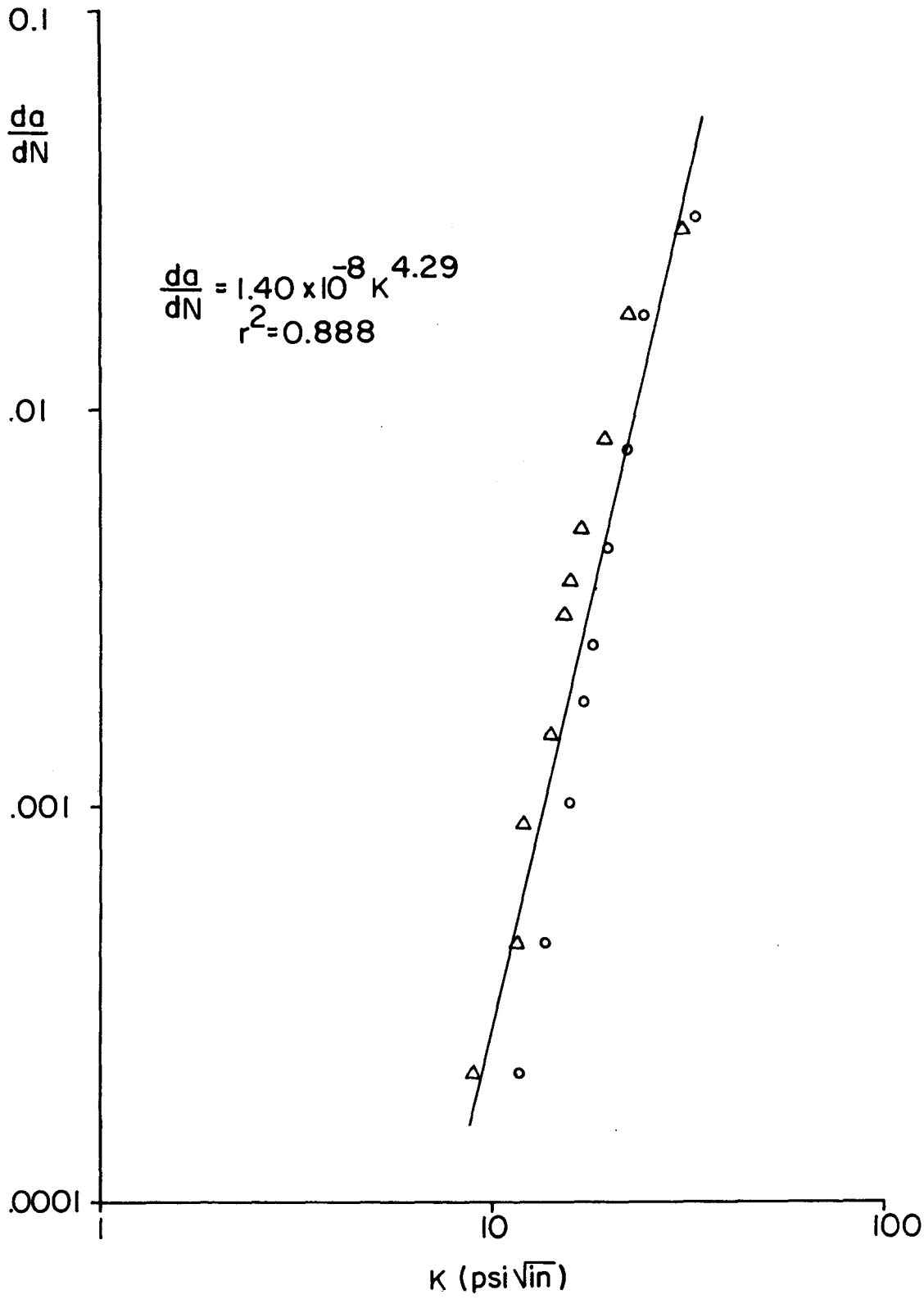

Figure 35. Log $\frac{da}{dN}$ Versus Log K for Test No. 10.

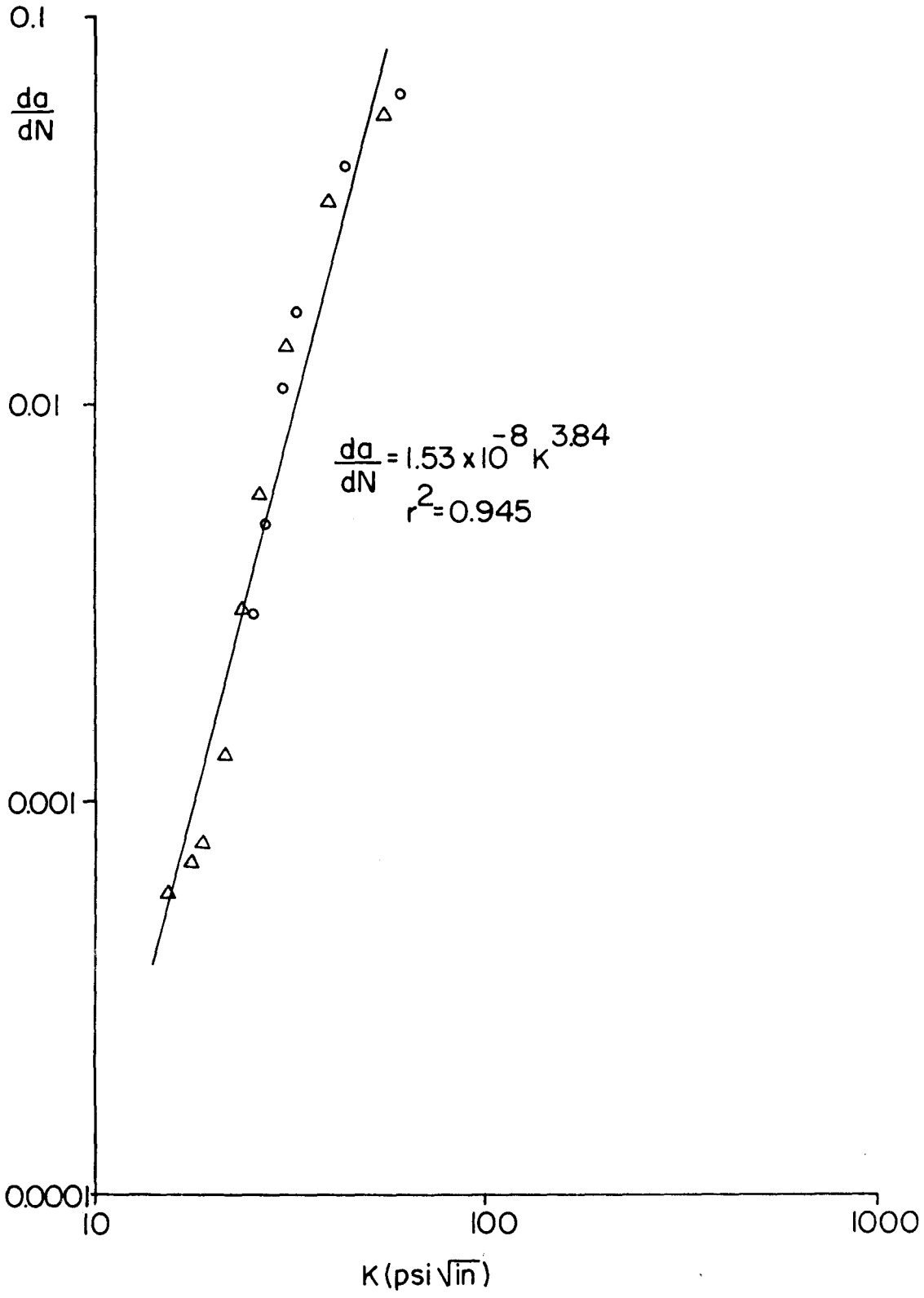

Figure 36. Log $\frac{da}{dN}$ Versus K for Test No. 11.

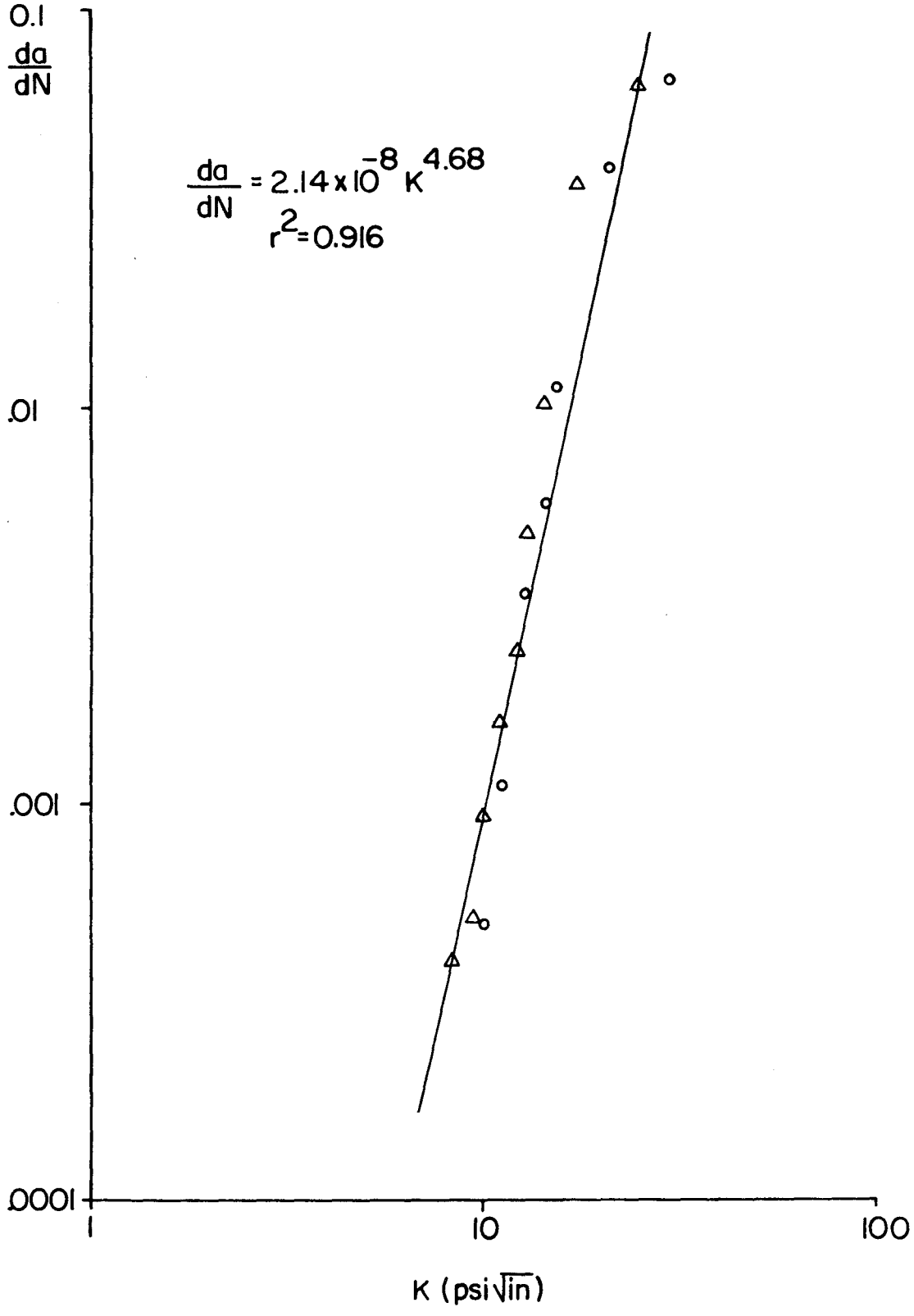

Figure 37. Log $\frac{da}{dN}$ Versus Log K for Test No. 12.

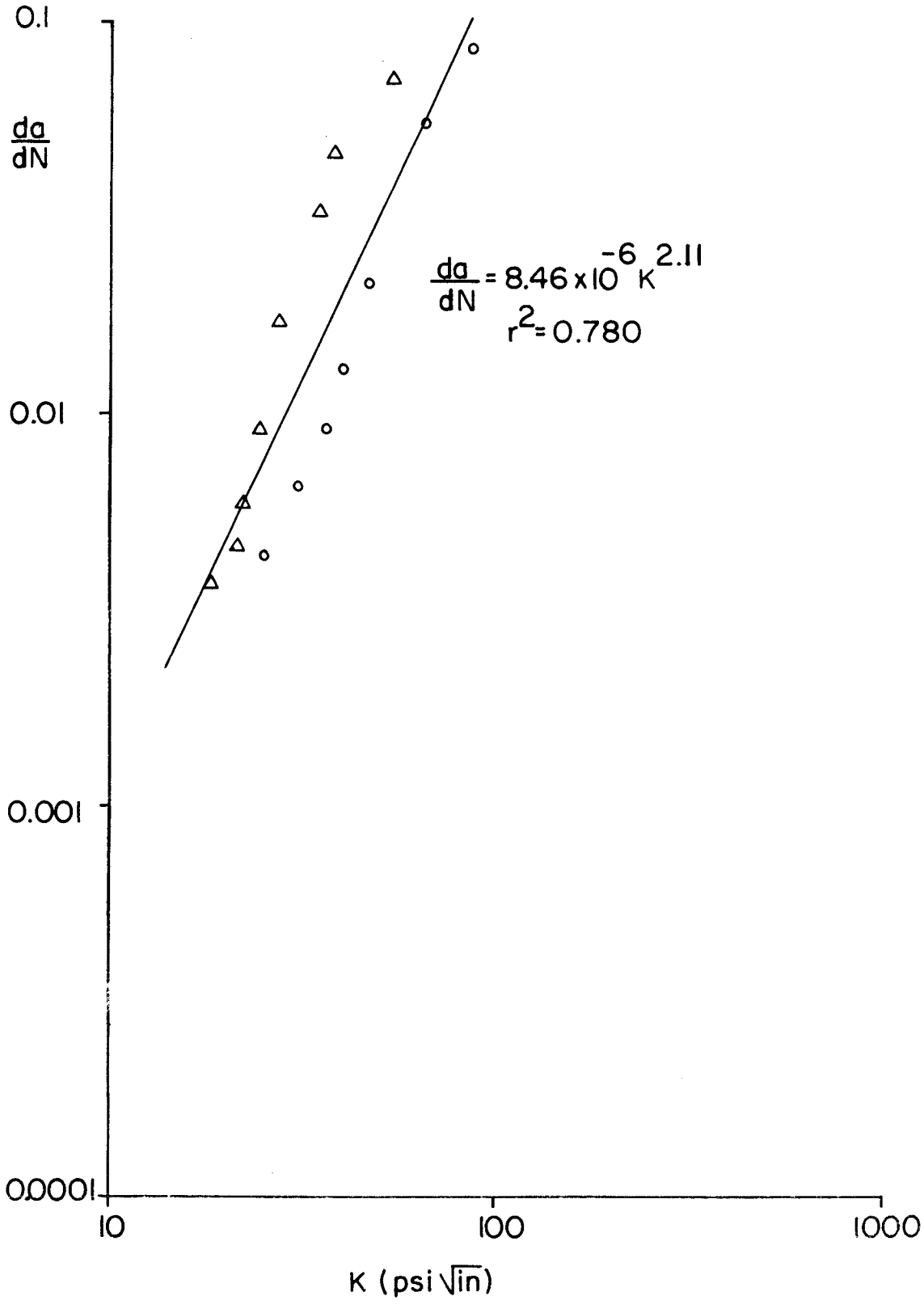

Figure 38. Log $\frac{da}{dN}$ Versus Log K for Test No. 13.

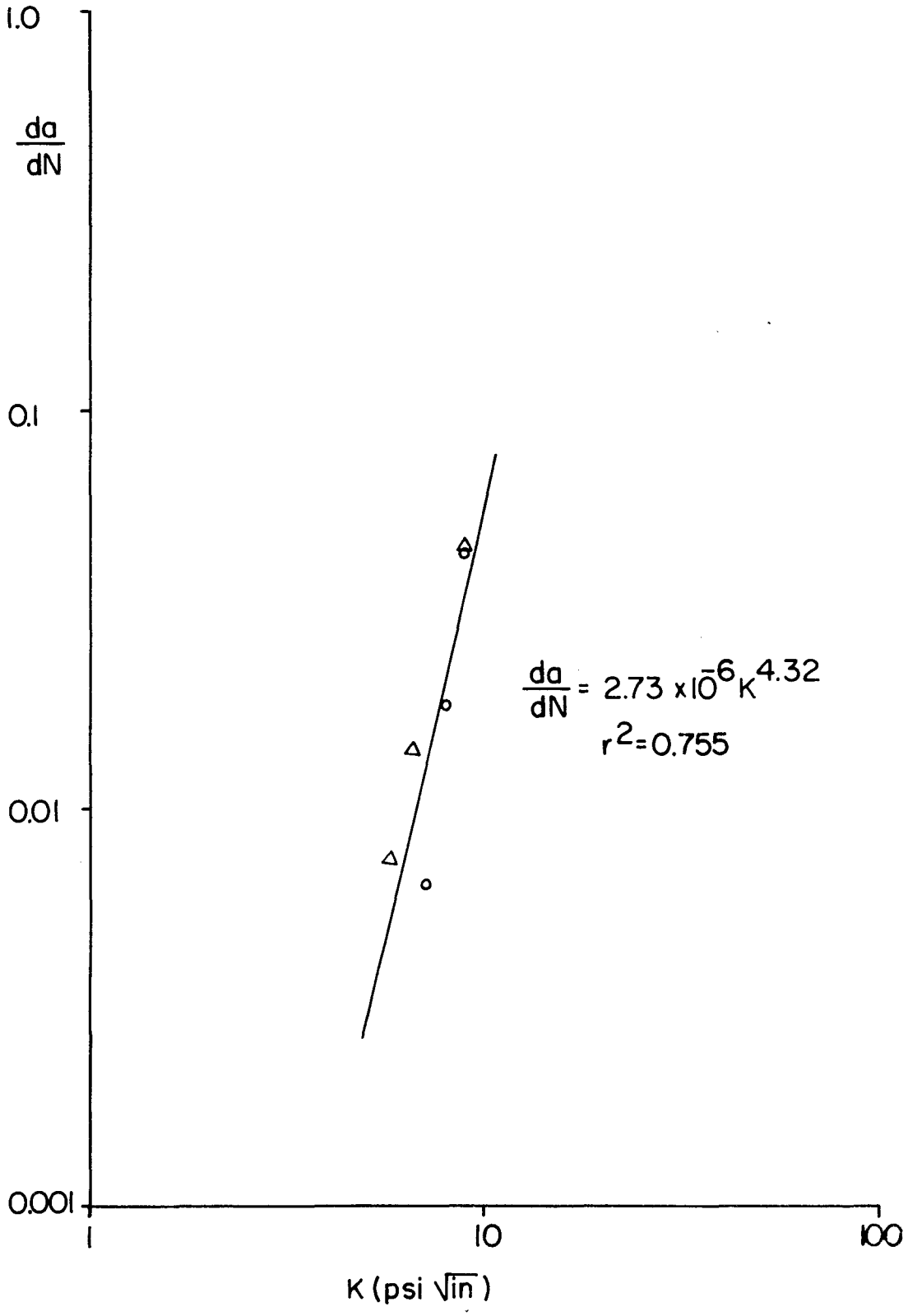

Figure 39. Log $\frac{da}{dN}$ Versus Log K for Test No. 14.